ACKNOWLEDGMENTS

I would like to thank Dr. Magne Kristiansen, Dr. Marion Hagler, and Dr. Lynn Hatfield for their invaluable assistance and guidance during the course of this research. I would also like to thank Dr. Russell Seacat, Dr. Erich Kunhardt and Dr. Albert Engelhardt for serving on my committee. I thank Mike Foster, Roger Dougal, George Jackson, Dr. John Marx, and Dr. Frazier Williams for assistance in the analysis and interpretation of this work. Special thanks goes to Hugh Kirbie, Kim Zinsmeyer, Randy Curry, and Ken Rathbun who all helped with the critical design and construction phases of this project. I would like to thank many others whose help on this project and processing this manuscript is appreciated. Some of these include Marie Byrd, Telesforo de la Cruz, Jim Semrad, and Dale Coleman. Some of the voltage distribution data was supplied by Richard Ness, and is greatly appreciated. The financial support by the Air Force Office of Scientific Research and Texas Tech University is appreciated. I owe my excellent education to the Department of Electrical Engineering at Texas Tech University. Finally, I would like to dedicate this work to my parents, C. M. Gordon and Barbara Gordon, who made it possible for me to achieve this goal, and to my wonderful wife, Jeanette, for her patience and encouragement.

TABLE OF CONTENTS

ABSTRACT

A flexible spark gap assembly was designed and constructed to investigate and characterize the chemical and physical processes involving the electrode, gas and insulator materials in a high energy spark gap. Materials studied were graphite and a tungsten-copper composite for the electrodes, Lexan and nylon for the insulators, and N_2 and SF_6 for the gases. The gas composition was monitored with a mass spectrometer, and spectroscopic and photographic techniques were used to characterize the arc channel. The self-breakdown voltage distribution was examined as a function of the material combinations. The electrode surfaces were studied with several surface analysis techniques, including scanning electron microscopy, electron spectroscopy for chemical analysis, Auger electron spectroscopy, and X-ray fluorescence. For the materials studied (graphite, copper-tungsten, N_2, and SF_6) results indicate that the least chemical erosion occurs in N_2 (compared to SF_6) and that the fewest mechanical changes occur on graphite. Blue nylon appears to contaminate the gap and alter the breakdown voltage distribution adversely.

LIST OF TABLES

LIST OF FIGURES

Figure Page

LIST OF ACRONYMS

ESCA - Electron Spectroscopy for Chemical Analysis

AES - Auger Electron Spectroscopy

SEM - Scanning Electron Microscopy

XRF - X-Ray Fluorescense

EMPA - Electron Microprobe Analysis

OMA - Optical Multichannel Analyzer

UV - Ultraviolet

K-33 - A 67% tungsten/33% copper composite manufactured by Metallwerk Plansee (see page 4)

LTE - Local Thermodynamic Equilibrium

LIST OF CHEMICAL SYMBOLS

H - Hydrogen

C - Carbon

N - Nitrogen

O - Oxygen

F - Fluorine

Al - Aluminum

Si - Silicon

S - Sulfur

Cl - Chlorine

Ar - Argon

Cu - Copper

W - Tungsten

LIST OF TRADE NAMES

Delrin - an acetal resin manufactured by E. I. duPont de Nemours and Co.

Lucite - an acrylic resin manufactured by E. I. duPont de Nemours and Co.

Lexan - a polycarbonate resin manufactured by General Electric Company, Chemical Materials Department.

Poco Graphite - often used to label any of the high density graphites manufactured by Poco Graphite, Inc.

K-33 - one of the many tungsten/copper composites manufactured by Metallwerk Plansee.

Pyrex - a heat-resistant glass manufactured by Corning

Sources - CRC Press Handbook of Chemistry and Physics, Websters Third New International Dictionary, Unabridged, and Manufacturers' Literature.

CHAPTER I

INTRODUCTION

This dissertation describes research done to characterize the chemical and physical processes occurring in high pressure gas spark gaps. The approach used was to study the electrode surfaces and the gas chemistry using both on-line diagnostics and post analysis techniques, and to relate the observations made to changes in spark gap operation for various combinations of spark gap materials. A dedicated pulsed power source and an accessible, interchangeable spark gap were designed and built. Analysis techniques were taylored to the study of these processes.

The historical need for gas spark gaps is described in Chapter II. The important spark gap parameters are listed, including a discussion of gap lifetime and its importance. A discussion of the materials chosen for this study is followed by a review of previous work done on understanding spark gap processes, including some work done with these materials.

Chapter III describes the experimental arrangement designed and built for this spark gap study. The diagnostic and post analysis techniques are briefly described in Chapter IV. In Chapter V, conclusions about the spark gap processes occurring in the different material combinations are described and some of the data taken are presented. The conclusions are summarized in the final chapter and further studies are suggested. Improvements to the diagnostic and analysis techniques are included.

CHAPTER II

BACKGROUND

Recent developments in high-technology, pulsed power areas, such as lasers and fusion, require considerable improvements in high energy switching methods.[1] Gas-filled spark gaps are one of the most widely used switch types in pulsed power technology due to their ability to switch large energies very rapidly. Each application of spark gaps in pulsed power technology has its own set of specifications to meet. These specifications include hold-off voltage, peak current, average current, charge transfer, delay time, recovery time, rep-rate, jitter, prefire probability, trigger method, lifetime, and reliability.[2,3] Because of the wide range of applications and the large number of specifications, spark gaps are usually custom built to fulfill the specific needs for that application.

As the need for high rep-rate increases and as the application of spark gaps moves from research to commercial usage, one of the biggest problems with gas gaps will be the switch lifetime. Spark gap lifetime is determined by the degradation of important switch parameters, such as hold-off voltage, delay time, jitter, and recovery time, and ultimately by the failure of some component, such as the insulator or electrode. Many factors affect spark gap lifetime. For instance, rep-rate capability is directly related to recovery, which is determined by gas flow rate, gas type and pressure, current, voltage, charge transfer, gap spacing, electrode

shape, and electrode material. Electrode failure is related to mechanical and thermal stresses and erosion, which is influenced by time rate of change of current, peak current, charge transfer, electrode material, gas type, electrode cooling, gas flow, etc. Other limitations on spark gap lifetime include insulator failure and gas contamination and decomposition.

One of the most important factors influencing all aspects of gap lifetime is the individual degradation and the mutual compatibility of the electrode, gas and insulator materials. The details of the electrode erosion processes, the insulator damage mechanisms, and the plasma chemistry in a spark gap are poorly understood. Electrode erosion processes include corrosion, electrical, mechanical, and thermal stresses, melt-zone displacement, microstructural and molecular alterations, and vaporization, sublimation and/or sputtering of electrode material. Insulator failure can be due to UV damage, shocks, metal vapor deposition, microparticle impact, and chemical interaction. Gas degradation is caused by decomposition product accumulation, chemical interaction with the electrode and insulator materials, and release of impurities within the spark gap system. Little information is available about the chemical and physical processes occurring and leading to degradation of these materials, or how these processes vary from material to material. Most material selections in past spark gap applications have been reached by trial and error methods with only limited understanding of the physical and chemical mechanisms. Degradation processes are certainly influenced

by the physical parameters (electrode, gas and insulator materials, electrode shape, gap spacing, and gas flow and pressure) and the electrical parameters (voltage, current, charge transfer, pulse length, rep-rate, etc.). Because of the large number of different spark gap applications it would be difficult to investigate processes under all conditions of all parameters. Therefore, this work has concentrated on varying the materials (electrode, gas, and insulator) for a fixed set of electrical and other physical parameters (gas pressure and electrode shape).

The division of material problems into erosion processes, insulator damage, and plasma chemistry suggests that there are three regions of interest in the spark gap: the electrode surface, the gas, and the insulator surface. This division has influenced the development and choice of the diagnostics used in studying each region. The diagnostic and analysis techniques will be described in Chapter III. A separate study of insulator surfaces is being conducted in conjunction with this work[4] so that this report is primarily concerned with processes occurring at the electrode surface and in the gas. The influence of insulators on the chemistry of the electrodes and gases is discussed briefly.

The development of spark gaps for different applications has been achieved in the past by studying the influence of different gap materials (mainly electrode and gas) on specific gap parameters. Erosion studies have been carried out on several electrode materials[5-8] and electrode vapor ejection has been observed.[9,10] A

variety of gases have been studied for breakdown strength[11] and recovery time,[12-16] and a few studies have considered chemical processes.[17] Very few detailed surface analysis studies have been done on electrodes or insulators. A preliminary surface study on a brass electrode was conducted;[18] some electrode surfaces have been visually inspected;[19,20] and insulator studies are in progress.[4]

From the studies done on spark gap materials it is apparent that the selection of possible materials is very large. Figure 1 illustrates some spark gap materials along with other variables which would influence gap degradation. The goal of the research described in this dissertation was to investigate the chemical and physical processes occurring in spark gaps. Hopefully this will lead to better understanding of materials needed to optimize spark gap performance and obtain the highest possible lifetime. However, the extensive range of materials apparent from Fig. 1 would cause a detailed study of all processes occurring in all combinations of materials to be prohibitively complex and time consuming. Fortunately, the trial and error study of materials for the optimization of certain gap parameters has helped to point out some promising candidates for durable gap materials. Two each of electrode, gas, and insulator materials were chosen to be examined in this study. The electrode materials chosen were a very fine grained, dense graphite, ACF 10Q, made by Poco Graphite (1601 South State St., Decatur, Texas 76234), and K-33, a tungsten-copper composite composed of 67 percent tungsten and 33 percent copper, manufactured by Metallwerk Plansee

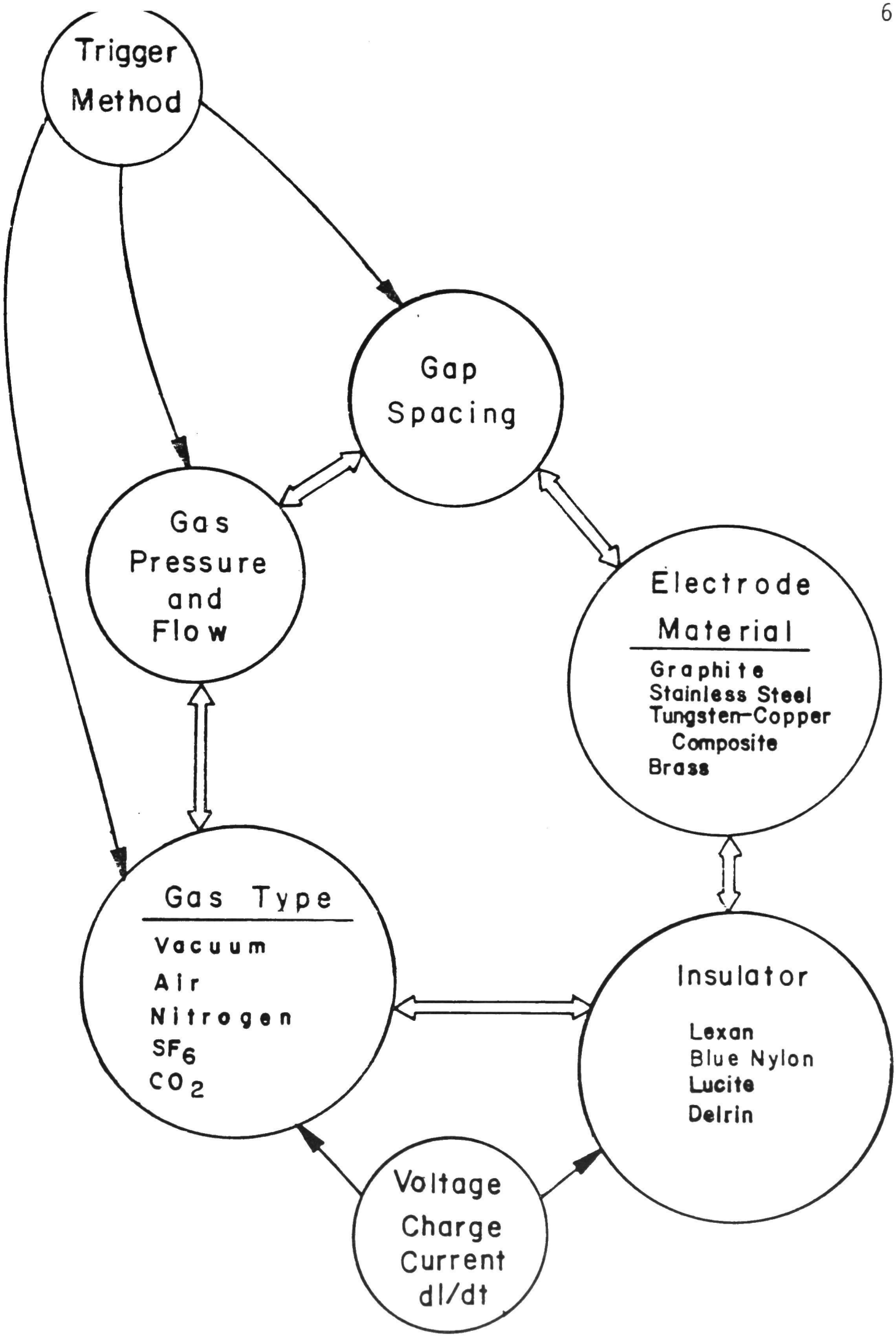

Figure 1. Spark Gap Variables.

in Austria (distributed by the Schwarzkopf Development Corporation, 1916 Old Middlefield Way, Mountain View, CA 94043). The gases used were spectroscopic grade (99.99 percent pure) nitrogen (N_2) and sulfur hexafluoride (SF_6). The insulators studied were Lexan and Blue Nylon, a special form of nylon.

Figure 2 gives the reduced material diagram showing the materials studied at a gauge pressure of 1520 Torr (2 Atm, not flowing), a breakdown voltage of 40-50 kV, and a charge transfer of about 0.03 C/shot. Since the electrode shape may affect the erosion processes, and the electrode polarity (i.e., anode/cathode) affects the degree of chemical interaction with the gas (from visual observation) and the erosion rates,[21] the variable space was further reduced by chosing a hemispherical electrode profile and by examining only the anode. These choices were made for convenience, since erosion and chemical processes may be significantly different for the cathode or for a different electrode profile. Thus, these studies do not attempt to determine the effects of gas pressure or flow, breakdown voltage, charge transfer, peak current, time rate of change of current, electrode shape, or polarity.

A few previous studies have been conducted on the materials selected. Very fine-grained graphites have been found to give erosion rates comparable to the best metal electrodes.[22] Affinito, et al.,[23] found that Poco Grahpite ACF 10Q has excellent erosion characteristics in air. Also, it is one of the best materials available for electrical

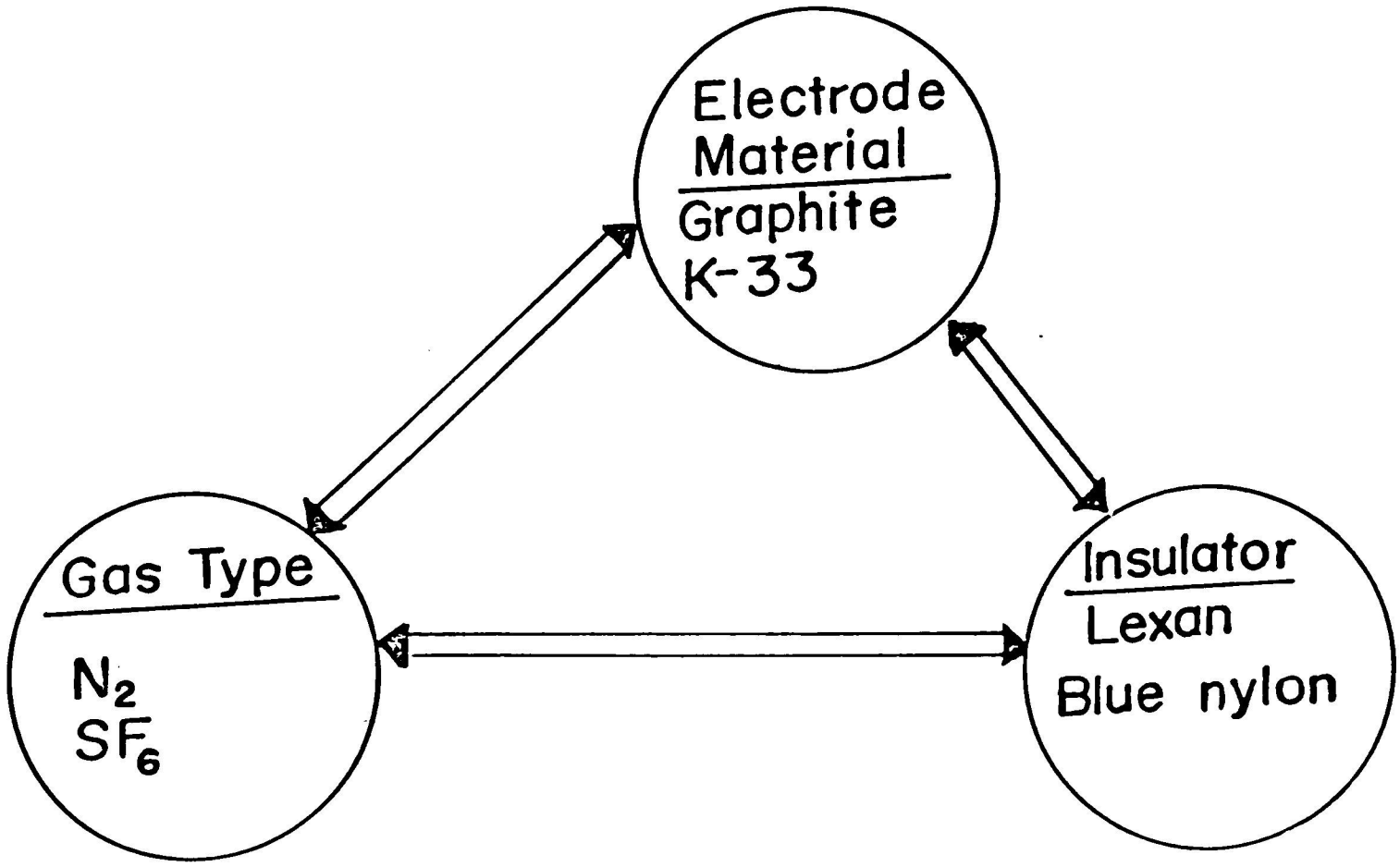

Figure 2. Spark Gap Materials Studied.

discharge machining.[24] Several studies have shown that certain tungsten-copper composites give excellent erosion characteristics compared to other metals.[5,25,26] Tungsten-copper composites have been studied in both N_2 and SF_6.[27] Few studies have been made of the chemical processes occurring in N_2, possibly because there may be no significant chemical interaction between N_2 and most metal surfaces. On the other hand, SF_6 has long been used as a high breakdown strength dielectric for high voltage applications in the utility industry. More recently it has found widespread use in spark gaps. Thus, there is a fair amount of literature concerning the decomposition and degradation of SF_6 when used as an insulator in electric utility industry switching,[28-32] some studies of SF_6 in a corona or low energy spark environment,[33-35] and a few studies when used in pulsed power switching.[36-40] These studies indicate a large number of stable and short-lived decomposition products, some being very toxic and others very corrosive.

All electrodes, insulators, and gas materials used in spark gaps are initially chemically stable; i.e., neglible interaction takes place before a discharge. However, when a spark gap closes, the gas breaks down, and the resulting discharge liberates tremendous amounts of energy in a small volume, causing dissociation, ionization, melting, vaporization, etc., of the exposed spark gap materials. Ultimately, the energy is dissipated as radiation and heat as the gas recombines and the arc extinguishes. In order to predict the potential chemical and physical degradation occurring in the gap it is

useful to look at the environment which a high energy discharge creates and how it might affect the gap materials.

A high energy spark gap in its "off" state typically holds off 10's to 100's of kV and conducts no current; i.e., no energy is dissipated in the gap. During a single-channel breakdown the voltage across the gap drops to 100 to 200 V and the current reaches the 1 to 100 kA range. Typically, 1 to 10 MW of power is transferred to the spark gap environment in a few microseconds. Assuming a 200 V drop across a 30 kA discharge channel in a few microseconds, as much as 1 to 10 J of energy is deposited in the arc channel volume. In a dc arc the channel radius expands to keep the current density low (10^6 A/m^2), regardless of the total current. In a high energy spark gap, however, the breakdown very rapidly (in 10^{-7} to 10^{-6}s) creates a high current discharge before the current channel can expand significantly. Thus, current densities of 10^9 to 10^{10} A/cm^2 are obtained in the initial breakdown channel (1 to 3 mm in diameter). As a result, high energy densities and very high temperatures are reached in the core of spark discharges. In N_2 the channel core reaches temperatures of around 40,000 to 45,000 K,[41-44] and in SF_6 temperatures up to 20,000 K have been measured.[45] Because local thermodynamic equilibrium (LTE) can be argued for the conditions found in the discharge channel,[46] the temperatures of the electrons and ions are approximately equal. At the electrode surfaces the arc channel is usually somewhat constricted and energy densities of 2×10^6 W/cm^2 are typical.[8,47] Electrode surface temperatures of 3000 K have been

measured in vacuum gaps,[48] and surface temperatures at arc spots range from 2000 K to 4000 K in gas gaps.[49-50]

For a typical arc channel volume of 0.07 cm^3 (3 mm diameter, 1 cm length), an initial deposition of 5 J of energy would result in an energy density of about 1.7×10^6 J/mole of gas (both N_2 and SF_6 provide approximately 3×10^{-6} moles of molecules in the arc volume). Since N_2 and SF_6 have bond strengths of 0.95×10^6 J/mole[51] and 1.8×10^6 J/mole,[52] respectively, N_2 is totally dissociated in the arc channel and SF_6 is 90 percent dissociated. However, this simple calculation grossly oversimplifies the real situation. The discharge creates a shock wave, expanding rapidly in the radial direction, which causes a lower density region to be formed in the arc channel. Thus, the energy density is probably higher (per molecule) than the initial guess above. Not only is sufficient energy available in the arc channel for complete dissociation of the gas, but almost all of the atoms are at least singly ionized, many doubly, and a few are triply ionized. (Indeed, the electrons resulting from the ionized atoms are the charge carriers for the switch.) The core of an arc channel of a pulsed discharge in N_2 at 40,000 K has been calculated to be composed of 0% N, 4% N^+, 93% N^{++}, and 3% N^{+++}.[43] Similarly, the core of an arc channel in SF_6 at 15,000 K has been calculated to be composed of 0% SF_6, 68% F, 24% S^+, 7% F^+, and 1% S.[30,53] These plasma composition calculations used the Saha and Boltzman equations, assuming that LTE is established very quickly (less than 10^{-7} s).[43,54] Although the exact results would certainly be different for different

gaps, and depend on the arc parameters, the general trend serves to illustrate that the plasma in the arc channel is composed of ionized atomic species of the original molecular gas. Actually, in a typical N_2 arc channel plasma N^+, N^{++}, and N^{+++} are observed[43] and in an SF_6 arc channel plasma S^+, S^{++}, F^+, and F^{++} are all observed.[45,46]

Many other phenomena would result from the violent deposition of energy in the gap. At the electrode surface, the high current densities lead to anode and cathode spots (the points of contact of the arc channel with the electrode surface) which often become small pools of molten metal. High electric fields occur just before breakdown and are certainly influenced locally by any imperfection on the electrode surface. Thermal and mechanical shocks in the electrode and insulating materials are caused by the expanding gas shock wave and the impact of the arc channel on the electrode surface.[55,56] The gas shock wave results in turbulence causing mixing and diffusion of the ions and gas molecules. Finally, demixing (separation of the S and F)[45,54,57] may occur in SF_6, due to the different ionization energies of sulfur and fluorine. The energy contained in the plasma is released as heat and radiation and partially converted back into chemical energy as the ionized gas atoms recombine.

The highly ionized plasma in the arc channel provides reactive gas species for chemical reactions. In addition to the ionized gas molecules, electrode vapor or particles may be ejected into the discharge region. In the case of N_2, very few chemical reactions

are probable. Most of the nitrogen ions probably recombine into neutral gas, although cyanogen (CN) compounds might be formed with graphite electrodes. A more likely candidate for chemical reactions is SF_6. In addition to the totally ionized atoms in the core, partially dissociated molecules from SF_6 are created by the high energy discharges. Several reports have noted the production of SF_5, SF_4, SF_3, SF_2, and SF molecules.[31,35] The recombining sulfur and fluorine atoms in the arc channel have many choices for forming new chemical compounds. Any metal vapor could react with the fluorine leaving an excess of sulfur. Demixing, due to the different ionization potentials of S and F, may occur within the discharge, causing S to migrate to the outside of the arc channel and F to accumulate toward the center. The fluorine is then likely to react with any Cu or W atoms emitted by the K-33 electrode or possibly with C released by the graphite electrode.[58] (WF_6 is an easily formed, highly volatile molecule). If 10 percent of the arc channel ions failed to recombine into SF_6 after each discharge then, after 50,000 shots, for the volume of the gap chamber in this report, as much as two percent of the original gas would have changed into other compounds. Any H_2O or oxides released by the discharge from the electrode and insulator surfaces would also be very likely to react with free S or F atoms. For example, Blue Nylon absorbs six percent water by volume, which will be gradually released in the spark gap environment. The results of prolonged discharges in SF_6 should be detectable gas

composition changes, possible metal corrosion by fluorine molecules, especially near the electrode spot regions, and possibly deposits of sulfur compounds or other solid debris.

CHAPTER III

EXPERIMENTAL ARRANGEMENT

The experimental arrangement consists of five parts: the spark gap assembly, the high voltage network, the vacuum-gas system, the diagnostic system, and the control system. Figure 3 illustrates the interrelationship of these basic subsystems. The spark gap diagnostics will be discussed in the next chapter along with the analysis techniques.

Spark Gap Assembly

The spark gap (Fig. 4 and 5) was designed to accommodate frequent electrode and insulator material changes, to allow accurate control over gap spacing, gas type and pressure, and to provide access for on-line diagnostics. The assembly consists of two electrodes, two header plates, the outer containment cylinder, two insulating plates, the load, and the current return rods. The electrodes are each composed of three components: the support, the holder, and the electrode insert (Fig. 6). The electrode supports are intended to be permanently installed in the system. Electrode inserts (5 cm in diameter, hemispherically shaped) are made from the various electrode materials to be studied and are shrunk fit into the aluminum holders to obtain a tight, high-current connection. For quick electrode changes, the aluminum holder-insert is removed and a new one substituted. However, since thread failure was caused by the chemical attack of fluorine on the aluminum holders (after many

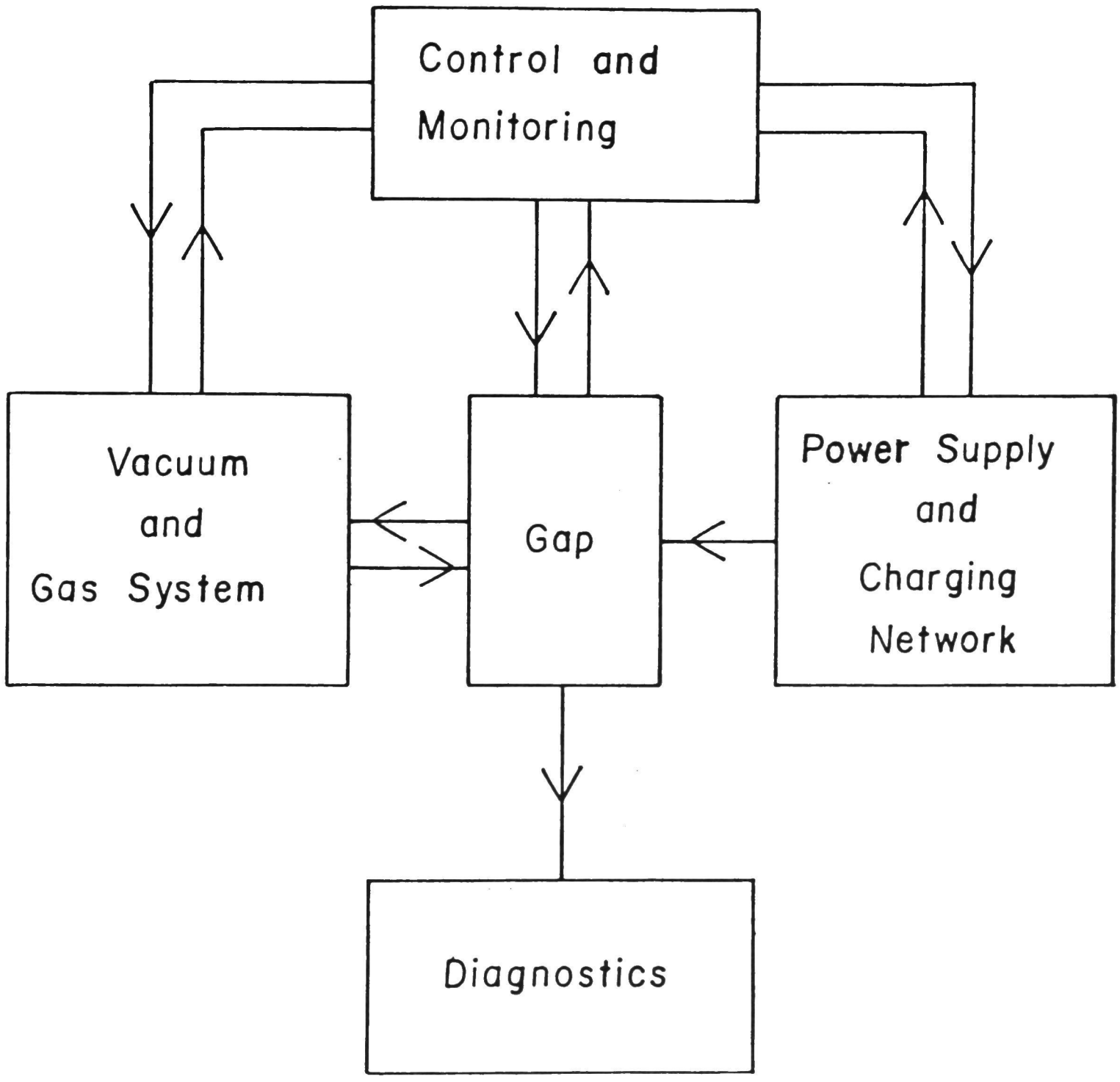

Figure 3. Basic Subsystems.

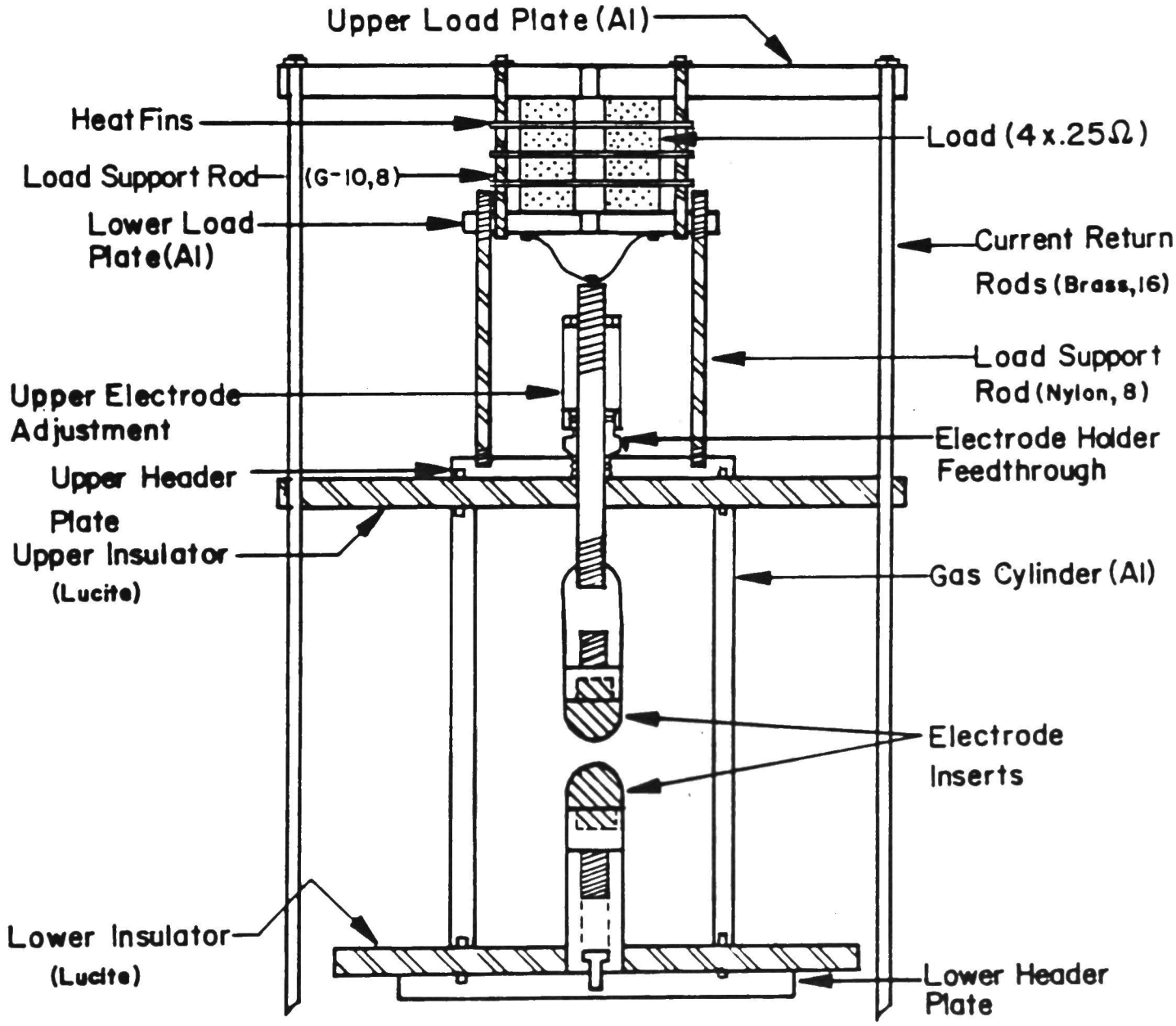

Figure 4. Spark Gap Assembly Cross Section.

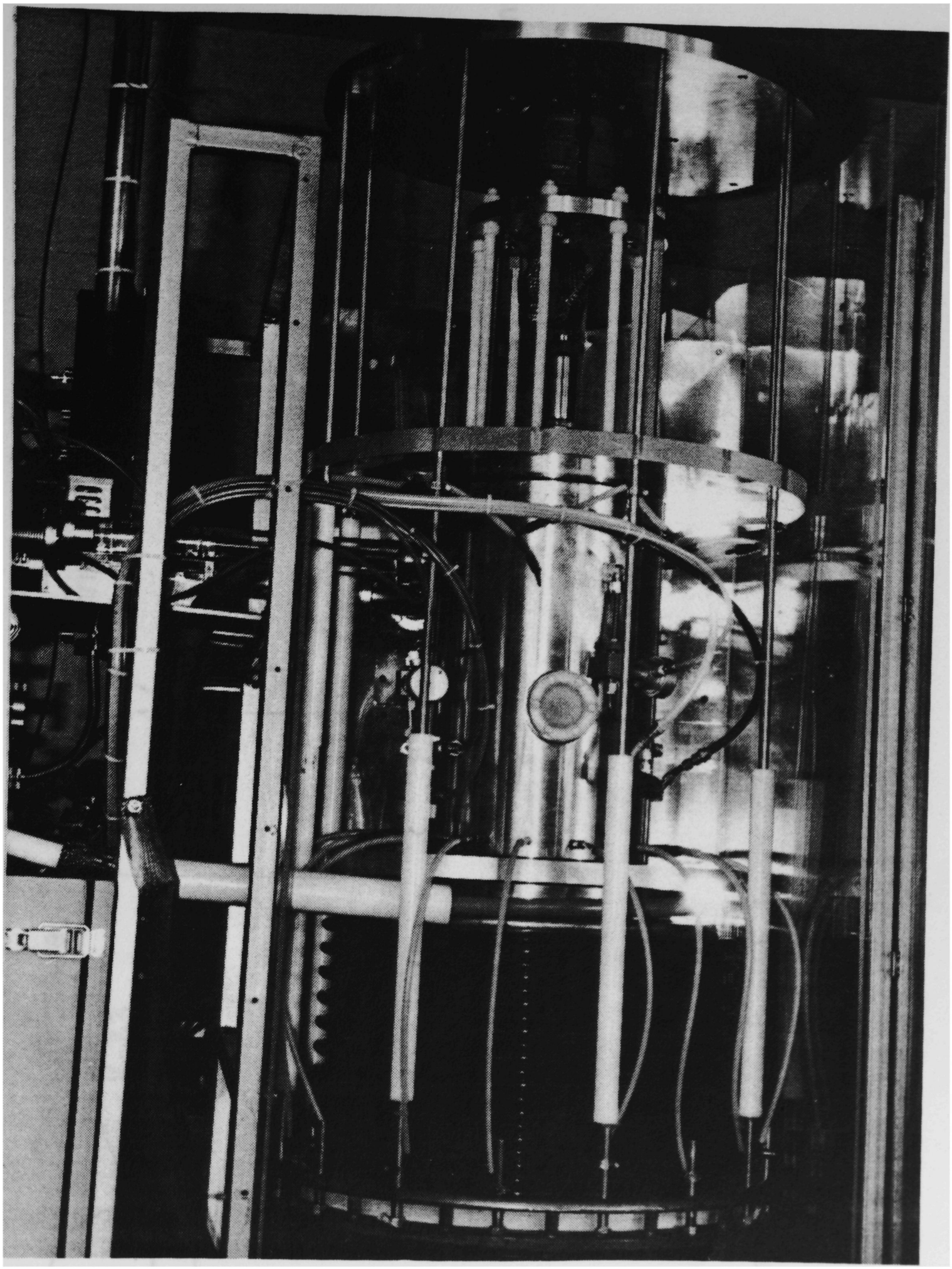

Figure 5. Photograph of Spark Gap and Load Assembly.

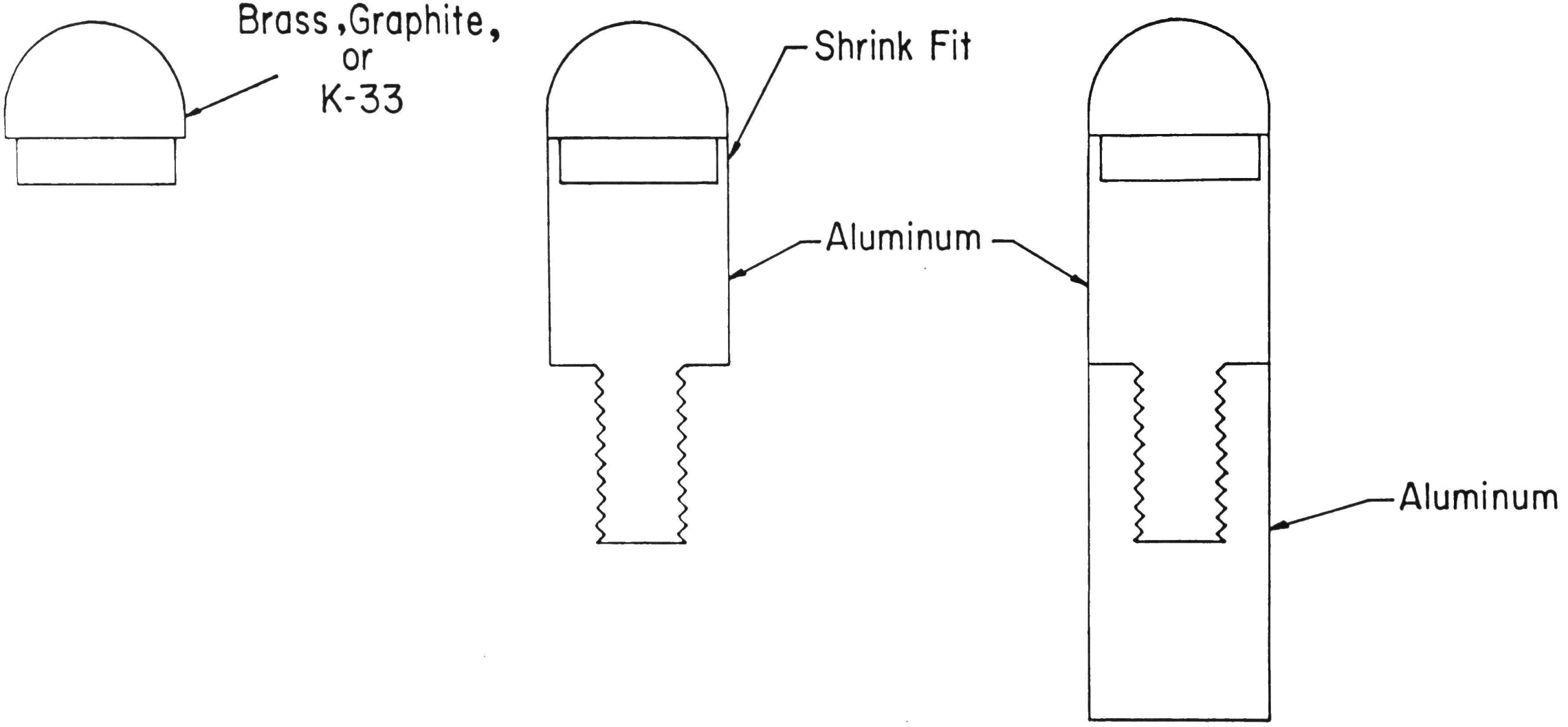

(a) Insert. (b) Insert and holder. (c) Insert, holder, and support.

Figure 6. Electrode Design.

shots), the holder support is made from one piece for SF_6 studies. The lower header plate connects the lower electrode to the capacitor and is also the lower containment surface for the chamber. The upper header plate supports the upper electrode and the discharge load, and is the upper containment surface for the chamber. A brass feed-through seals against a stainless steel rod which supports the upper electrode and allows adjustment of the gap spacing.

The aluminum cylinder surrounding the electrodes provides containment for the gas and supports the upper electrode and load. The large diameter of the cylinder (20 cm ID) allows the spark gap to be operated without an insulator adjacent to the discharge region. Thus, electrode-gas interactions can be studied with or without the effect of nearby insulators. Two 2.5 cm thick acrylic plates separate the containment cylinder from the header plates and the joints are sealed by O-rings. Although these dielectric plates are exposed in the spark gap chamber, they are at least 10 cm from the discharge region and appear to have neglible influence on the spark gap chemistry for the samples taken in this study. The cylinder has ports for connection to the vacuum and gas systems and windows for spark channel observation and diagnosis. The cylinder is also used as part of the current return path from the load to ground to reduce the inductance of the discharge circuit.

In order to support the vacuum and diagnostic connections to the gap, and to support a shielding cage, the energy storage capacitor and spark gap assembly are surrounded by a steel framework.

Brass sheets on the framework provide electromagnetic shielding between the gap and the diagnostic instruments.

High Voltage Network

The high voltage network consists of the energy storage capacitor, the power supply, the charging network, and the load. The circuit is shown in Fig. 7. The energy storage capacitor is rated at 120 kV, 0.8 μF with 60 nH inductance. It is charged to 40-50 kV with a 75 kV, 250 mA power supply through a 1 MΩ, oil-cooled resistor network. At a 40 kV breakdown voltage, the power supply is capable of a rep-rate of about two pulses per second. When the gap breaks down the capacitor discharges through a 1 Ω resistive load mounted on top of the spark gap assembly (see Fig. 4). The load consists of a series stack of four, 0.25 Ω, carbon-ceramic resistors. Brass rods serve as a coaxial return from the resistive load to the cylinder, and from the cylinder to the capacitor ground and hold the complete header plate, cylinder and load assembly rigidly on top of the energy storage capacitor. A computer analysis of the discharge circuit was done and the predicted output waveform and the actual current waveform are shown in Fig. 8. The actual current waveform shows a higher circuit impedance (a lower peak current and faster decay) than predicted by the model used. This was probably due to the fact that the simple model did not account for the discharge impedance, the distributed resistances, conductor skin effects, or the nonlinearities in the circuit.

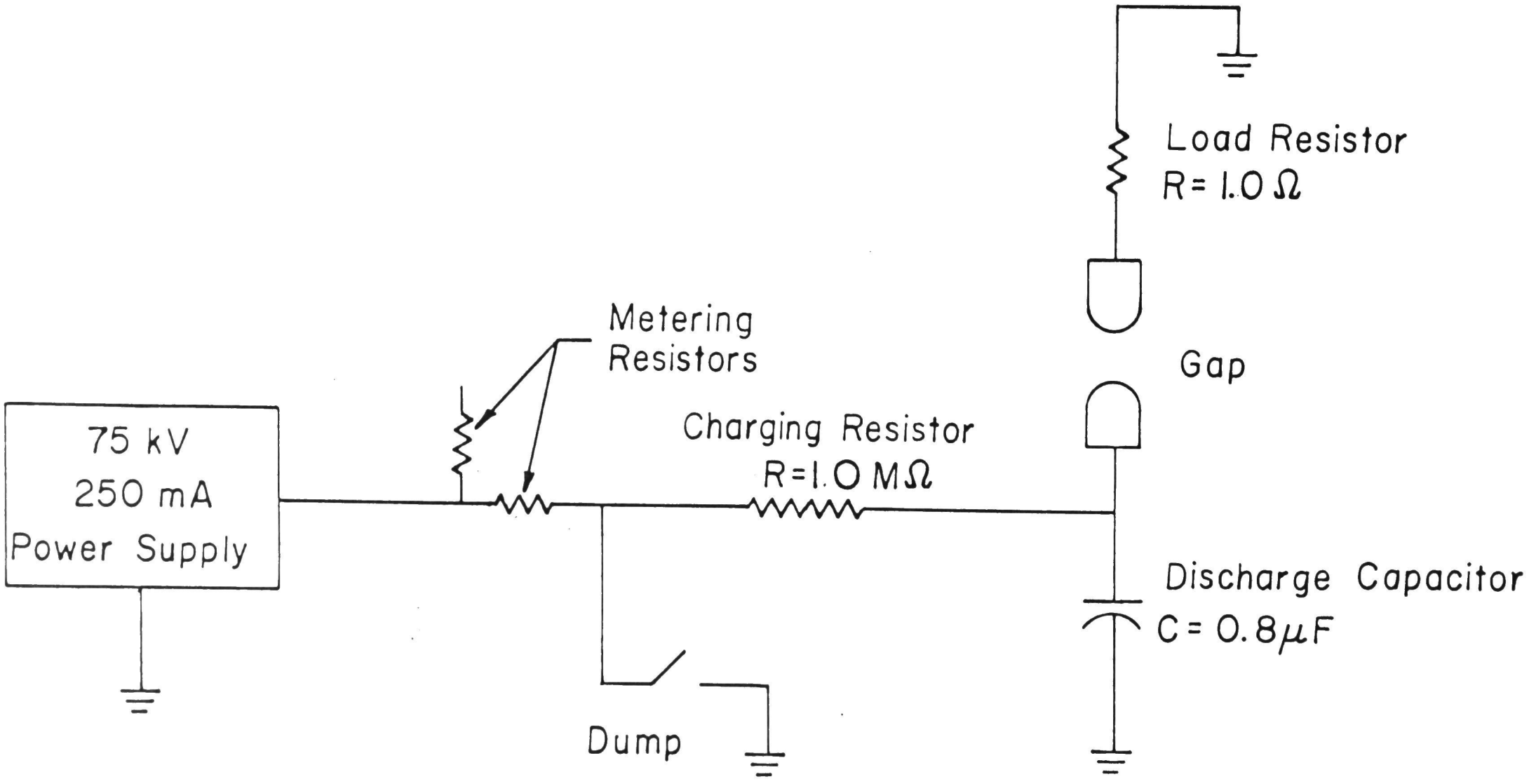

Figure 7. High Voltage Network.

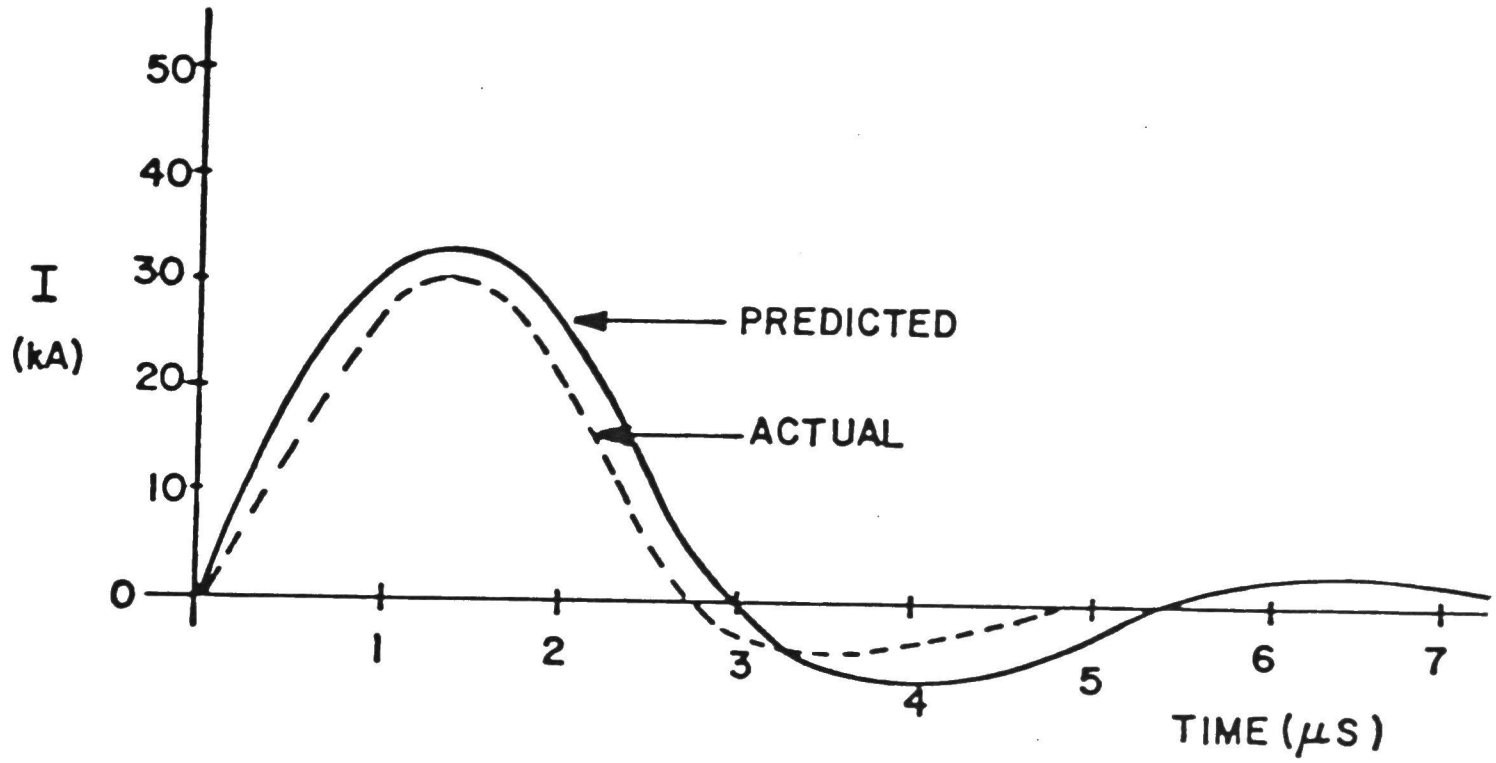

$V_{breakdown}$ = 45 kV

Figure 8. Predicted and Actual Current Waveforms.

Vacuum and Gas System

The vacuum pumping system has two purposes: to evacuate the spark gap chamber for removal of used gases and to supply the vacuum necessary to operate the quadrupole mass analyzer. A pressure conversion system is necessary to sample the gas in the gap whenever the pressure is above 1×10^{-4} Torr. For gap pressures above 1 Torr, a two-stage pressure reduction system is necessary to interface the gap to the quadrupole mass analyzer, which operates in the 10^{-5} Torr range.

The vacuum system is shown schematically in Fig. 9. The high-vacuum pump is a 260 ℓ/s turbomolecular pump, which can achieve an ultimate vacuum of 5×10^{-8} Torr. The large number of O-rings and the upper electrode feedthrough prevent the pump from achieving much better than 1×10^{-5} Torr in the spark gap chamber. A turbomolecular pump was chosen because it is very clean (necessary for the mass analysis), does not become contaminated by the various gases used in the studies, and can operate over a wide range of gap pressures. The chamber cylinder is isolated from the vacuum system with Pyrex sections. Four thermocouple and two ionization gauges measure the vacuum at various points in the system.

The pressure converter shown in Fig. 9 is used to sample the gas in the chamber and reduce it through two stages of pressure conversion to a pressure suitable for the mass analyzer. The first stage consists of a mechanical roughing pump, pumping the gas sample through a long, stainless steel capillary tube to achieve a pressure reduction

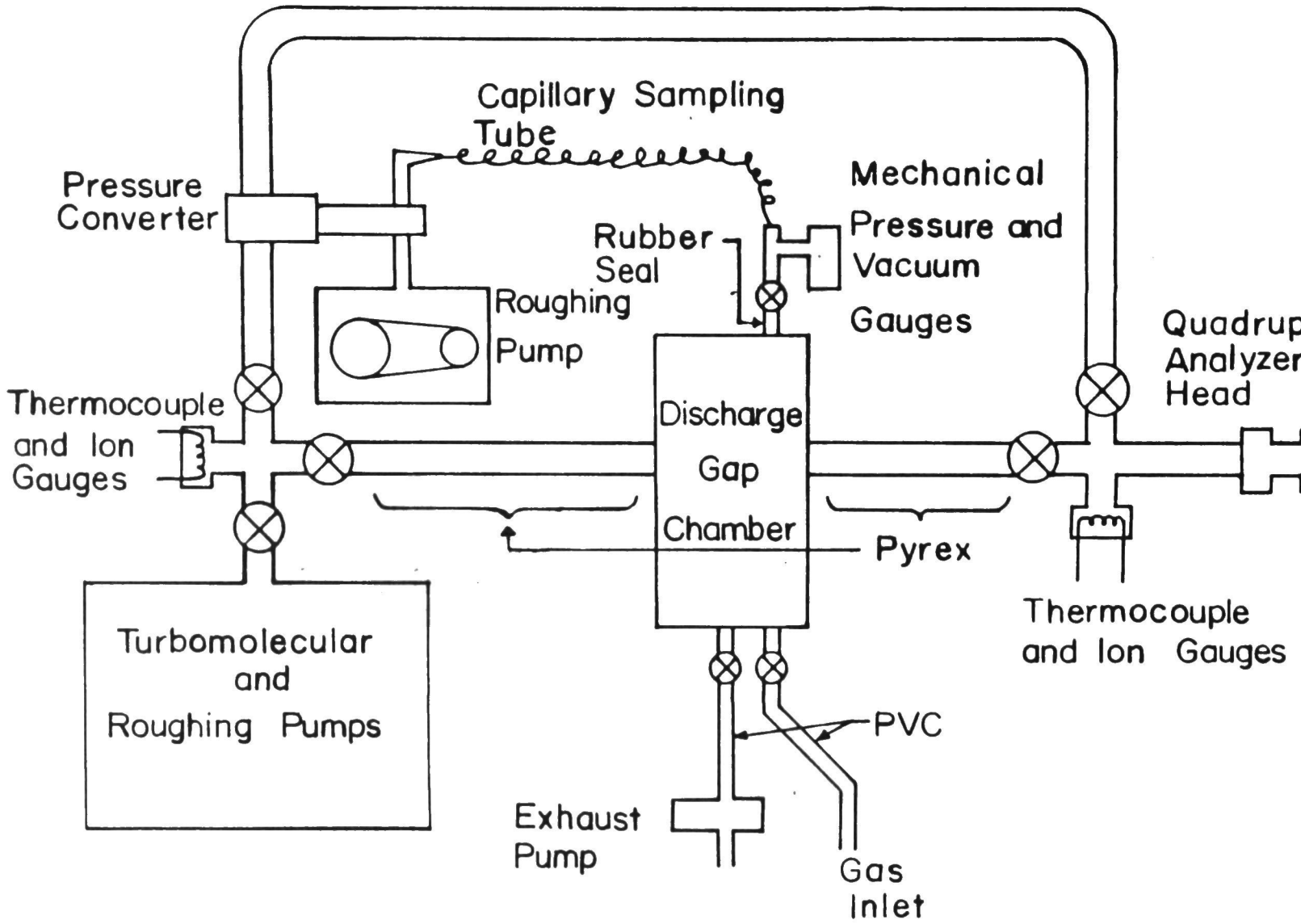

Figure 9. Vacuum System.

down to about 1 Torr. The second stage uses the turbomolecular pump, pumping through a small orifice, to drop the pressure to 1×10^{-5} Torr. The pressure converter and quadrupole detector are continually heated to reduce gas sample condensation.

In addition to the vacuum system, a gas metering and mixing system is necessary to supply the different gases for the spark gap studies. Figure 10 is a block diagram of the gas system. The evacuation pump is an air-driven, venturi type and is exhausted to outside the building, since many of the discharge products in the gap are toxic.

Control System

The control system is necessary to observe and control the experimental system manually in the single-shot mode, and to monitor and control the system automatically in the rep-rate mode. The vacuum system must be continually monitored to assure that a vacuum is maintained at all times on the mass analyzer sensing head. The sensing head becomes contaminated if exposed to pressures exceeding 1×10^{-3} Torr for more than a few minutes, and loses its sensitivity. Also, the routing of the vacuum pumping must be changed when switching between the various vacuum and pressurized modes of the spark gap chamber. Most of the valves in the vacuum system are pneumatically controlled, and the thermocouple and ion gauges have relay control set-points for indicating various threshold pressures. The turbomolecular pump, the three oil pumps (turbo forepump, pressure converter forepump, and cylinder evacuation pump), and the

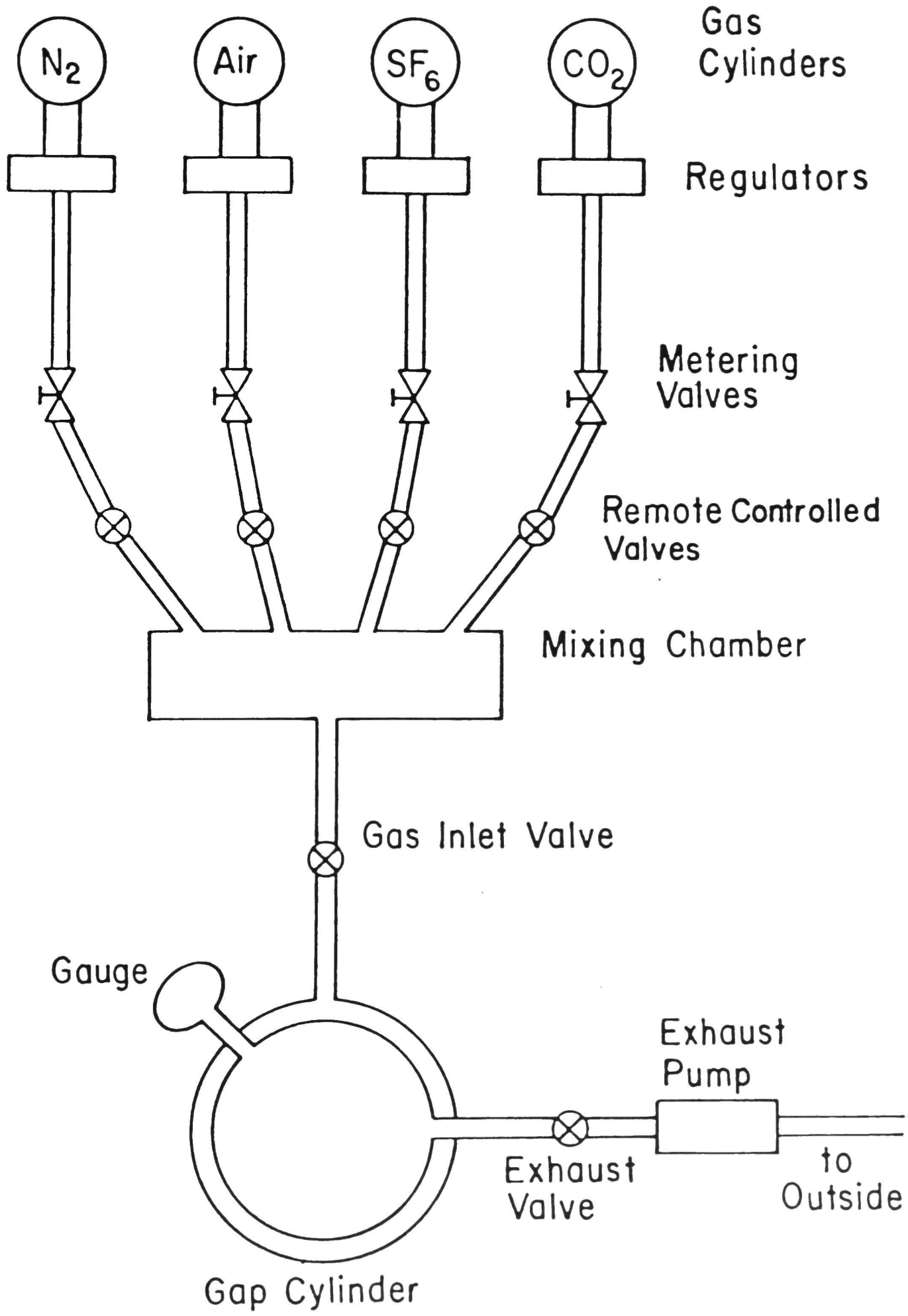

Figure 10. Gas System.

cylinder venturi exhaust pump can also be controlled automatically.

For rep-rate studies, the gas system is controlled automatically. The pressure and flow rate are monitored and the inlet and exhaust valves at the cylinder are pneumatically controlled. For exhausting gases in the cylinder, an air-driven venturi pump is first used, followed by evacuation with an oil-filled forepump. The venturi exhaust pump prevents contamination of the oil-filled pump and allows safe and easy exhaust of the spark gap gases.

The power supply control system monitors the charging voltage and current, and interfaces with several safety interlocks and other components of the control system. It is designed to terminate charging under several conditions: overvoltage, overcurrent, vacuum system failure, mass analyzer malfunction, etc. The control system recharges the spark gap capacitor automatically after each shot, and records the total number of shots for rep-rate studies.

Some monitoring and control of the major diagnostics (such as the mass analyzer and the spectrometer) are used both for instrument protection and for automatic data recording during rep-rated operation.

CHAPTER IV

DIAGNOSTIC AND ANALYSIS TECHNIQUES

The methods of obtaining information for the study of spark gap processes can be divided into two general categories: active on-line diagnostics and post analysis techniques. The active on-line diagnostics are used to study the gas composition and evolution and to study the arc channel characteristics. They include a mass spectrometer for gas analysis, optical spectroscopy, voltage and current measurements, and image converter and open shutter photography. The post analysis techniques are used to study the electrode and insulator surfaces and the chemical deposits removed after operation of the gap. They include Electron Spectroscopy for Chemical Analysis (ESCA), Auger Electron Spectroscopy (AES), Scanning Electron Microscopy (SEM), X-Ray Fluorescence (XRF), Electron MicroProbe Analysis (EMPA), mass spectroscopy, and some more conventional analytical methods. Table I summarizes the principal techniques and their application.

Gas Mass Spectroscopy

The composition of the spark gap gas is studied with an Inficon IQ 200 mass analyzer. A sample from the gap chamber is reduced from 1520 Torr (2 Atm) to 1×10^{-5} Torr through the pressure converter, as described earlier. The mass analyzer consists of a heated filament ion source, a quadrupole mass separator, and an electron multiplier

METHOD	PURPOSE	USEFULNESS & INTERPRETATION
Gas Mass Spectroscopy	to study composition of gas as a function of # of shots	difficult, but good as a verification diagnostic
Spectroscopy	to identify ionized species in the discharge	useful in N_2, very difficult in SF_6
Voltage & Current	to study current waveform and breakdown voltage distribution	change in voltage distribution as a function of materials
Photography	to verify qualitative characteristics of discharge	to monitor discharge, some interesting anomalies observed
SEM	to study erosion processes on electrodes and insulators	starting point for all other diagnostics, measure surface features
ESCA	to study chemical changes in surface structure	good for large spot, non-destructive analysis
AES	to study chemical changes in surface structure	good for small spot, slightly destructive
XRF	to study distributions of heavier elements on surface	good for studying metal deposition or redistribution
EMPA	to study small details at a fair depth on surface	too deep, does not detect light elements, sometimes useful
Chemical Analysis	to identify deposits	some results, often difficult

Table I. Summary of Diagnostics.

detector. The output can be recorded from the CRT screen onto film or from a hard copy unit onto paper. The IQ 200 can measure masses from 1 to 200 amu with a resolution of approximately 1 amu. The gain, dwell (number of counts per sweep), scan width, starting mass, and electron multiplier voltage are programmable to allow a range of sensitivities and selectivities. Three modes of operation are possible. The analog mode displays the actual peak shapes in the mass spectrum and is good for resolving fine details on a small scale. Figure 11 is an example of the analog mode. Figure 11 (a) shows the water content (17:OH and 18:H_2O) in a graphite-nitrogen-Blue Nylon combination gap and Fig. 11 (b) illustrates the increase in H_2O and OH after 10,000 shots. The bar graph mode displays the amplitude (but not the shape) of all peaks in a selected portion of the mass spectrum and is much more suited to monitoring masses over a larger scan width. The table mode, used for specific mass component monitoring, gives a numerical display of the amplitude of one to ten mass peaks. It also permits the measurement parameters (dwell, gain, and calibration) to be programmed individually for each peak, and for the amplitude to be compared to a limit set point. Figure 12 is an example table output for SF_6, showing some of the ion fragments produced in the mass spectrometer detector after 50,000 shots in a graphite-SF_6-no insulator system. Typically, increases in SF_4, SF_2, H_2O, SO, SO_2, and CF were observed in the mass spectrum. Some of these, such as SO and CF, are a result of the fragmentation patterns of larger molecules, such as SO_2 or CF_4.

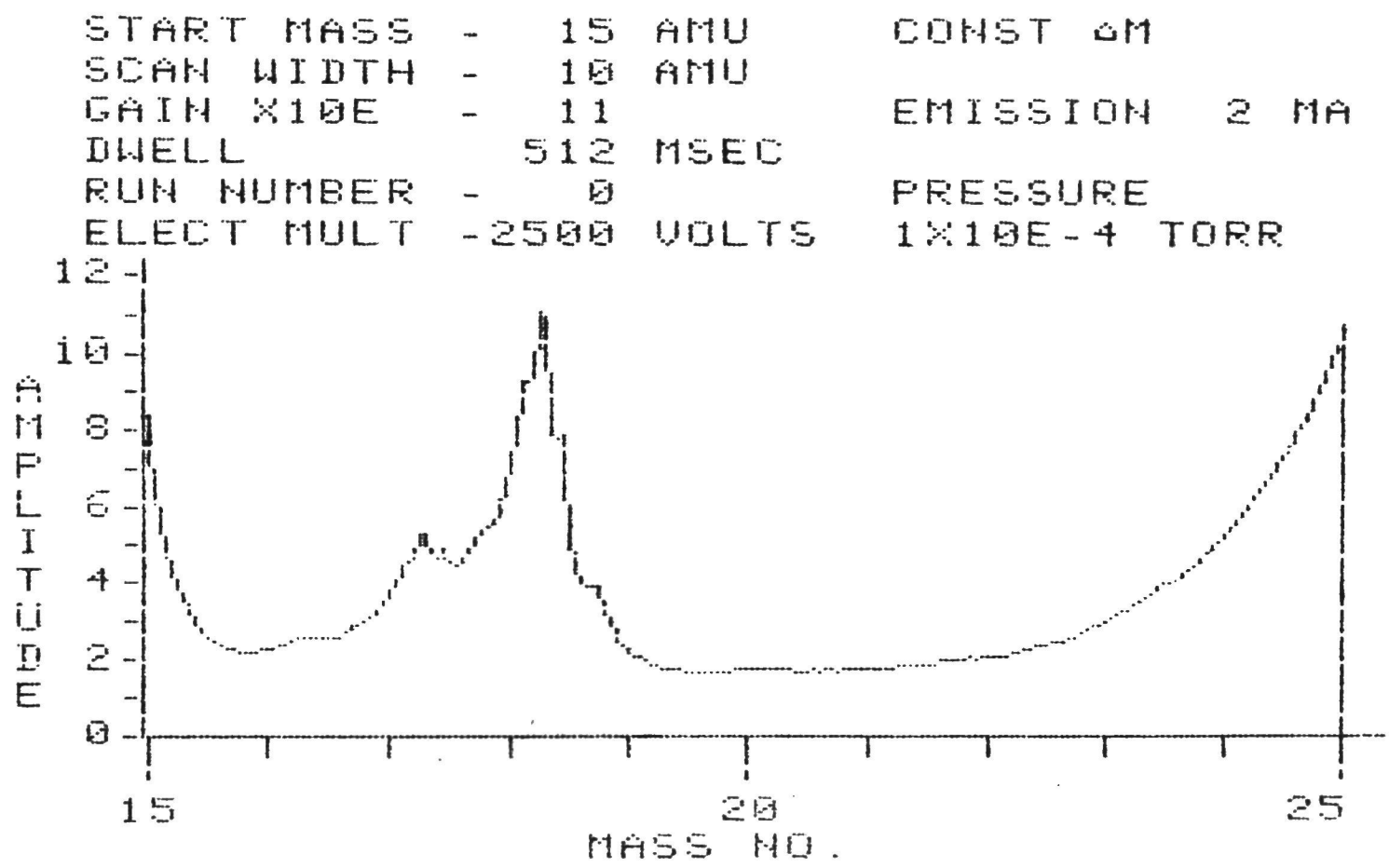

(a) Spectrum before firing.

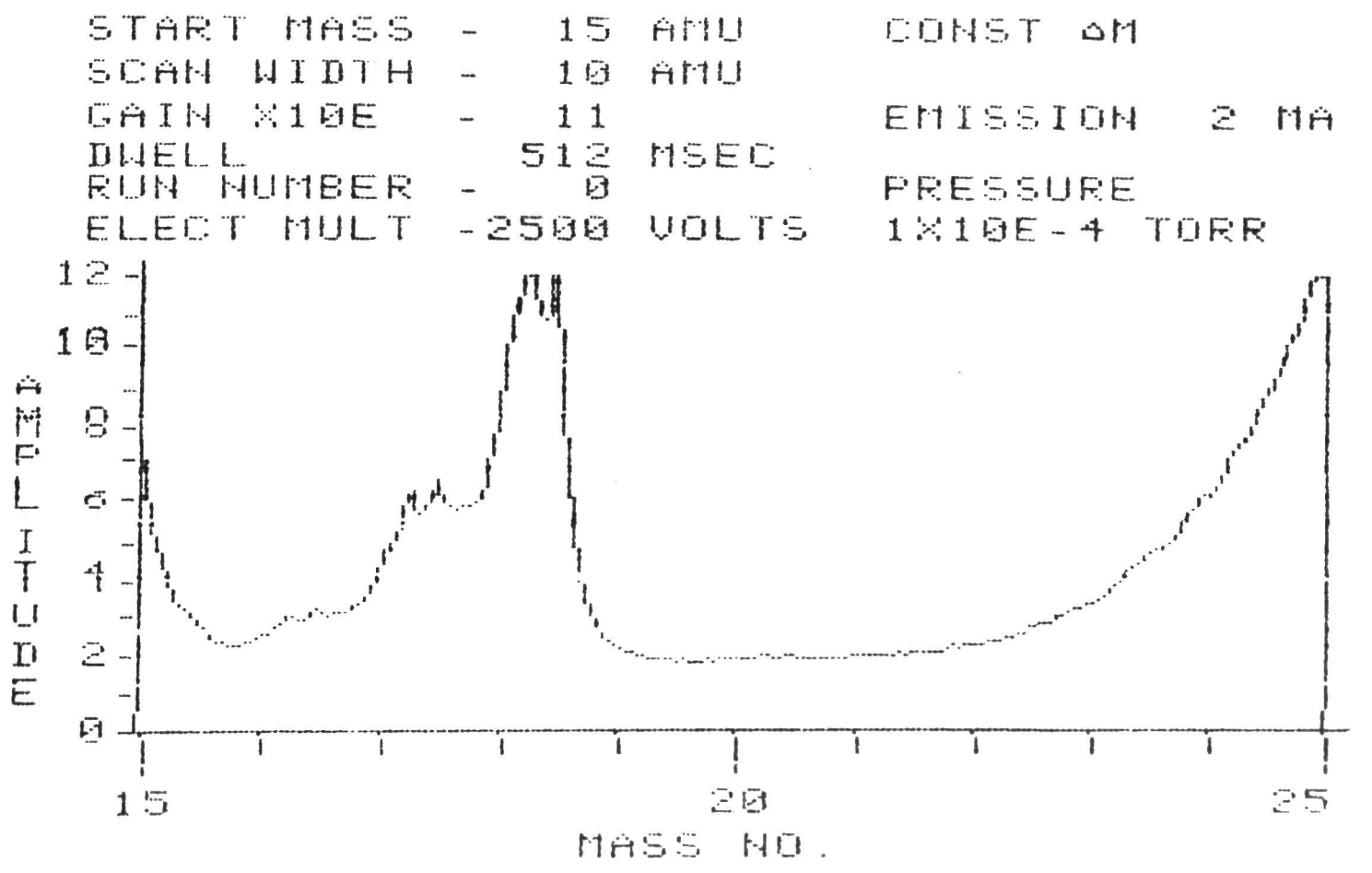

(b) Spectrum after 10,000 shots.

Figure 11. Mass Spectrometer Output - Analog Mode.

INFICON IQ 200
MASS ANALYZER

CONST TRANS

RUN NUMBER - 0 EMISSION 2 MA

ELECT MULT -2100 VOLTS PRESSURE
1X10E-4 TORR

	CHAN	MASS	VALUE	CALIB	GAIN	DWELL	LIMIT
SF_5^+	1	127	18.8	1.0	9	2048	90.0
SF_4^+	2	108	16.4	1.0	10	2048	90.0
SF_3^+	3	89	24.6	1.0	10	2048	90.0
SF_2^+	4	70	18.4	1.0	11	2048	90.0
SF^+	5	51	5.2	1.0	11	2048	90.0
CF^+	6	31	1.7	1.0	11	2048	90.0
H_2O^+	7	18	1.7	1.0	11	2048	90.0
SO^+	8	48	1.6	1.0	11	2048	90.0
SO_2^+	9	64	4.0	1.0	11	2048	90.0
SF_4^+	10	54	4.6	1.0	11	2048	90.0

Figure 12. Mass Spectrometer Output - Table Mode.

The mass analyzer is used to measure accurately the composition of the gas before the discharges, by making detailed scans in the analog mode. After several thousand shots, the scans are repeated to detect minute changes in the components of the gas. The delay time for a sample to go from the high pressure spark gap, through the pressure converter and the quadrupole filter to the electron multiplier detector is about two seconds. Thus, highly reactive ionized species, molecules of low volatility, or readily absorbed molecules are impossible to detect. Since pure gases are used, the difference in signal level between the background gas and the gas impurities is several orders of magnitude. Minute changes in gas impurities are difficult to detect due to the sample delay time, the high background level, and the calibration drift of the instrument. Also, the mass analyzer detection and controlling circuits must be carefully shielded from the electromagnetic noise generated by the pulsed discharge. Despite these problems, several changes in gas composition have been observed with the mass analyzer.

Spectroscopy

Spectroscopy of the arc discharge is done with a Jarrel-Ash, 0.5 m Ebert monochromator, Model 82-010 and a 0.5 m Spex spectrometer with an EG&G, Princeton Applied Research (Model 1420) Optical Multichannel Analyzer (OMA). The OMA looks at a 200 Angstrom section of the optical spectrum in a single shot, and was used to identify the ionized species present during discharges. The Jarrel-Ash

monochromator was used for relative intensity comparisons of specific lines. In a N_2 filled gap many ionized atoms were identified, including O, C, Cu, and N. In an SF_6 filled gap, the spectroscopy is difficult due to the complex spectrum of the discharge and problems caused by reactions of the fluorine generated in the gap with the quartz observation windows. Figure 13 is an example of an OMA scan showing two Cu I lines in a K-33 - nitrogen gap. Due to the relatively low boiling point of copper, the Cu I lines were very strong in all K-33 combinations.

Voltage and Current Measurements

Measurements of the discharge current are made with an integrated Rogowski coil placed around the upper electrode support rod. Thus, the total current passing through the spark gap is measured. The breakdown voltage is measured with a resistive voltage divider at the anode, and is recorded on a Hewlett Packard Model 7004B X-Y recorder. Using a slow horizontal sweep rate on the recorder up to 300 breakdown voltage values per page are recorded. The voltages are measured by hand, normalized by counting the percentage of shots occurring at a specific voltage for a given sample, and plotted vs breakdown voltage. Distributions of 500 shot samples are taken several times during a 50,000 shot test series. Typically, samples are taken at the start, after 2500 shots, after 5000 shots, after 10,000 shots, and after 20,000 shots. Often the distribution stabilized after 5000 or 10,000 shots and the series was terminated.

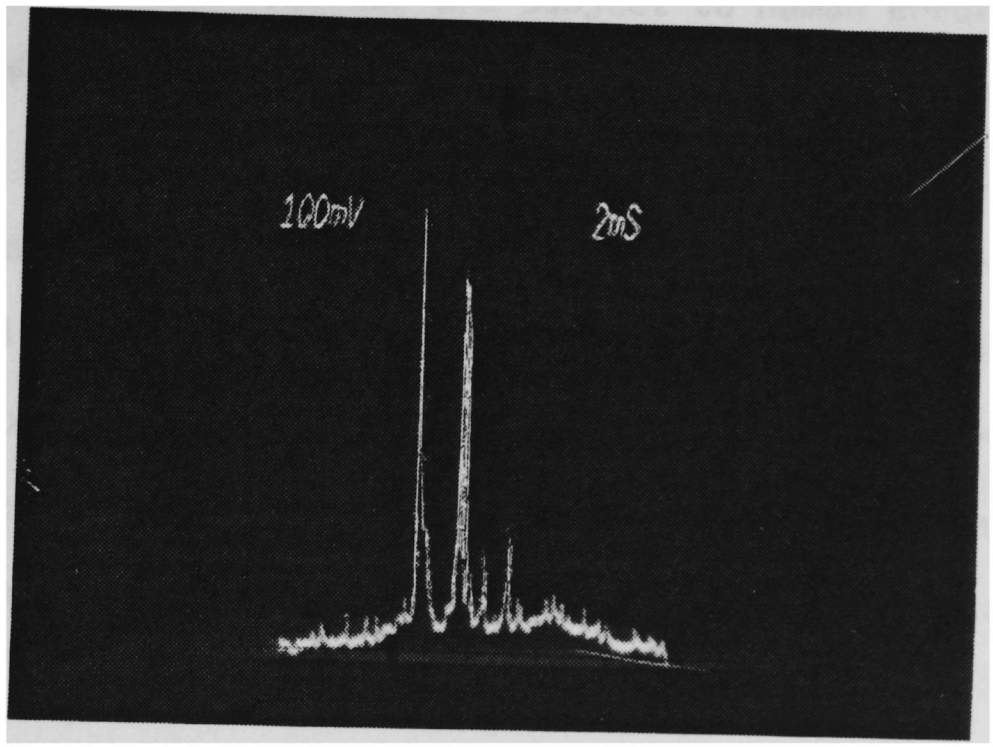

Figure 13. Example Output of OMA.

The accuracy of the voltage distribution measurements relies on close control of gas pressure, gap spacing, electrode alignment, charge voltage, and misfires (to the cylinder wall). Due to the long period of time involved in performing 50,000 shots at a repetition rate of 1 pps, it was difficult to maintain accurate control over many of these parameters. In addition, the manually measured voltage values from the X-Y recorder are subject to human error. Lack of control of the external mechanical parameters, measurement error, and averaging over a small sample (500 shots out of 2500) contribute to low reproducibility of the distributions. Since the errors in quantitative results are large, the breakdown voltage distributions are used primarily for qualitative evaluation of the different material combinations. Since these data were accumulated, several changes have been made to the voltage distribution measurement methods, increasing the usefulness of this technique.

Photography

The arc discharge is viewed through a quartz window and is recorded with an open-shutter camera or a TRW Model 1D image converter streak camera. Observation of the arc discharge is used to verify proper gap operation, and to identify malfunctions caused by electrode holder failure or insulator tracking. The diagnostic windows are also used to observe gap faults, prefires, and arc channel wander. Figure 14 illustrates some discharge channel photographs. The double discharge in SF_6 occurred in about 1 out of 30

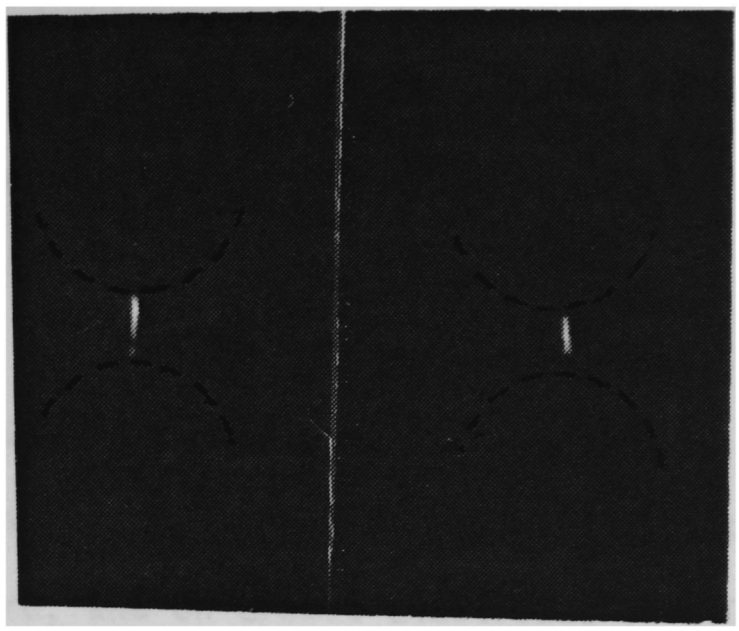

Anode

x 0.4

Cathode

(a) N_2 filler gas.

Anode

x 0.4

Cathode

single discharge double discharge

(b) SF_6 filler gas.

Figure 14. Arc Channel Photographs.

shots. In Fig. 14b the reflection above and to the right of the discharge is caused by the windows.

Electrode Sample Preparation

Surface studies were conducted on electrodes subjected to a single shot to study the effect of one discharge on the electrode surface structure, and on eroded electrodes (50,000 shots) to study long term damage. At a breakdown voltage of 40 kV, each shot transfers a total of 650 J of energy and conducts 0.03 C of charge.

For single shot studies, the electrode is first polished to expose the internal matrix of the material (i.e., to get rid of machining artifacts). The polishing techniques are described later for each electrode material. The polished electrode is subjected to one shot and the single discharge site, including some of the virgin material, is cut from the electrode surface and analyzed with SEM, AES, or EMPA. From a single shot site (typically 4 mm in diameter) three regions are usually observed: the central high-temperature or melting zone (1-2 mm in diameter), a surrounding ring exposed to the discharge, and the region outside the discharge site (virgin material).

Eroded samples are produced by exposing electrodes to 50,000 shots, resulting in a total charge transfer of about 1.5×10^3 C. Since 2 to 3 mm depth of electrode material is lost in the central region, initial electrode surface conditions are not critical and

these electrodes are not polished. As shown in Fig. 15, samples are taken from the anode surface in two regions. The inner discharge region is the site of all of the individual discharges and has undergone erosion. The outer region is the electrode surface immediately outside the discharge region and contains chemical deposits formed by the discharge. Figure 16 shows these regions for a K-33 electrode.

All electrode samples are cut, stored and shipped while exposed to air. Thus, surface contaminants (mainly CO, CO_2, O_2, H_2O, metal oxides, and hydrocarbons) accumulate prior to surface analysis. Since ESCA and AES are both very shallow (30 to 80 Angstrom) surface analysis techniques, light etching with a neutral argon beam is necessary to remove hydrocarbons, oxides, and adsorbed gases from the surface before the analysis.

ESCA and AES

Electron Spectroscopy for Chemical Analysis (ESCA) is a surface analysis technique which is used to identify atomic species and give information on chemical bonding in the first 50 to 80 Angstrom depth of the electrode surface.[59,60] A monochromatic x-ray beam is incident upon a few square mm of the surface, causing no appreciable damage to the surface, and stimulating the emission of photoelectrons. The energy spectrum of the emitted photoelectrons is used to identify atomic species, since the energy of an emitted photoelectron is related to the binding energy of the ionized element and the incident x-ray photon energy. ESCA can identify all elements except H and He,

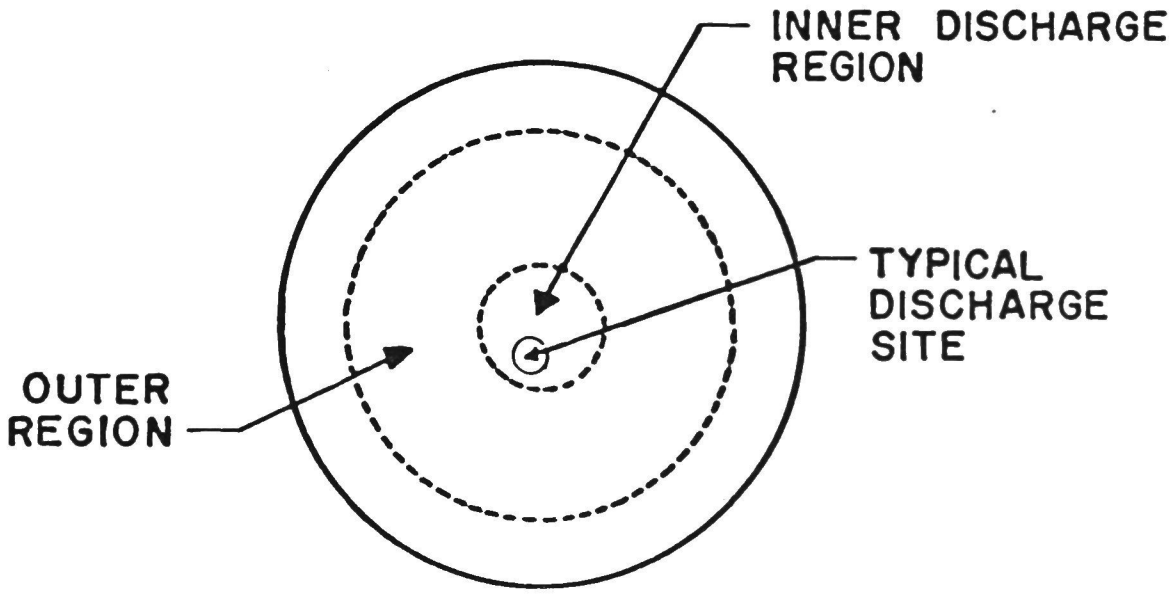

Figure 15. Electrode Sample Regions.

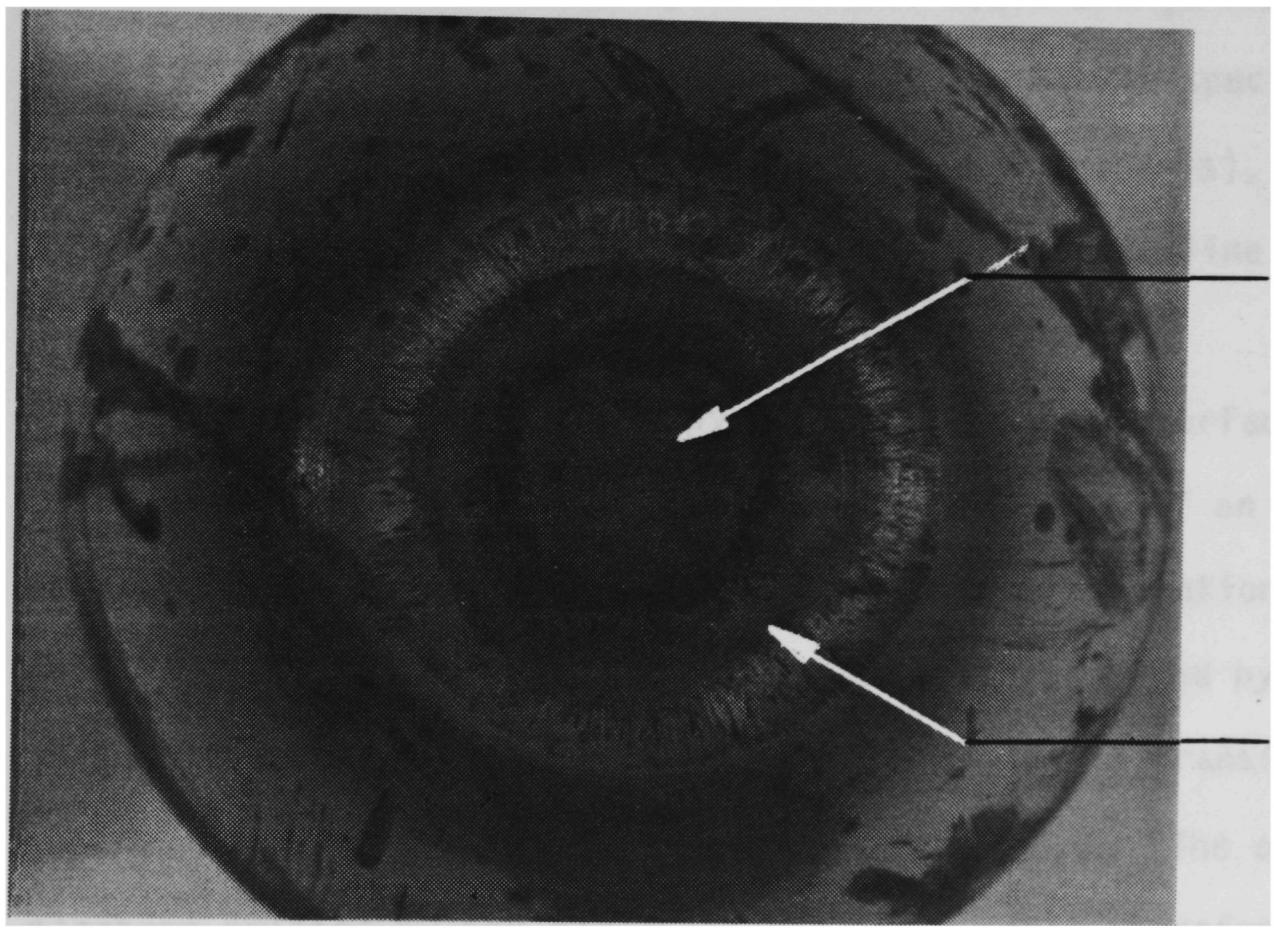

Figure 16. Photograph of K-33 Electrode Surface after 50,000 shots.

and by carefully observing energy shifts of an emission line some chemical bond information can be obtained. The quantitative accuracy of ESCA is limited to about 20% of the concentration indicated by the observed peak. Figure 17 illustrates a typical ESCA energy spectrum for the discharge region of a K-33 electrode in SF_6. The discontinuity at 560 eV is caused by a vertical scale change from 10 kcpi to 3 kcpi (kcpi = kilo counts per inch). The atomic species are identified from the energy of the peak (horizontal axis), and the relative concentration of elements is found from the line intensity (vertical axis) using sensitivity scaling factors.

Auger Electron Spectroscopy (AES) is a similar surface analysis technique used to examine the top 30 to 60 Angstrom of an electrode surface.[59,60] An incident electron beam causes ionization of the inner atomic shells. The vacancy is immediately filled by an outer shell electron. The energy from this transition is transferred to another outer shell electron, causing its emission. The outer shell electron emitted by the radiationless inner shell transfer is called an Auger electron. The energy analysis of the emitted Auger electrons identifies the atomic species. AES also detects all elements above He, but has the potential (over ESCA) of examining a smaller sample area (approximately 400 μm^2). It is not generally used for chemical bonding information, however, and is less accurate quantitatively (40% of the concentration indicated by a peak). Since the sample is being bombarded by electrons with an energy of 5 to 25 keV, some damage can occur to the sample. Figure 18 is an example of

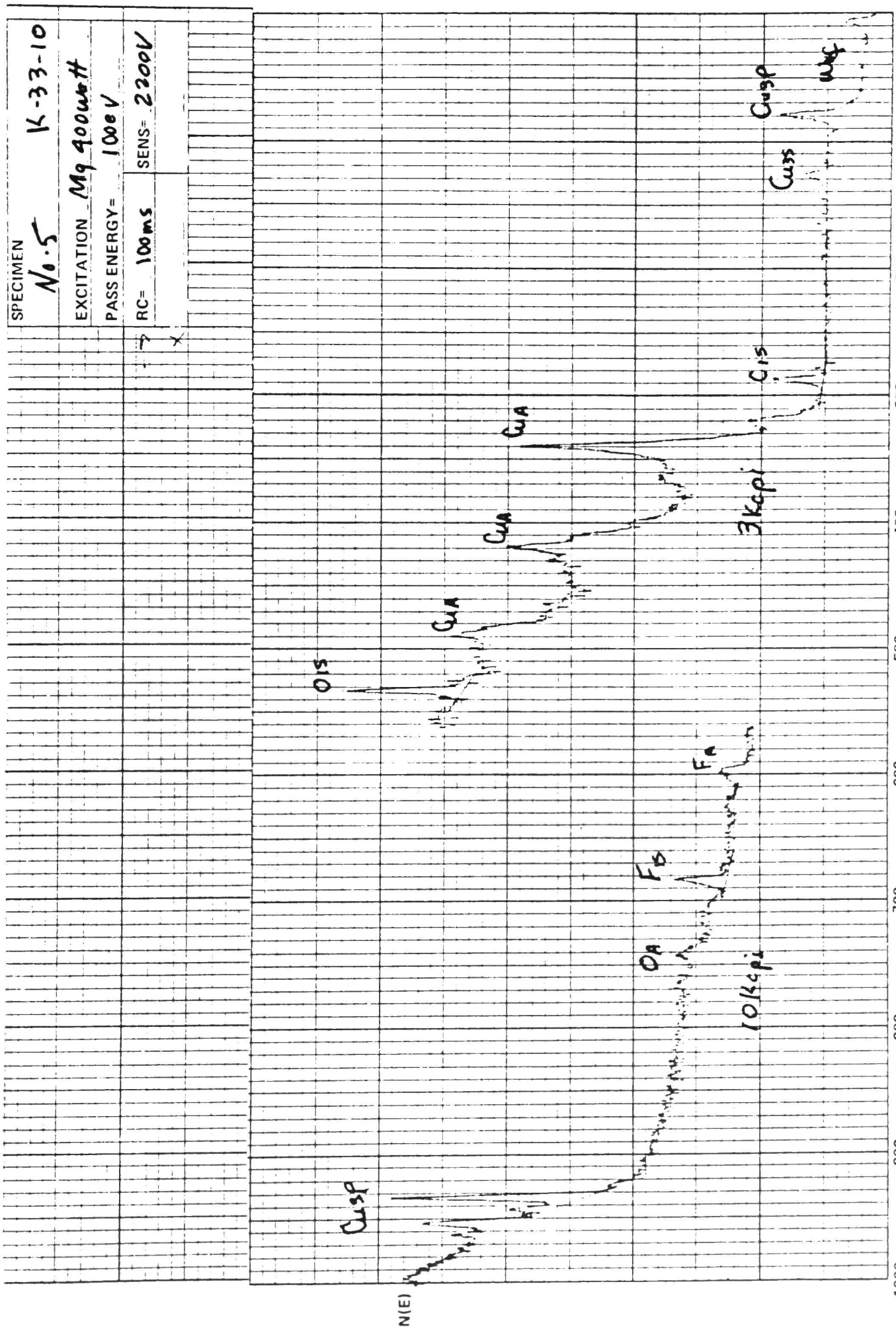

Figure 17. Example of ESCA Energy Spectrum.

some damage can occur to the sample. Figure 18 is an example of an AES energy spectrum of the inner discharge region of a K-33 electrode sample used in SF_6. The largest peak in the center of the spectrum is a Cu line. Also present are S, C, O, F, and W lines.

SEM, XRF and EMPA

Scanning Electron Microscopy (SEM) is used to study electrode surfaces under magnifications from x25 to x4500. The photographs obtained show surface deterioration, suggesting damage mechanisms and chemical processes, which are obviously different for different combinations of electrode, gas, and insulator materials. Interpretation of the photographs gives an excellent starting point for further surface analysis. The SEM photographs will be used in the next chapter as the focal point for describing the processes occurring on the electrode surfaces.

X-Ray Fluorescence (XRF) is used in conjunction with the SEM photographs to study the distribution of a specific element on a sample.[61] The x-rays emitted by an electron-beam-excited surface are analyzed at a specific frequency to give the surface distribution of the element which fluoresces at that frequency. The XRF maps (also referred to as metal maps or dot maps) help identify the composition of certain surface features observed in the SEM photographs.

an AES energy spectrum of the inner discharge region of a K-33 electrode sample used in SF_6. The largest peak in the center of the spectrum is a Cu line. Also present are S, C, O, F, and W lines.

SEM, XRF and EMPA

Scanning Electron Microscopy (SEM) is used to study electrode surfaces under magnifications from x25 to x4500. The photographs obtained show surface deterioration, suggesting damage mechanisms and chemical processes, which are obviously different for different combinations of electrode, gas, and insulator materials. Interpretation of the photographs gives an excellent starting point for further surface analysis. The SEM photographs will be used in the next chapter as the focal point for describing the processes occurring on the electrode surfaces.

X-Ray Fluorescence (XRF) is used in conjunction with the SEM photographs to study the distribution of a specific element on a sample.[61] The x-rays emitted by an electron-beam-excited surface are analyzed at a specific frequency to give the surface distribution of the element which fluoresces at that frequency. The XRF maps (also referred to as metal maps or dot maps) help identify the composition of certain surface features observed in the SEM photographs.

It is also possible to use a small stationary electron beam to study the composition of very small surface features observed in an SEM photograph (referred to as EMPA, Electron MicroProbe Analysis). Areas as small as 2 μm in diameter can be analyzed, although the technique gives information from a greater depth (1 to 2 μm) than ESCA or AES. The principle disadvantage of EMPA is that it is limited to elements of atomic mass above that of sodium (Na).

Miscellaneous Analysis Techniques

Deposits collected from the electrode surfaces and from the bottom of the spark gap chamber have been analyzed using conventional mass spectrometry, atomic absorption spectroscopy, and some conventional chemical analysis techniques. Other observations such as the color and smell of the discharge gas, the erosion of the electrode, and deposits on the insulators help to supply qualitative information concerning chemical and physical processes occurring in the gap.

CHAPTER V

RESULTS

The chemical and physical interactions were investigated for the six materials (graphite, K-33, N_2, SF_6, Lexan, and Blue Nylon). Since a separate study at TTU investigates the insulator processes,[4] this study was primarily concerned with the electrode and gas processes. Thus, each of the four combinations of electrode material and gas type is discussed in detail, and the effects of insulators in the vicinity of the discharge are only discussed briefly in a separate section. The four electrode-gas combinations are presented in order of increasing complexity: graphite-N_2, graphite-SF_6, K-33 -N_2, and K-33 -SF_6; assuming that graphite is the simpler electrode material (chemically) and N_2 is the simpler gas. Figures 19-31 and the accompanying discussion describe these four combinations. Note that no insulators were involved in these tests; the insulator discussion starts with Fig. 32. Also note that all electrode photographs and analyses are of the anode only.

Graphite Electrode

The graphite used is ACF-10Q made by Poco Graphite of Decatur, Texas.[62] It is a very dense, fine-grain graphite with a maximum particle size of less than 20 μm. The hemispherical electrodes are made on a lathe with a steel cutting bit and show a surface structure representative of fine grained fractured graphite (Fig. 19a). No

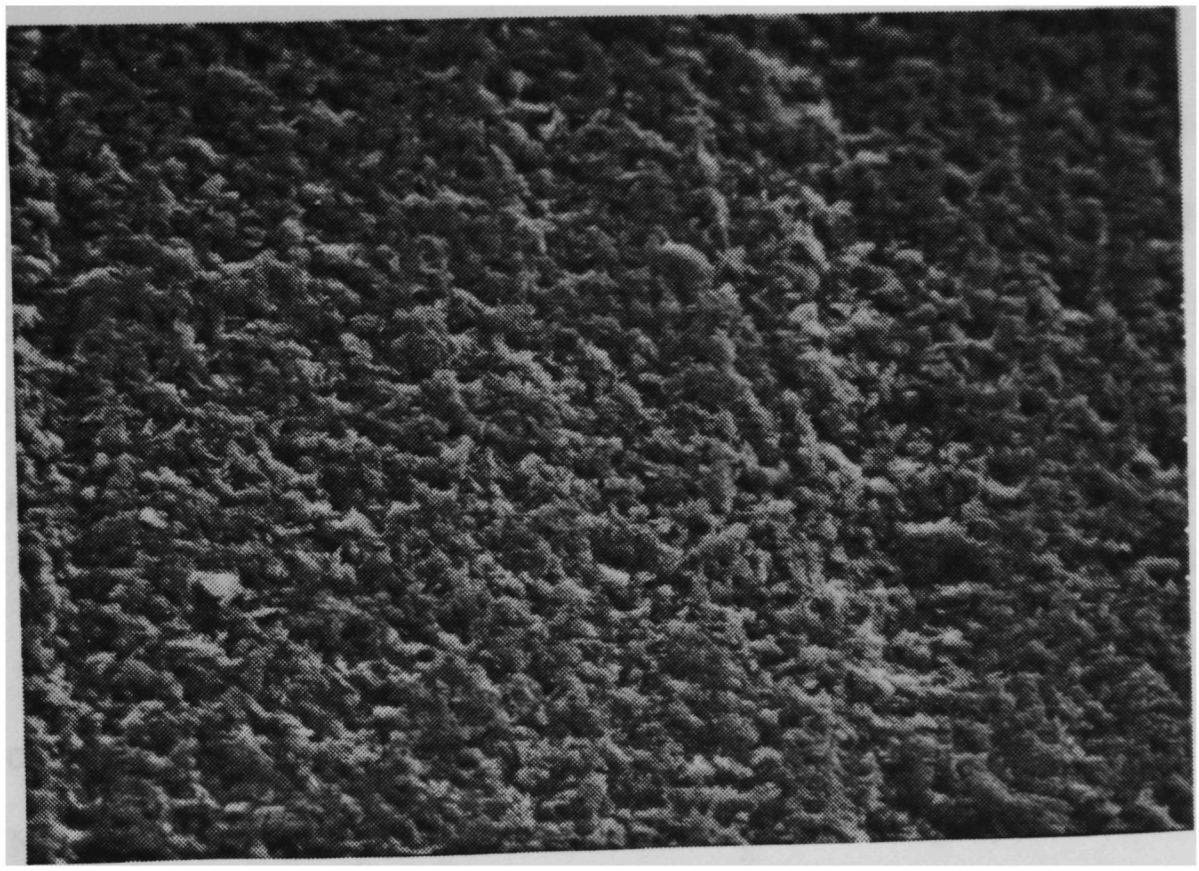

(a) Unpolished. (x 500)

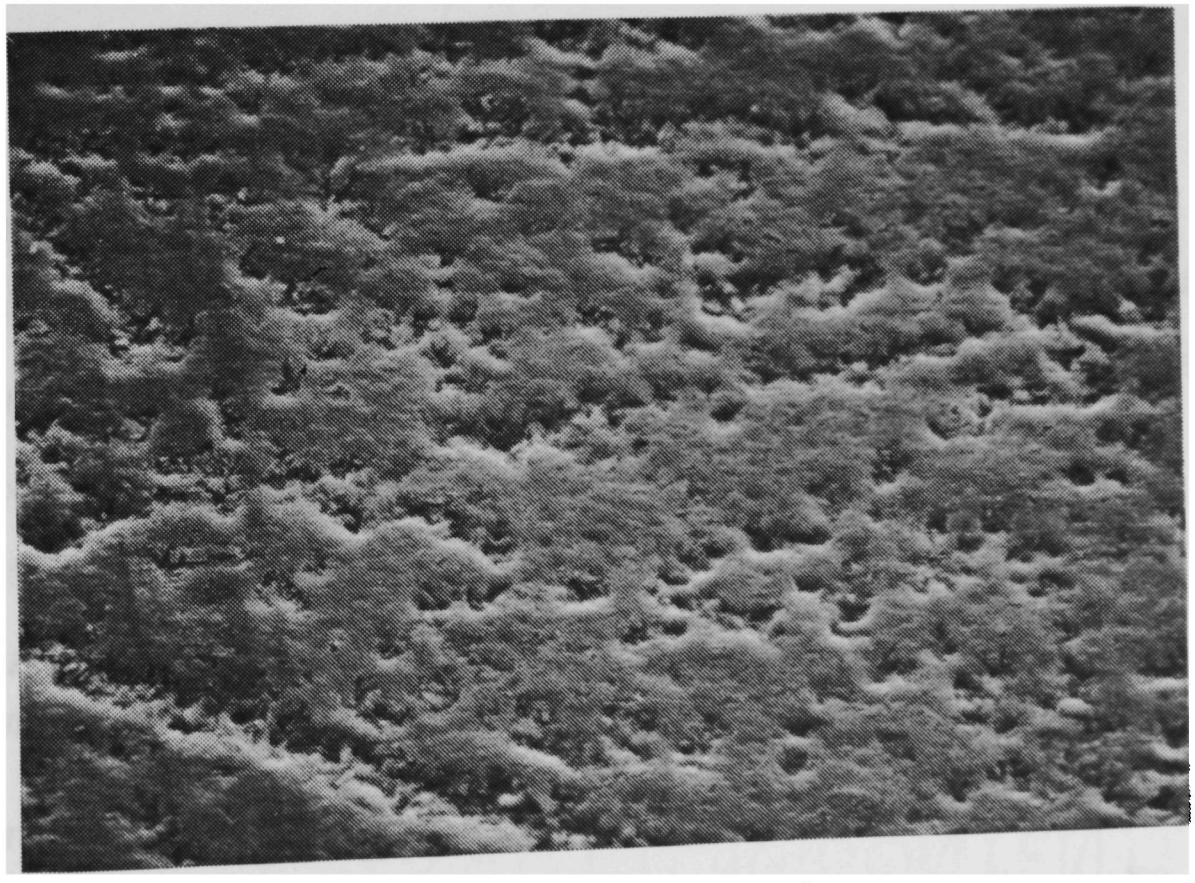

(b) Polished. (x 500)

Figure 19. Virgin Graphite.

chemical agents are used and few machining marks are visible. Some of the graphite electrodes are polished (Fig. 19b) for single shot experiments, to reduce the sharp fractured texture which is difficult to analyze with SEM and ESCA. Polishing is done using very clean steel cutting tools (files and steel wool) and abrasive oxide papers. Using ESCA, SEM, and AES, no contaminants from the polishing process are found on the graphite surface. The only cleaning technique used on the graphite is to blow loose graphite dust from the surface with clean, dry freon (in gas form). From ESCA the surface of the virgin electrode is composed of 94% carbon and 6% oxygen. The oxygen is probably adsorbed as O_2, H_2O, CO, and CO_2 on the graphite surface. Some hydrocarbons are also invariably adsorbed on the surface, but are difficult to detect on the carbon background.

Nitrogen Filler Gas

The erosion mechanism occurring in N_2 is a combination of vaporization, sublimation, and microparticle ejection. Graphite does not have a molten state at the pressures found in the gap and is mechanically stable at very high temperatures. Graphite begins to vaporize in the temperature range of 2200-2700 K and sublimes at 3640 K.[63,64] The inner region of the discharge surface is very smooth, with an extremely fine grain structure, less than 0.1 μm particle size, and was apparently eroded at the point of discharge by sublimation and vaporization at surface temperatures in excess of 2500 K. Figure 20 compares the drastic difference between the electrode

(a) Virgin. (x 5000)

(b) 50,000 shots. (x 5000)

Figure 20. Graphite Electrode Erosion in N_2.

surface before firing and after 50,000 shots. The erosion process (vaporization and sublimation) removes all traces of the original sharp, fractured, graphite edges, and leaves a smooth, ablated surface. Also, the surface shows some very small, 3 μm long, thermally induced, cracks, and a few craters, 2 to 3 μm in diameter. Some graphite particles, 1 to 10 μm in diameter, are found on the insulator surfaces exposed to the graphite electrodes (see Fig. 21).[65] Ejection of graphite particles, however, is probably not the major erosion mechanism, since analysis of a single shot on a graphite electrode surface shows no pitting or craters, only preliminary smoothing. Also, the black deposits throughout the gap appear to be monoatomic layers of amorphous carbon and not polycrystalline like the original graphite. Thus, the major erosion mechanism at the graphite electrode surface is vaporization of the carbon. The few craters were probably the result of an occasional particle ejection or occurred at impurity sites or lattice vacancies which could be subject to accelerated chemical reactions (with released gases and water vapor).

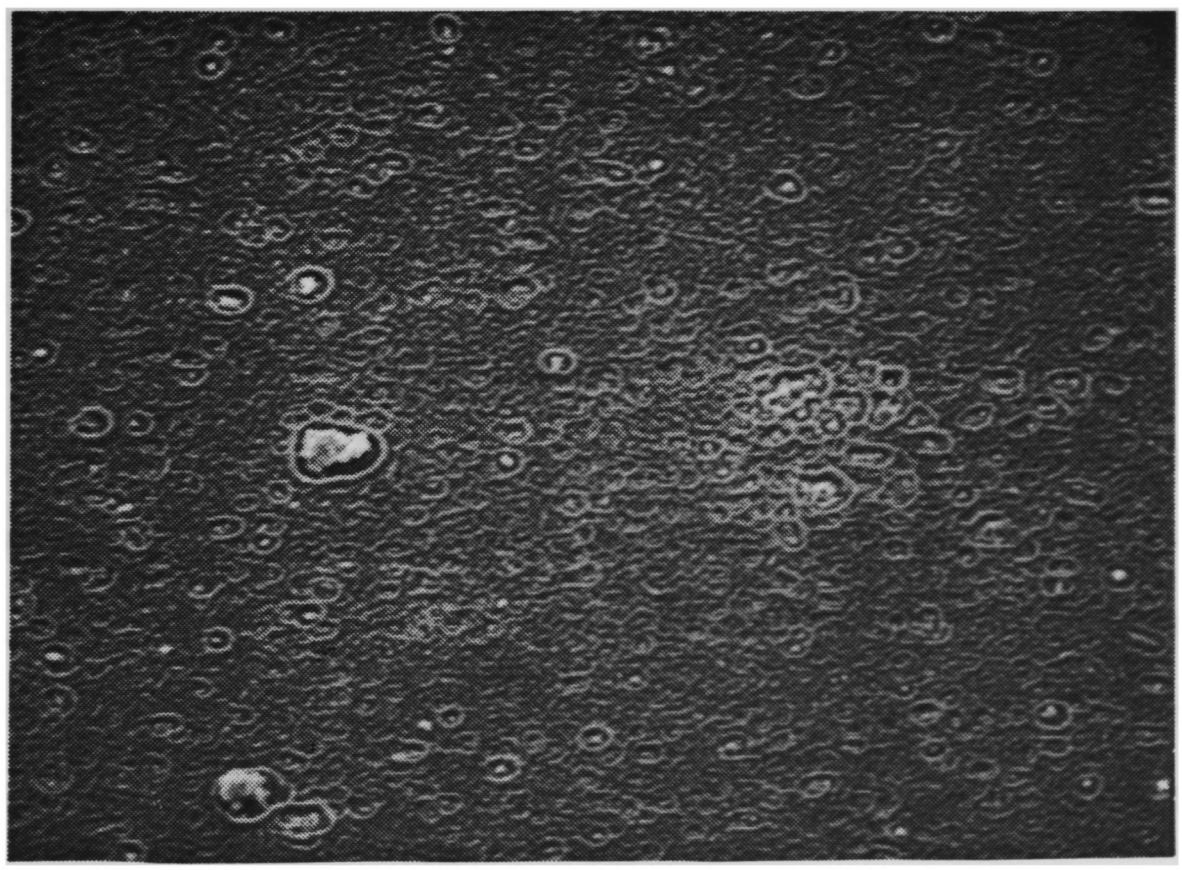

x 2000

Figure 21. Lexan Insulator in N_2, Exposed to Discharges Between Graphite Electrodes.

From the ESCA spectrum, the virgin surface (94% C, 6% O) changes to 52% C, 14% O, and 31% N in the inner region and 70% C, 11% O, and 16% N in the outer region after 50,000 shots (Fig. 22). In both cases, about 3% miscellaneous contaminants were found. Some fluorine contamination (less than 2%) was present, probably due to system contamination from previous SF_6 studies.

Two chemical processes were determined from the ESCA results and analysis of the gas content. First, the change in O on the surface (after allowing for about 6% O adsorbed from air) is due to an increase in oxides (CO and CO_2) formed on the surface. Above 700 K carbon oxidizes in the presence of any available oxygen and above 1000 K carbon reacts readily with water.[66] Primarily CO and CO_2 are formed, depending on the relative abundance of C and O. The oxygen is obtained from water released by all surfaces in the gap during firing, and to a lesser extent from absorbed O_2, which is also released. In the colder regions of the gas, the vaporized carbon may combine with oxygen molecules to account for the increase in CO and CO_2

$$\begin{aligned} O_2 + 2\,C &\rightarrow 2CO \\ O_2 + \;\; C &\rightarrow \;\; CO_2 \end{aligned} \qquad (1)$$

More of the chemical reaction probably occurs in the arc plasma, where molecules are highly dissociated. In the plasma

$$\begin{aligned} C \;+\; O &\rightarrow CO \\ CO + \;\; O &\rightarrow CO_2 \end{aligned} \qquad (2)$$

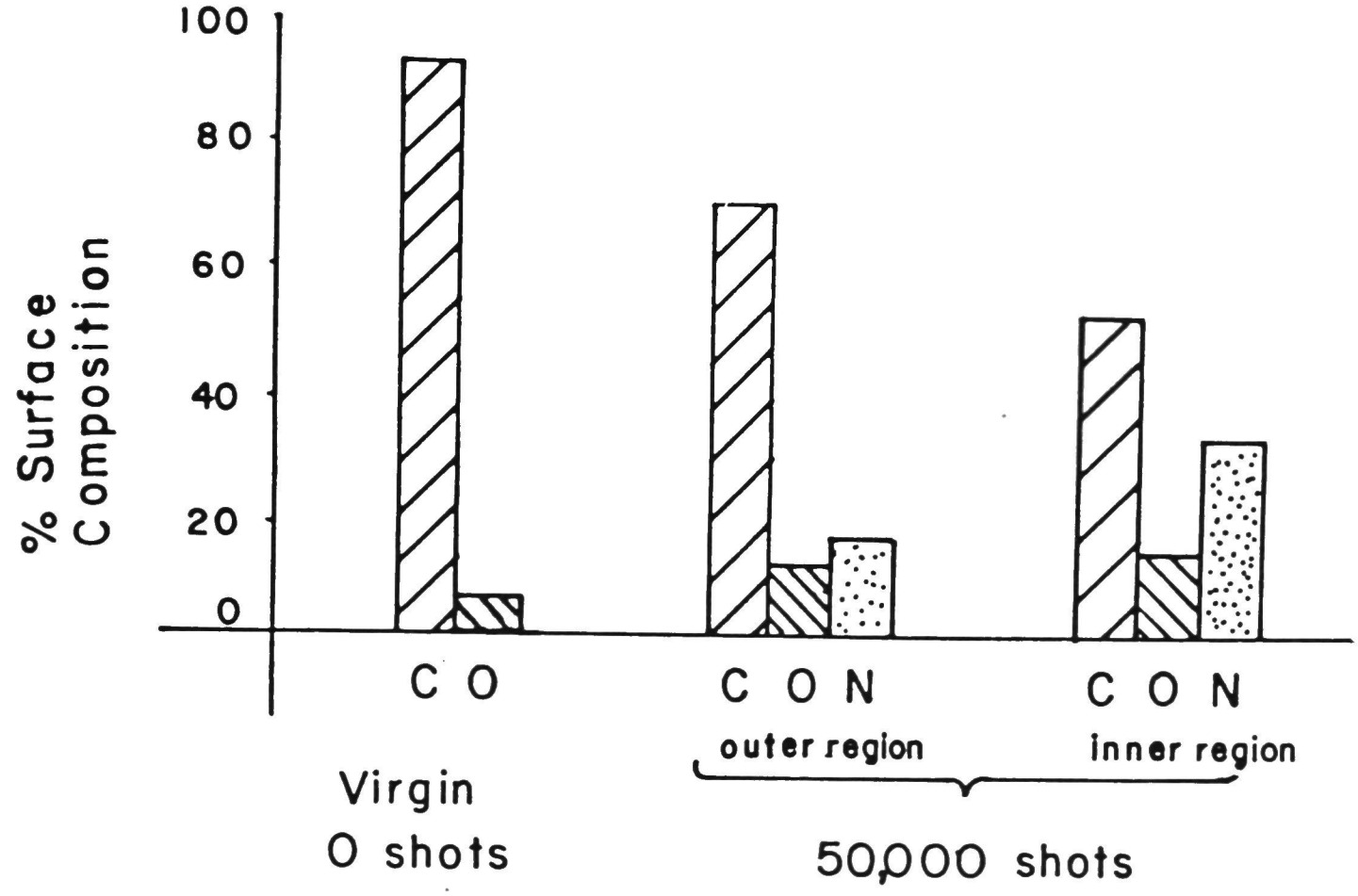

(a) Graphite electrodes in N_2.

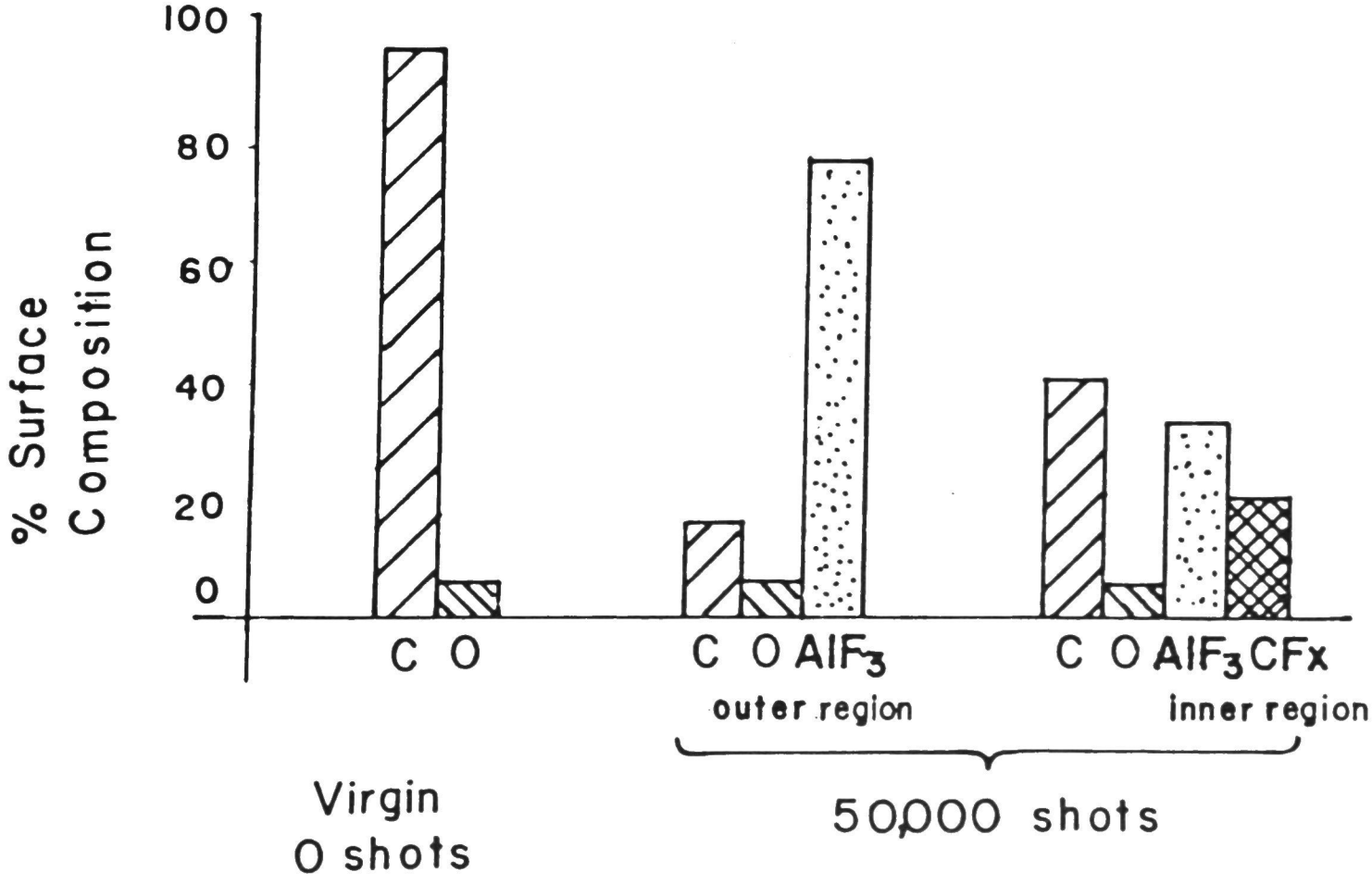

(b) Graphite electrodes in SF_6.

Figure 22. Surface Composition of Graphite Electrodes.

At the electrode surface O_2, H_2O and oxygen atoms may combine directly with the bound carbon atoms, especially at the arc site where the loss of a carbon atom leaves unfilled shells in other carbon atoms on the electrode surface.

The gap was not baked under vacuum to remove the water prior to firing, since this would not be representative of a real spark gap situation. Also, the gas in the chamber is not flushed during operation, but remains statically pressurized at 1520 Torr. The gas mass analysis indicates an increase in CO_2 in the gas, directly proportional to observed increases in H_2O (2 to 3 times higher when insulators are present). It was not possible to detect CO (amu 28) with the mass spectrometer, because of the presence of N_2 (also amu 28). Optical spectroscopy showed an increase in the OI line intensity after several thousand shots, indicating that the available O was indeed increasing as water was released from the surfaces.

The second significant chemical process occurring at the electrode is nitrogen attachment to the surface. In the inner region, N accounts for 31% of the surface atoms. The increases in both N and O are higher in the inner region, indicating either that the inner region (higher temperatures) is the site of more chemical activity, or that the outer region is being covered by a pure carbon layer. The increased energy spread of the ESCA carbon line on the electrode inner region (compared to the virgin sample) indicates the presence of carbon bound with another atomic species (i.e., N).

Cyanogen molecules $(CN)_2$ have been spectroscopically observed by others in graphite-air discharges.[67] The exact nature of the C-N bond on the surface, or if it has any effect on erosion, is not yet understood.

Sulfur Hexafluoride Filler Gas

Graphite in SF_6 undergoes different erosion processes than in N_2. The surface (Fig. 23a) is uniformly covered with holes (craters), 5 to 10 μm in diameter and hemispherically shaped. The uniform density and shape imply that chemical erosion is occurring at the discharge sites. Analysis of the ESCA spectrum reveals that the graphite surface contains several different carbon bonds, i.e., the broadened carbon line is composed of several components. Some of the C bonds can be identified as CF_x compounds formed on the surface and monitoring of the gas with the mass analyzer shows a peak at 88 atomic mass units (probably CF_4) within the gas. In the arc discharge region, the gas is essentially fully ionized. Thus, some free fluorine atoms are likely to combine with carbon atoms, instead of recombining back to SF_6. The CF_x compounds on the electrode surface are formed when F atoms react with the hot carbon. Some of the CF molecules are released in the gas or are formed in the discharge region. This is evident from the peak at 88 (CF_4) and a smaller peak at 69 (CF_3), an unstable fragment from CF_4 generated by the mass spectrometer.

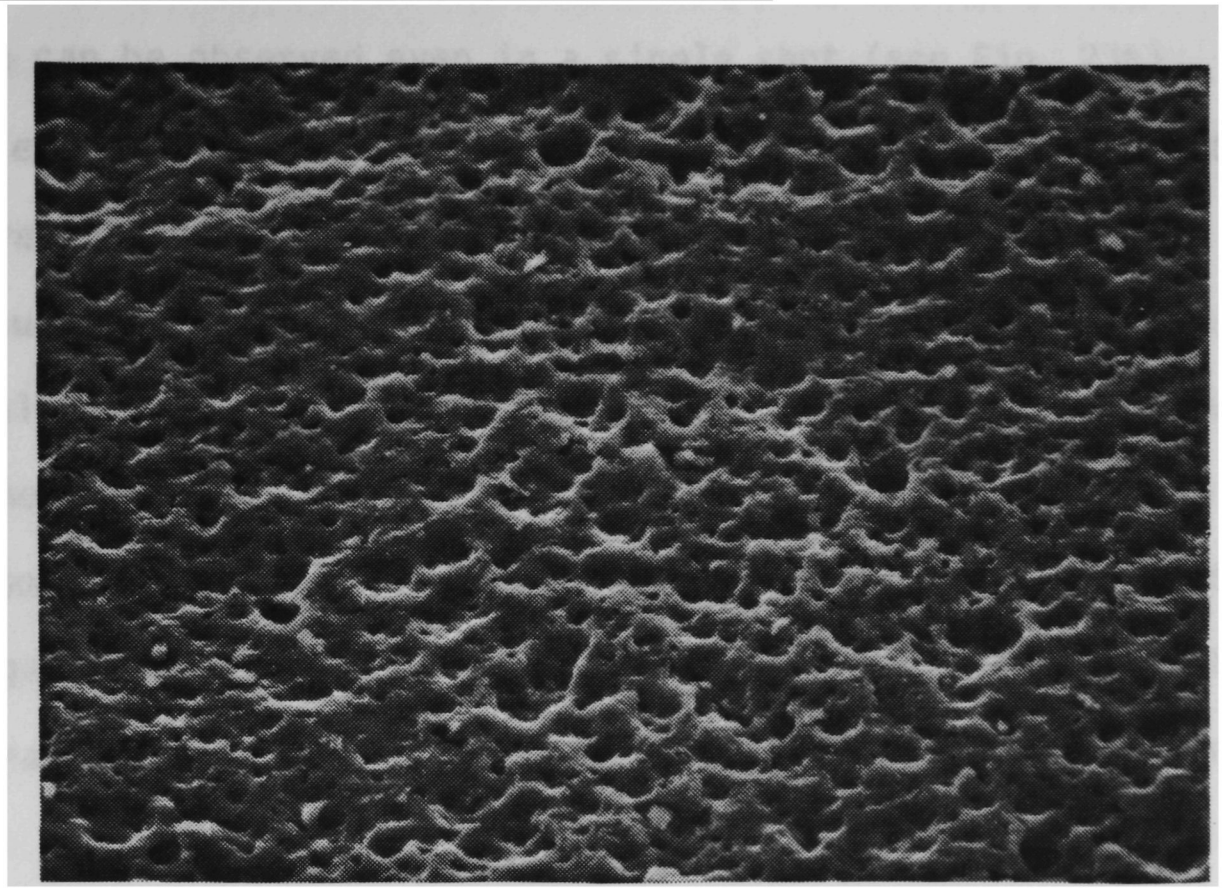

(a) 50,000 shots. (x 500)

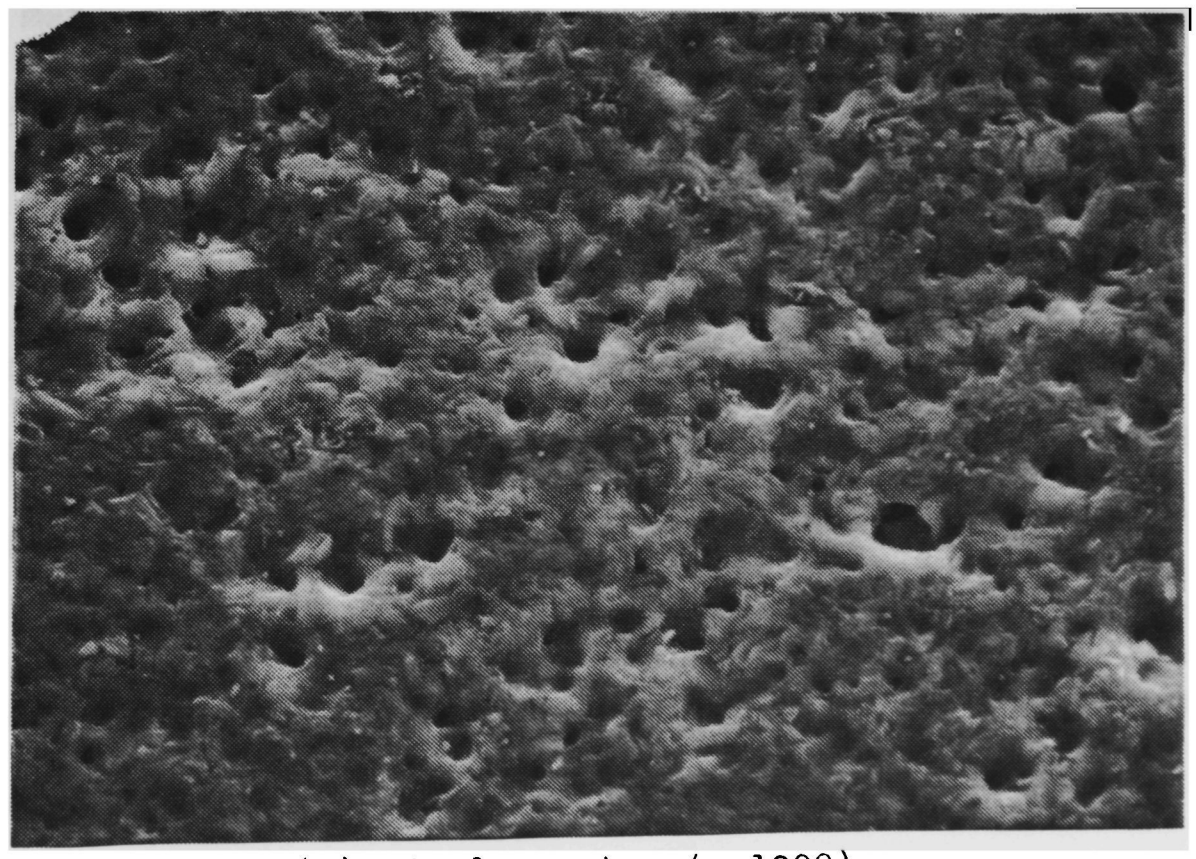

(b) Single shot. (x 1000)

Figure 23. Graphite Electrode Erosion in SF_6.

The formation of CF, CF_2, and CF_3 groups on graphite surfaces in microwave discharges has been observed.[58] The start of the chemical erosion can be observed even in a single shot (see Fig. 23b). After a single shot, some of the sharp graphite peaks have been smoothed (compare to Fig. 20a) and a few craters have formed.

Study of the graphite surface in SF_6 is complicated by another chemical process taking place in the gap. Fluorine and reactive fluorine molecules (such as HF) are generated in the discharge from the decomposition of SF_6. Reaction with aluminum surfaces in the spark gap chamber produces AlF_3. Also, any free Al atoms in the gas react rapidly with SF_6 to form AlF_3. The following reactions may occur:

$$\begin{array}{lrl} \text{at metal surface} & Al + 3F \rightarrow & AlF_3 \\ \text{in the gas} & 2Al + SF_6 \rightarrow & 2AlF_3 + S \\ \text{or} & 2Al + 3SF_6 \rightarrow & 2AlF_3 + 3SF_4 \end{array} \qquad (3)$$

The AlF_3 (a white powder) covers all surfaces and collects at the bottom of the gap. The reaction is greatly increased when aluminum vapor is ejected into the cylinder from an occasional misfire between the bottom electrode and the outer cylinder (1 in 500 shots, evidenced by arc spots on the cylinder wall) or by arcing (creating more fluorine at aluminum surfaces) at electrical connections in the upper electrode holder. The inner electrode region shows a composition of 40% C, 6% O, 32% AlF_3, and 20% other F. The 20% extra F is bonded to the graphite in the form of the CF_x compounds

(refer to Fig. 22).

The outer electrode region is composed of 77% AlF_3, 16% C, and 6% O. The C and O result primarily from surface adsorption of oxides and hydrocarbons after the electrodes are removed from the gap. Thus, before exposure to air, the outer region was almost entirely masked by AlF_3. This is verified by an XRF metal map of Al (Fig. 24) showing virgin graphite beneath the AlF_3 crust, where a flake of deposit was removed. The AlF_3 crust has the appearance of a hot chemical deposit which has been cooled, leading to cracking and curling (10 μm diameter flakes).

The constant O content (6%) in the virgin, and the inner and outer SF_6-eroded samples is due to surface adsorption, after removal from the gap, implying that there was no oxygen available for reaction with the graphite surfaces, as occurred in N_2. This is consistent with observations of the gas composition showing a sharp decrease in H_2O and some increase in m/e peaks at 64, 34, and 48 (probably SO_2, H_2S and SO fragments, respectively), after several thousand shots. Apparently, any water released in SF_6 reacts in the gas discharge environment before it reaches the graphite. The oxygen in the water probably ends up as SO_2. The hydrogen forms H_2S (detected by the odor of the gas products), and HF (probably responsible for the etching of the quartz diagnostic ports). For instance, one possible reaction (likely, if any SF_4 molecules are present) would be

$$SF_4 + 2H_2O \rightarrow SO_2 + 4HF \qquad (4)$$

(a) SEM of outer region, showing removed flake of deposit. (x 2000)

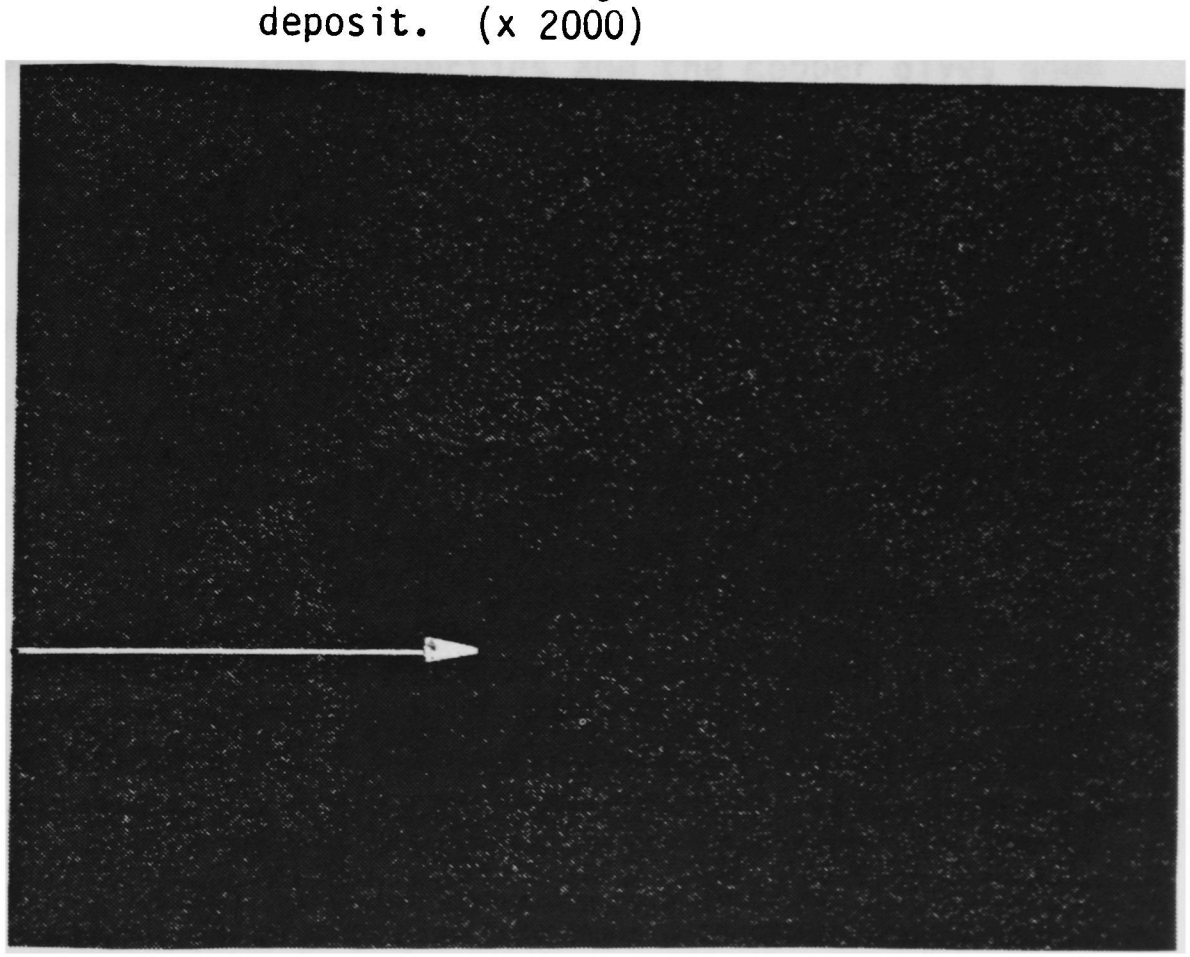

(b) Al metal map, showing uniform Al distribution except at removed flake of deposit. (x 2000)

Figure 24. Graphite Electrode Outer Region in SF_6.

After 50,000 shots in SF_6 the bottom of the gap is covered with up to 2 mm of powder. Chemical analysis has shown a high content of elemental sulfur and AlF_3, mixed with some H_2S and elemental aluminum.

Tungsten-Copper Electrode (K-33)

The metal electrode studied is a composite of 67% W and 33% Cu (designated K-33) developed and manufactured by Metallwerk Plansee of Austria and distributed by the Schwarzkopf Development Corporation in the U.S.[68] It is made by forming a porous tungsten substrate from a sintered tungsten powder, and then infiltrating molten copper. The tungsten gives good erosion properties and the copper gives good thermal and electrical conductivities. Figure 25a shows an SEM photograph of an unpolished, machined electrode surface. Machining marks are clearly visible and ESCA shows a freshly machined surface to be composed of 61% Cu, 3.6% W, and 35.5% hydrocarbon and oxide contaminants. The machining process turns over the soft copper and masks the tungsten, so that the surface distribution of metals is not representative of the interior composition. Some K-33 electrode inserts were polished with steel wool, oxide papers, and oxide and diamond pastes. The electrode inserts were then cleaned ultrasonically, rinsed with ethanol and baked at 300 C for 2 hours. No residues from the polishing or cleaning chemicals were detected by any of the surface analysis techniques. Figure 25b is an optical photograph of a highly polished K-33 sample. The copper (dark

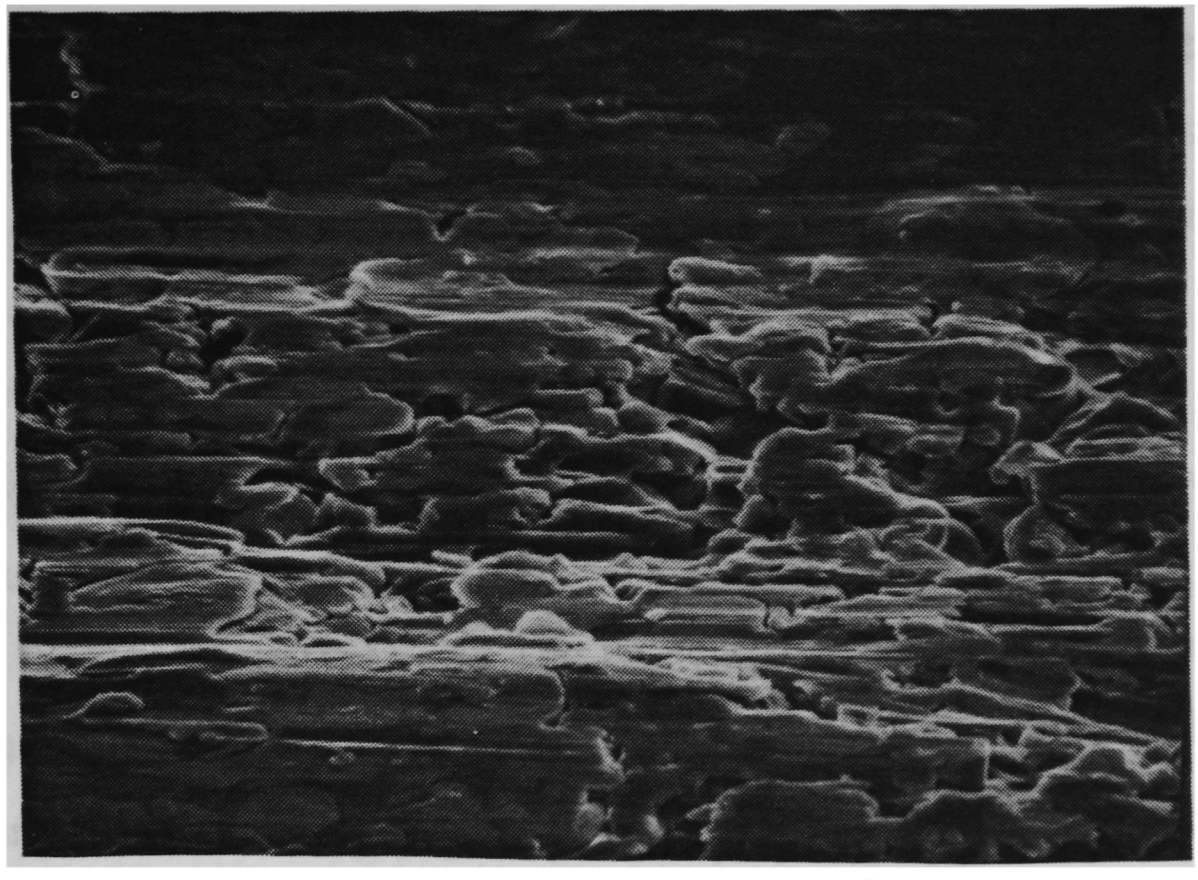

(a) Unpolished. (x 2000)

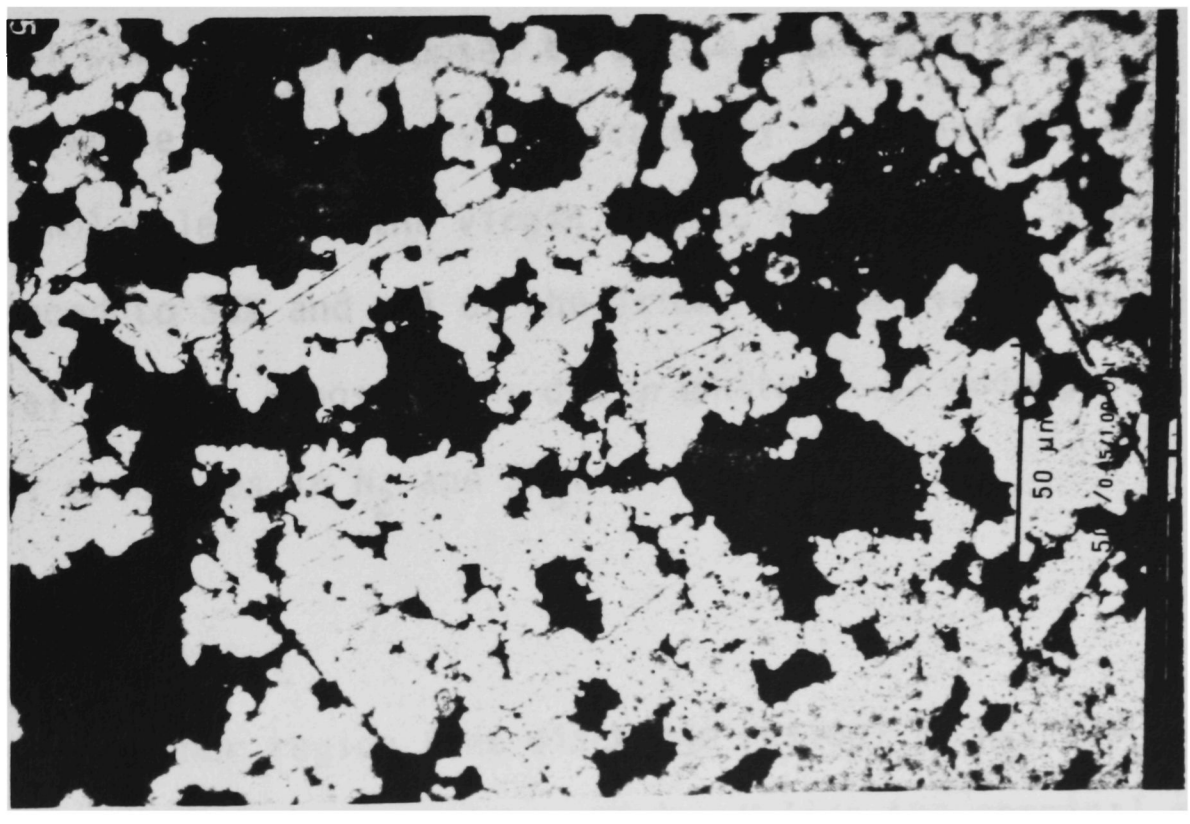

(b) Polished. (x 430)

Figure 25. Virgin K-33.

region) was slightly etched to give sharper contrast with the tungsten (lighter region). The sintered tungsten particles are typically 3 to 8 μm in diameter. The pockets left among the aggregates of tungsten particles are filled with copper and are typically 10 to 50 μm across.

Figure 26a shows a crudely polished section of K-33 and Fig. 26b and 26c are the Cu and W metal maps, respectively, showing the Cu-W matrix. In this electron microscope photograph, the raised, interconnecting light material is the W and the filler, the dark material, is the Cu. From ESCA, the electrode samples show a high surface contamination (up to 50%), after removal from the spark gap and exposure to the atmosphere. To reduce this masking contamination, all metal samples were exposed to a weak argon beam for about two minutes (while in the ESCA vacuum chamber) to remove the adsorbed surface molecules. On the virgin sample, for example, hydrocarbons are reduced to 36% and all of the oxides are removed, leaving 65% of the metal surface exposed. As did graphite, K-33 undergoes different chemical processes in N_2 and SF_6.

Nitrogen Filler Gas

In the inner region (the discharge region) in N_2, the resulting K-33 surface is very rough (Fig. 27a). Unlike the chemical erosion of graphite in SF_6 or the vaporization of graphite in N_2, this sample appears to have undergone violent physical processes, such as melting or boiling. The material surrounding the many pores is very

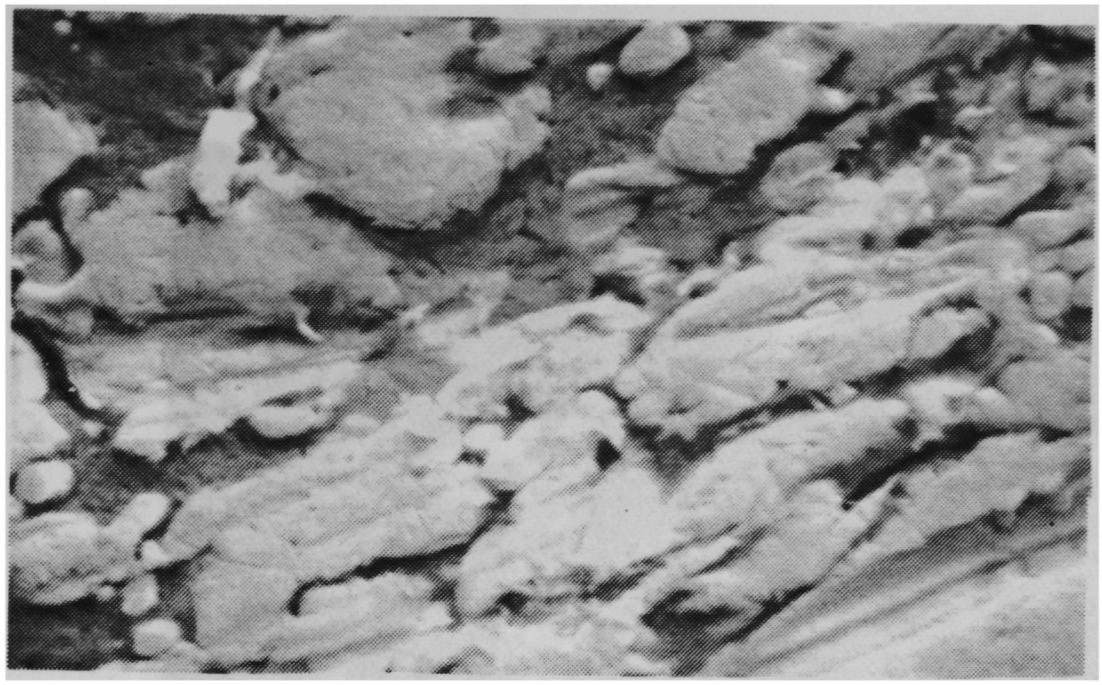

(a) SEM.

(x 4000)

(b) Cu metal map.

(x 4000)

(c) W metal map.

(x 4000)

Figure 26. Polished Virgin K-33 Metal Maps.

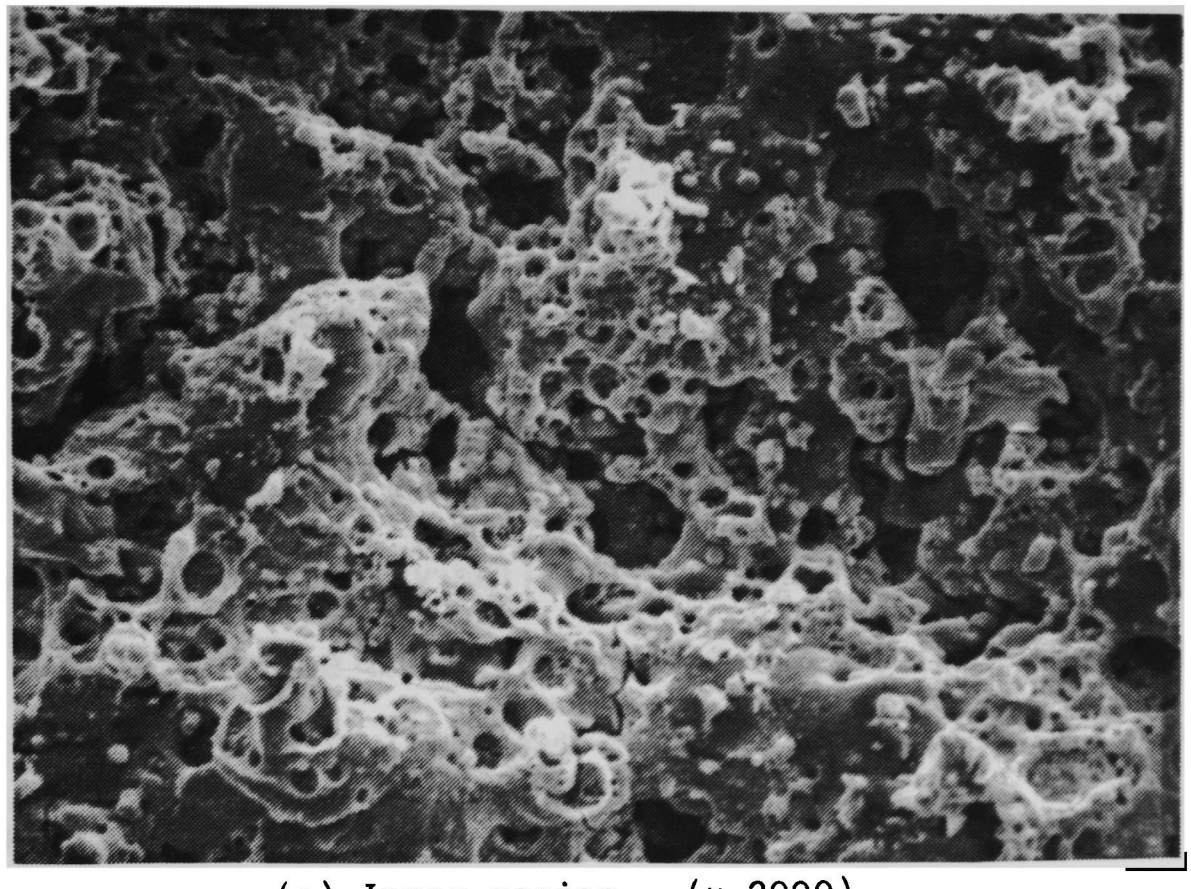

(a) Inner region. (x 2000)

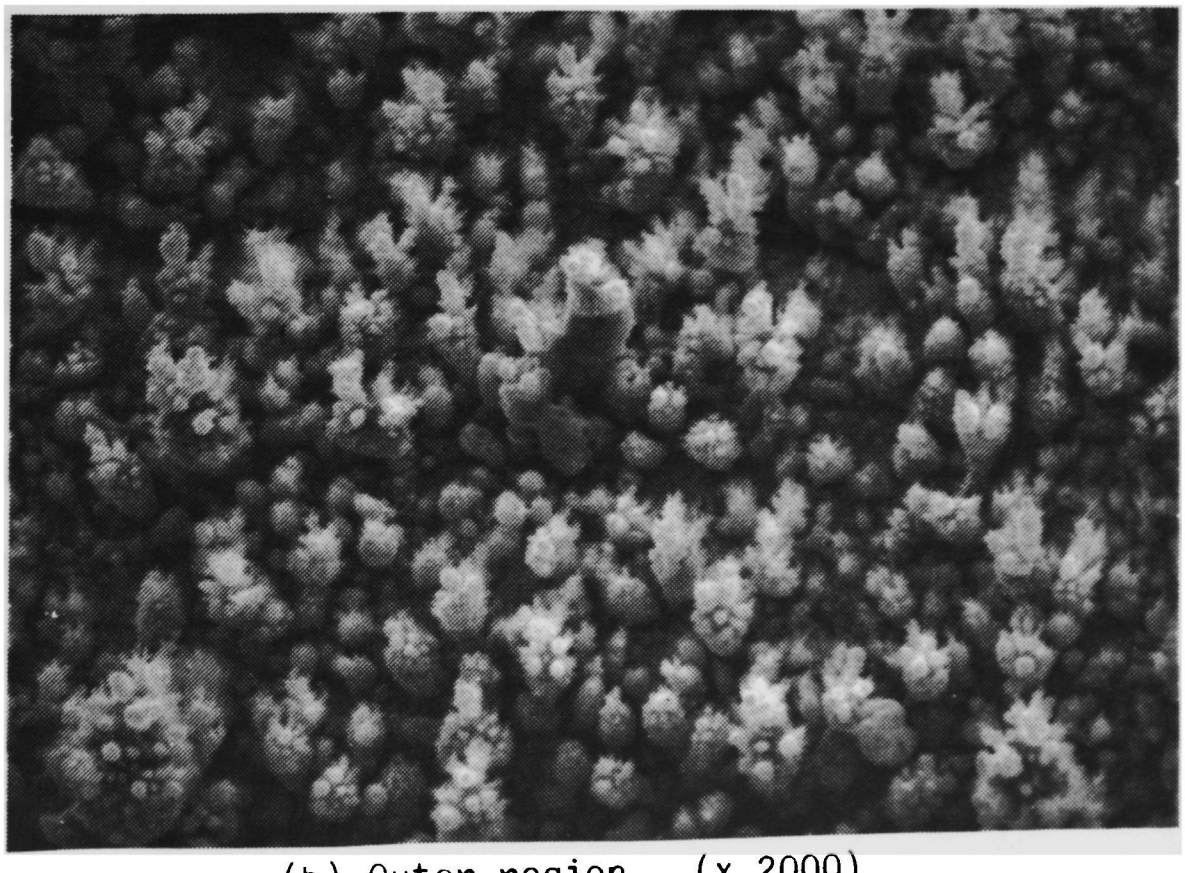

(b) Outer region. (x 2000)

Figure 27. K-33 Electrode Erosion in N_2.

similar to the appearance of the original tungsten matrix in a polished cross-sectional view of a virgin sample, with one material depleted. Analysis of the ESCA spectrum indicates a relative decrease in Cu and some increase in W in the discharge region. Very strong Cu I lines were observed in the arc plasma while W was undetected. Although the initial excess surface copper, due to the machining process, makes interpretation difficult, it seems that the copper has been selectively boiled out or ejected from the surface. This is feasible, since the melting point of copper is 1339 K and its boiling point is 2823 K, whereas W melts at 3660 K and boils at 6186 K.[66] Thus, copper boils at a temperature which is 1000 K less than that at which W melts. It is very likely that the anode spot temperature exceeds the melting and boiling points of copper. However, no electrode surface temperatures have ever been reported as high as the melting point of W.[50] After etching, the oxygen content of the N_2 exposed K-33 electrode is significantly higher than the virgin sample. From ESCA, it is found that all of the surface tungsten has been oxidized, while most of the surface copper is pure. Tungsten has a much higher reduction potential than copper and thus, readily uses the oxygen released in the gap by the discharge.

Although the SEM photograph of the surface (Fig. 27a) gives the indication of fairly deep structural changes (at least compared to graphite), examining a cross-section of the eroded sample shows the damage to be only 3 to 5 μm deep, on the average, and 10 μm deep in places.

The outer region (Fig. 27b) is entirely covered with vapor redeposited, metal crystals. The vertical crystalline growth is composed of dendrites, 1 to 4 μm in diameter and 2 to 8 μm tall, and are primarily composed of tungsten oxides and metallic copper. Detailed analysis of the dendrite composition is very difficult due to their small size.

Sulfur Hexafluoride Filler Gas

The processes involved with K-33 in SF_6 are interesting and somewhat more complex than the previously described combinations. This combination is the first to show a definite effect of each individual discharge. In graphite, for instance, individual shots have no different regions and detailed analysis of the many-shot surface shows no distinct pattern made by the most recent shots. In K-33, however, each of the last few shots has masked the effects of the previous shots. On a many shot sample (50,000 discharges), the last few shots (3 to 8) are individually discernable. Two distinct regions are apparent at each of these individual discharge sites within the inner discharge region (Fig. 28a). A single discharge site (3 mm in diameter) has a center (1 to 2 mm in diameter) which appears to have been a molten pool of material that underwent rapid cooling from the bottom up. During cooling, recrystallization of the material produced a large scale (400 μm across) cellular pattern (Fig. 29a). The pattern is most likely caused by the rapid

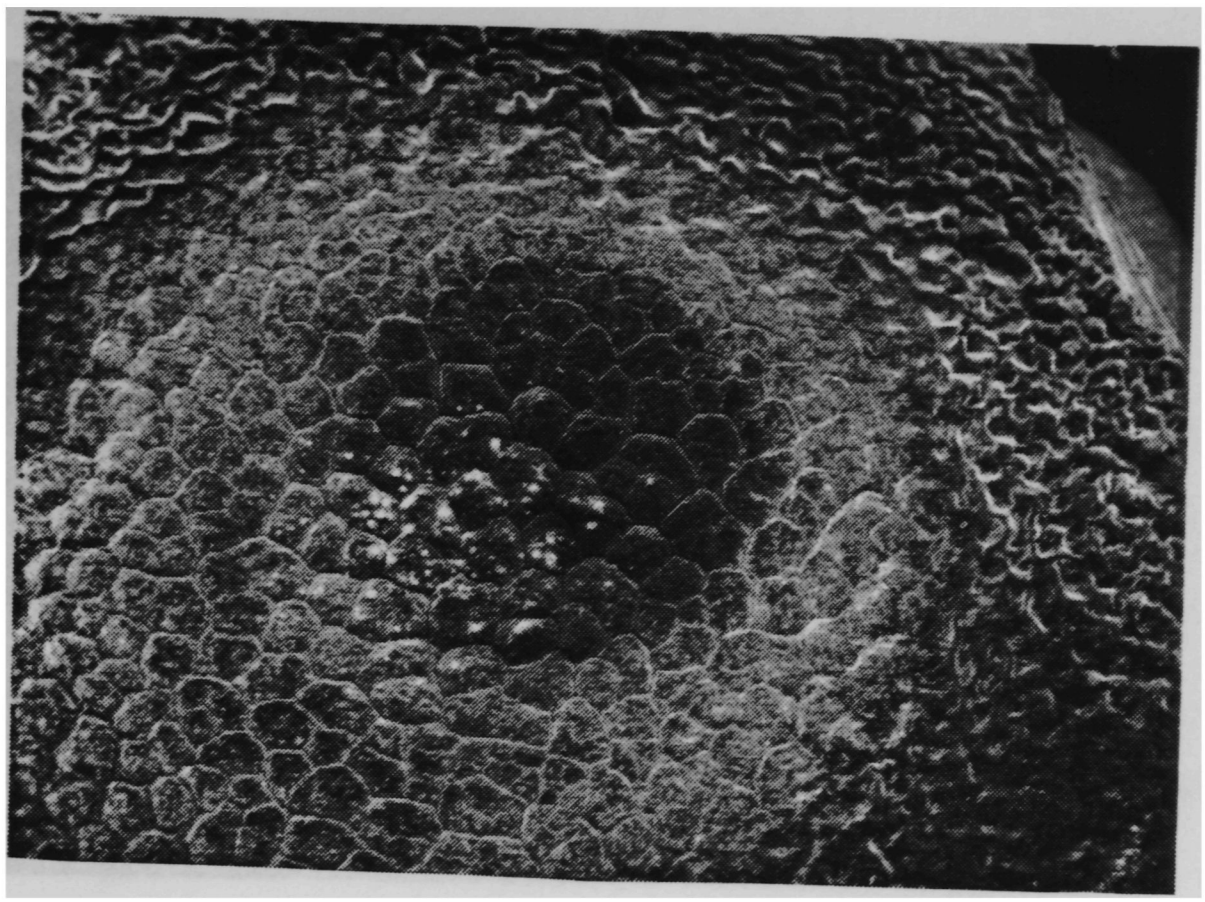

x 20

(a) A single discharge site in the inner region of a 50,000 shot electrode sample.

x 500

(b) Outer electrode region (outside discharge region).

Figure 28. K-33 Electrode Regions in SF_6.

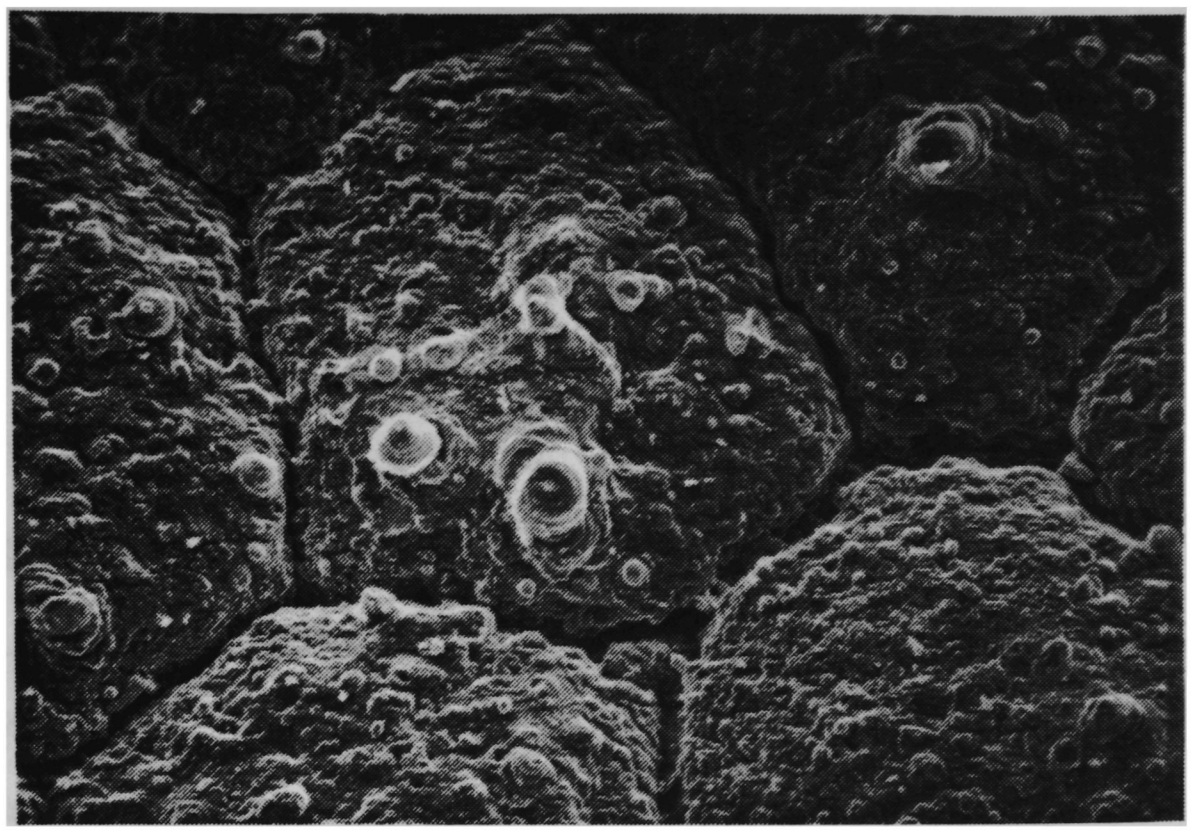

x 200

(a) Center of discharge site (from center section of Fig. 28a).

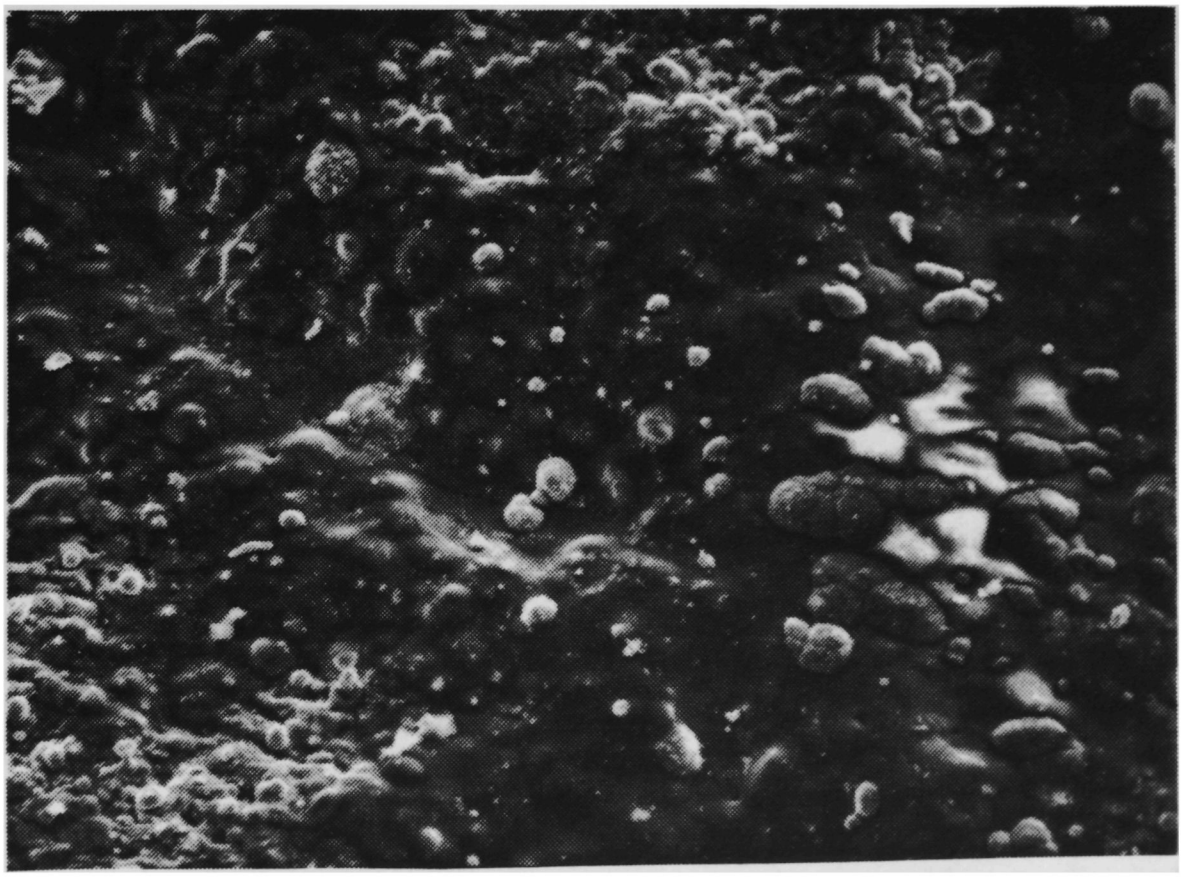

x 500

(b) Outer area of discharge site (from fringe area of Fig. 28a).

Figure 29. Discharge Site on K-33 Electrode in SF_6.

recrystallization of CuF_2 or CuF. The molten copper at a discharge site reacts with free fluorine to form the fluoride.

$$Cu + 2F \rightarrow CuF_2 \qquad (5)$$

The region around the recrystallized center of the individual site (still within the inner electrode region) is composed of two materials (Fig. 29b). The difference in texture and form of the two materials suggest that one has a much lower melting point than the other. Possibly one of these materials was ejected from the center of the discharge site (Cu or Cu fluorides). The exact composition of the two materials has not been resolved, except for the presence of a high fluorine content.

Since ESCA covers a relatively large spatial area (2-5 mm in diameter) it is not selective enough to study each of the regions at a single discharge site, but gives an average of the surface content of the two regions. Analysis of the AES spectrum of the different areas of a single shot discharge site, however, gives very useful information concerning the effect of the single shot. A single shot on a polished K-33 electrode surface in SF_6 did not show the same cellular pattern (Fig. 28a) as the single discharge site on a multiple shot electrode. This implies that a buildup of certain chemical structures, such as CuF_2, over a period of many shots leads to the cellular structure. However, analysis of the single shot on a polished virgin surface did show three distinct regions.

The center of a single discharge, about 1.5 mm in diameter, was a very bright dark orange star. Surrounding the center spot and filling the rest of the discharge site, about 6 mm in diameter, was a light, copper-colored ring. Outside the discharge site the polished K-33 surface is a silvery gray color (the original color of the polished material). Analysis of the AES spectrum shows the virgin area to be 39% Cu, 14% W, 22% O, and 4% F; the light colored ring to be 56% Cu, 8% W, 19% O, and 6% F; and the dark center spot to be 63% Cu, 0% W, 7% O, and 18% F (see Fig. 30). The remaining 10 to 20% of the surface is miscellaneous contaminants, primarily carbon. Several important conclusions can be made. First, either W is being chemically removed by F ($W + 6F \rightarrow WF_6$), or the copper is being selectively drawn to the surface, at the center of the discharge site, to mask the W. Second, since there is no W exposed in the inner region, no W oxidation occurs and the 7% O is probably all adsorbed, whereas on the virgin region, much of the 22% O present is in the form of oxidized tungsten. Finally, more fluorine is chemically bound to the copper in the inner region than in the virgin region.

Careful analysis of the ESCA spectrum shows a very broad fluorine line (on the many-shot sample) indicating the presence of several fluorine compounds, including CuF_2, CuF, CF_x and possibly CuOHF. There are two forms of carbon on the inner electrode region: the normal hydrocarbon contaminants plus some other carbon compound (probably CF_x). The carbon available for chemical reaction with F comes from prior hydrocarbon contaminants or from impurities in the

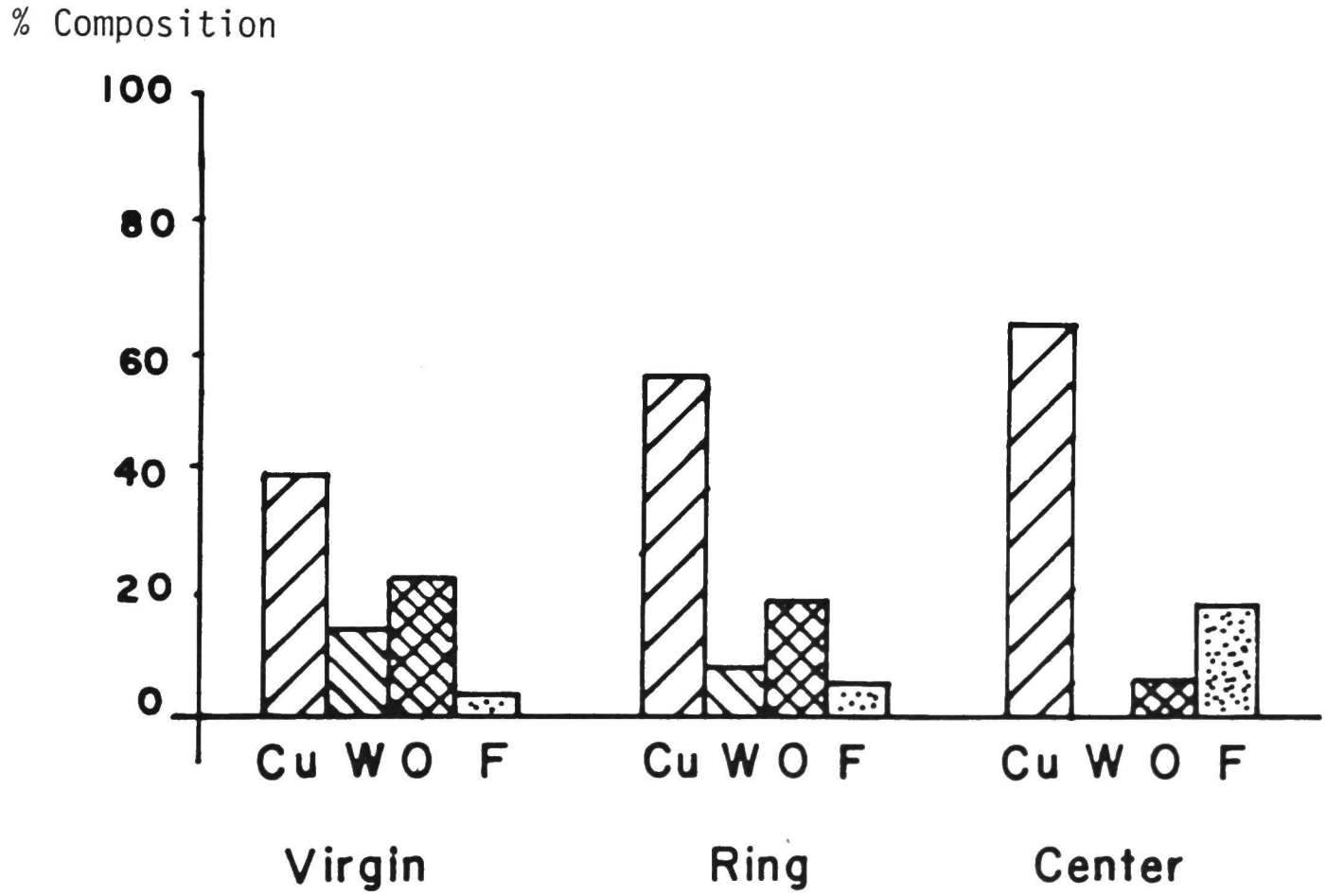

Figure 30. Surface Composition of a Single Discharge Site on a K-33 Electrode in SF_6.

metal. Although no tungsten lines are observed in the discharge (possibly due to masking from the very strong Cu, S, and F lines), more tungsten and copper is found on insulator surfaces exposed to the K-33 electrodes in SF_6 than on insulators in N_2. It is very likely that some WF_6 is formed in the discharge plasma. No WF_6 is detected on the electrode surfaces due to its high volatility and it is, of course, too heavy a molecule to detect with the mass spectrometer used. An accumulation of chlorine (less than 5%) on the electrode surface is observed after 50,000 shots. Most likely the Cl is obtained as an impurity from the SF_6, which is often manufactured using Cl in the processing. Cross-section photomicrographs show the damage depth to be less than 10 μm (similar to the N_2 case), as seen in Fig. 31. It is very likely that the electrode spot temperatures are less in SF_6 than in N_2, since the plasma temperatures in SF_6 are generally less than in N_2. (Much more energy is used in disassociating the more complex SF_6 molecule.) Thus, it is possible that more chemical erosion, due to fluorine, and less mechanical erosion, due to the boiling of copper, occurs in SF_6 than in N_2.

The outer region of a multishot electrode (outside all discharge sites) is composed of a redeposition of material in a flake pattern, characteristic of chemical deposits (see Fig. 28b). It is composed of 43% F with less than 20% metal content and is very complex and difficult to analyze (from the ESCA spectrum).

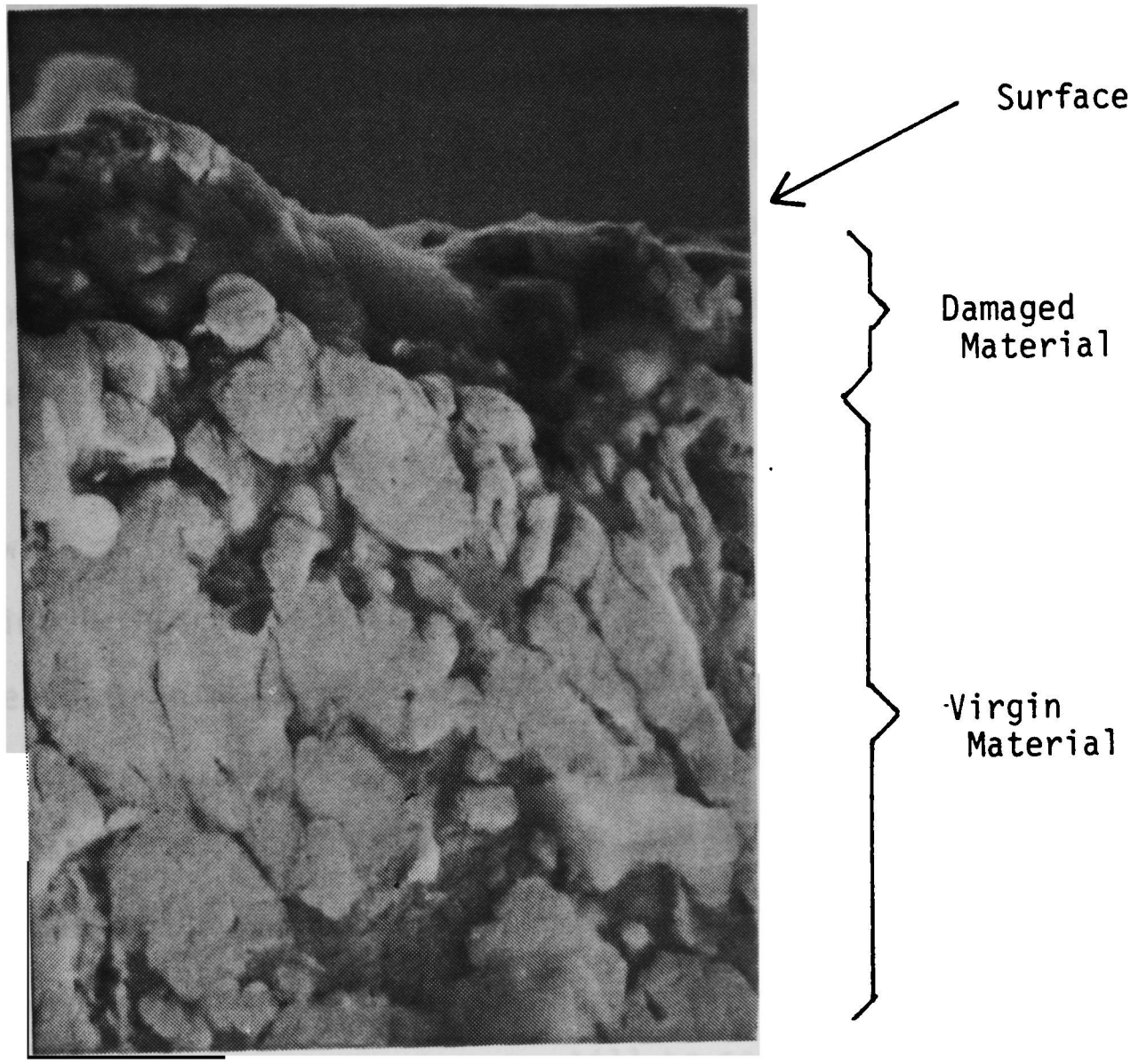

(x 4000)

Figure 31. Cross Section of K-33 Electrode in SF_6.

Insulators

Square insulator samples (20 cm x 20 cm x 8 mm thick) were placed 5 cm from the discharge region to: (1) produce discharge-exposed samples for study in another project looking at insulator degradation (10,000 shots), and (2) to study the effect of the insulator's presence on the electrode and the gas (for 50,000 shots). Examination of the electrode surfaces exposed to insulators reveals similar characteristics, independent of the electrode material. Differences were noted between the two insulator types and a few differences were detected between operation in N_2 and SF_6.

When comparing an electrode sample taken after 50,000 shots, without an insulator, with one taken after 50,000 shots with an insulator, it is apparent that the erosion mechanisms for the electrode material are basically the same (although rates may change). The electrode sample exposed to the insulator, however, is masked with organic molecules most likely deposited after the electrode surface has cooled. The erosion details, holes and cracks, seen previously without an insulator, are now filled and covered, although their outlines can still be seen. In all cases, (all combinations of K-33, graphite, N_2, and SF_6), ESCA shows a higher surface content of organic carbon compounds on the surface. Since both inner and outer areas are equally covered and since organic molecules have a low melting point (compared to the electrode materials), the material is probably deposited after each discharge.

An increase in H_2O is observed in N_2 when insulators are present, Blue Nylon showing the greatest increase. This is due to the fact that Lexan absorbs 3% water and Blue Nylon absorbs 6% water by volume. In an SF_6-graphite gap, an increase in the CF_3 fragment is observed when an insulator is present, indicating some reaction of flourine with the insulator, producing CF_4.

In the graphite-SF_6 system, exposure to Lexan for 50,000 shots leaves a thick organic layer on the electrode (Fig. 32, compare to Fig. 23a). Besides an increase in organic carbon, the surface oxygen concentration is up to 23%, as compared to 14% without an insulator. On K-33 surfaces exposed to Lexan in both N_2 and SF_6, the organic layer shows a somewhat crystalline pattern (Fig. 33a and 34b). In both cases, the electrode erosion characteristics seem to be the same as without an insulator (compare to Fig. 27a and 29a, respectively); i.e., the underlying electrode structure (vertical relief, crystalline matrix, holes, etc.) is unchanged. In SF_6, organic fluorine compounds were found on both graphite and K-33. Analysis of the ESCA spectrum shows only that the contaminants are organic in nature, and does not resolve the exact chemical structure of the organic molecules.

Three important differences are observed when Blue Nylon is present in the discharge region (Figs. 35, 36, and 37). First, more visible deposits are observed when compared to Lexan (compare Fig. 35b to 32, and 36 to 34). Second, more water is released into the spark gap chamber, supplying increased oxygen for production of

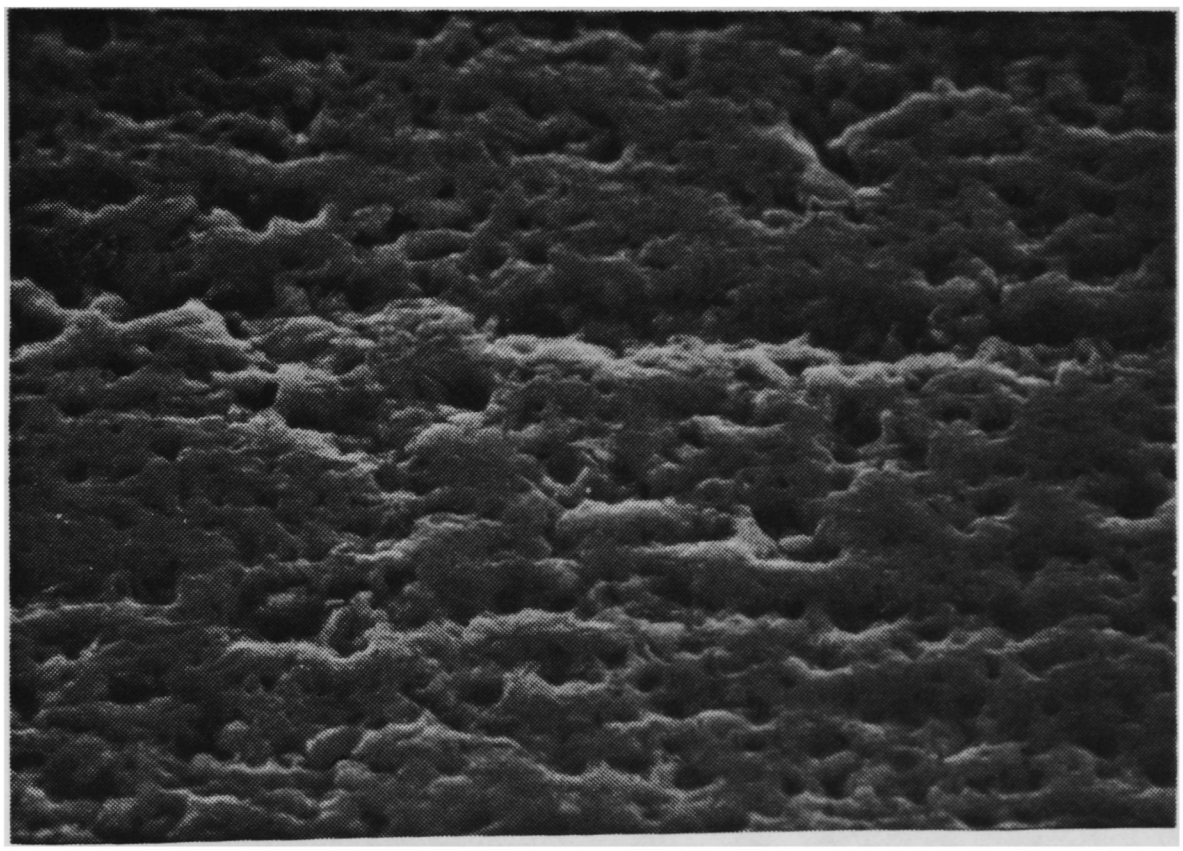

(x 1000)

Figure 32. Graphite Electrode in SF_6, Exposed to Lexan.

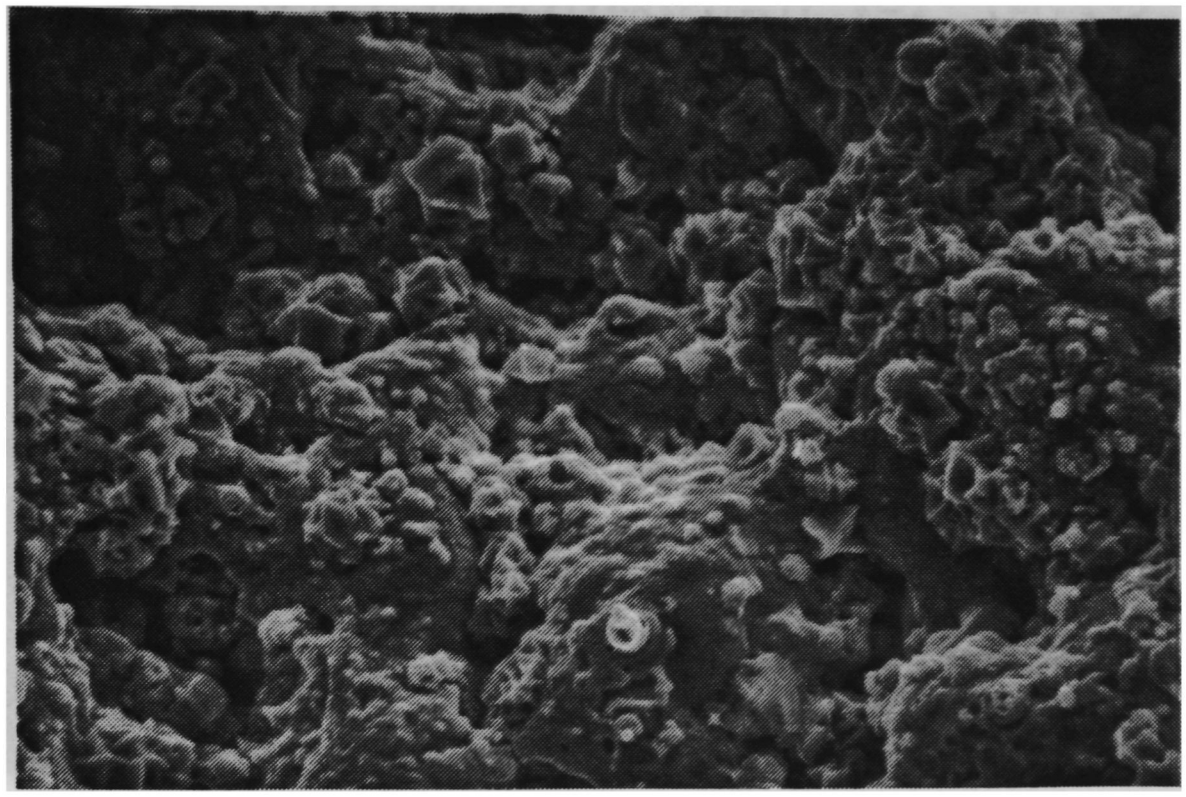

(a) Lexan exposed. (x 2000)

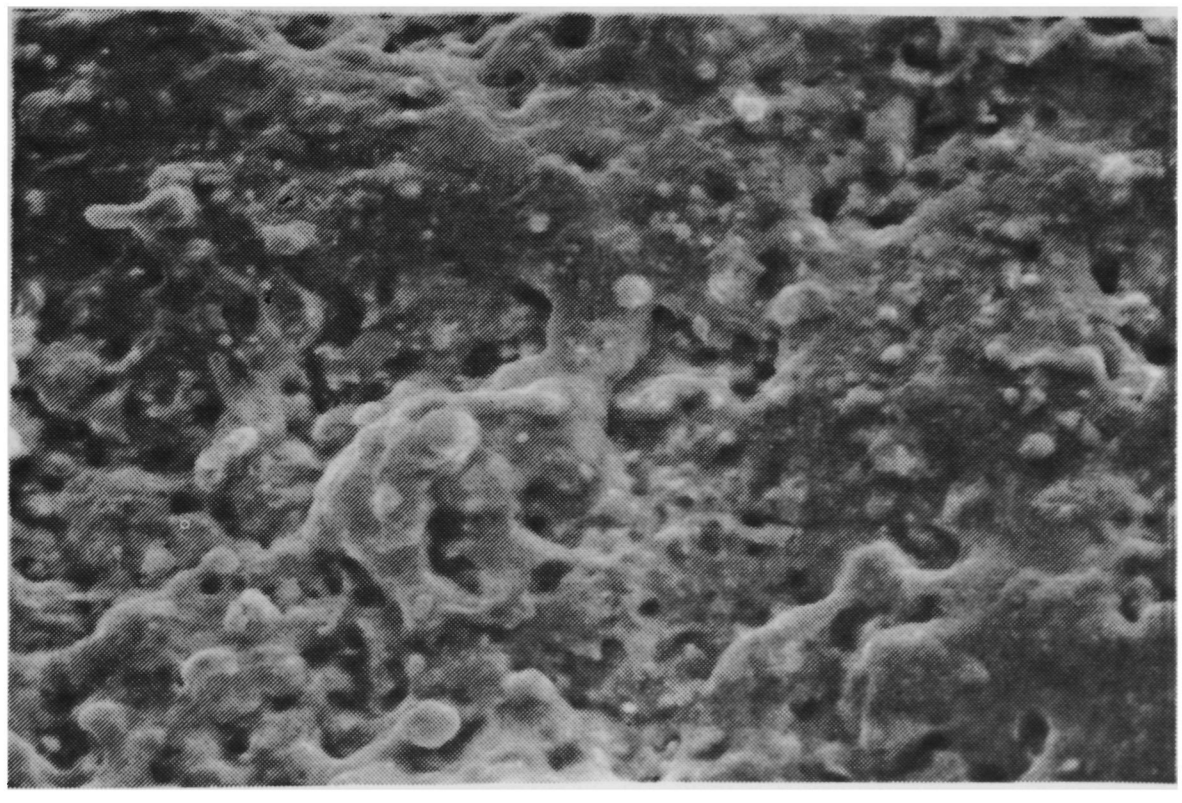

(b) Blue Nylon exposed. (x 1000)

Figure 33. K-33 Electrodes in N_2, Exposed to Insulators.

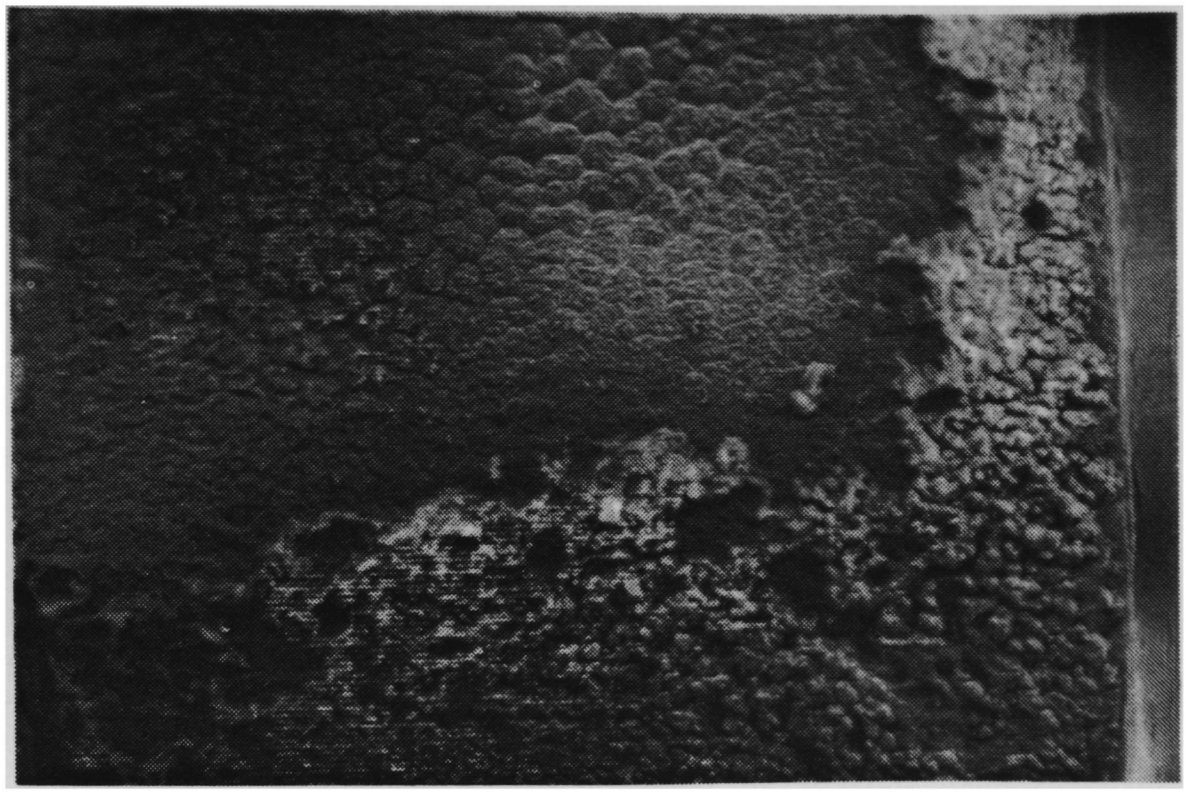

(a) Discharge site. (x 15)

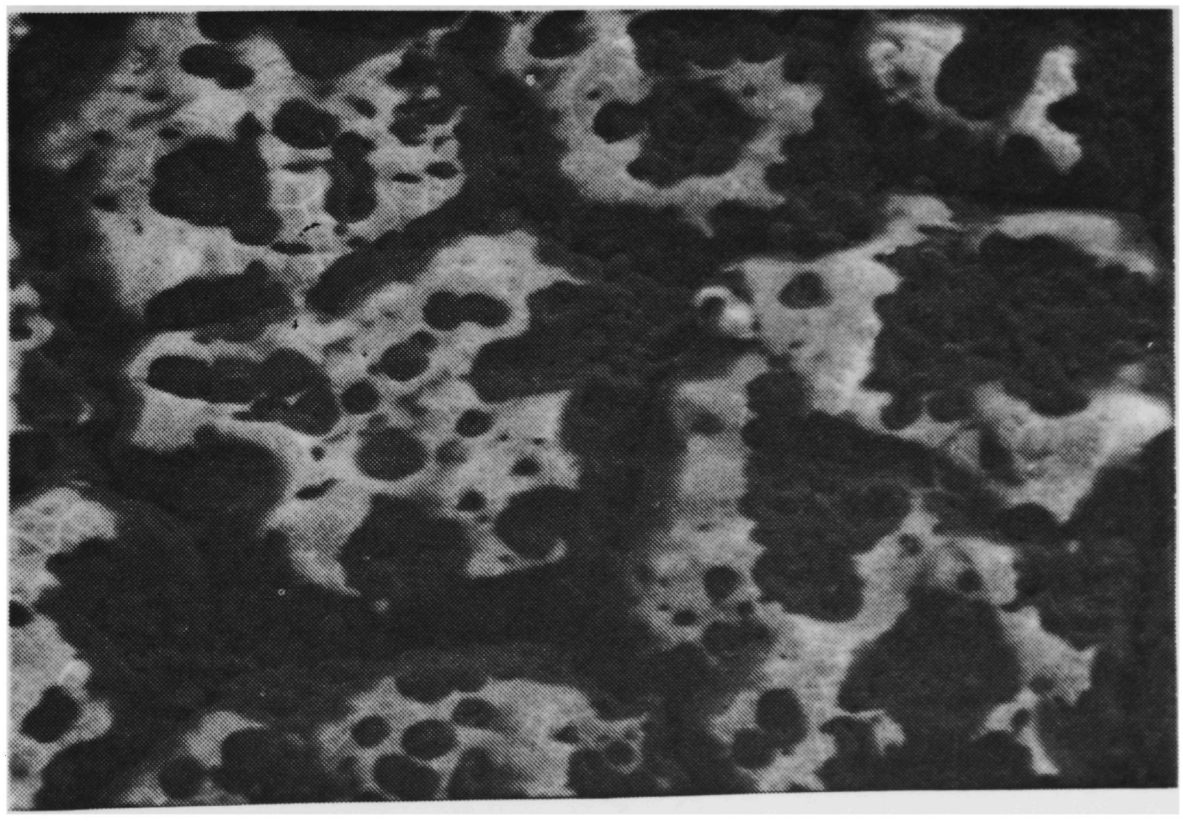

(b) Central region of discharge site. (x 200)

Figure 34. K-33 Electrodes in SF_6, Exposed to Lexan.

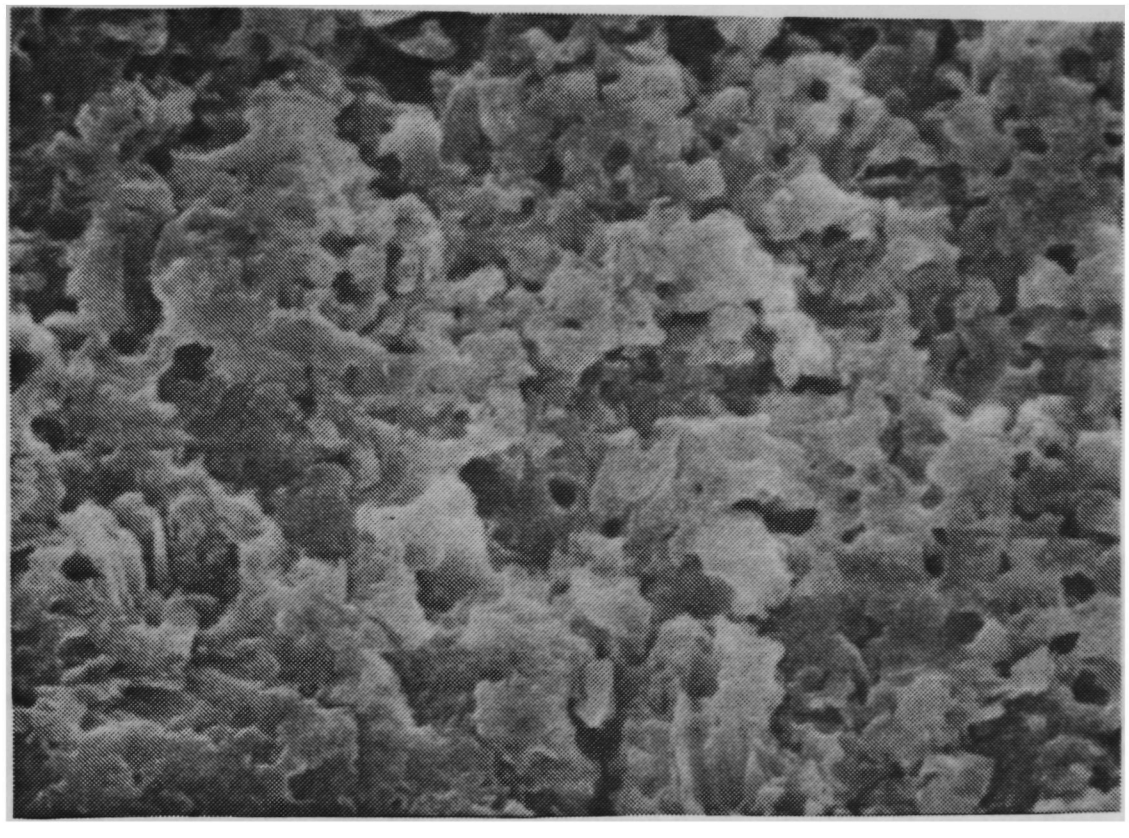

(a) N_2 filler gas. (x 1000)

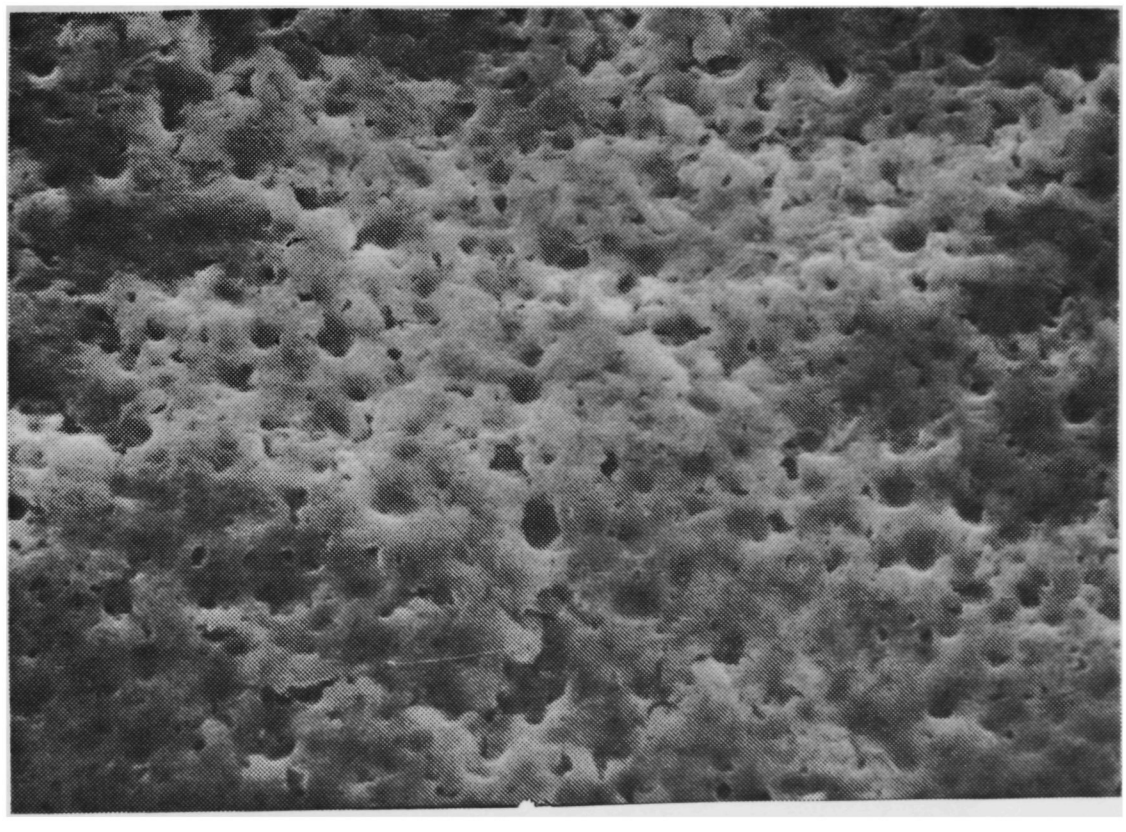

(b) SF_6 filler gas. (x 500)

Figure 35. Graphite Electrodes Exposed to Blue Nylon.

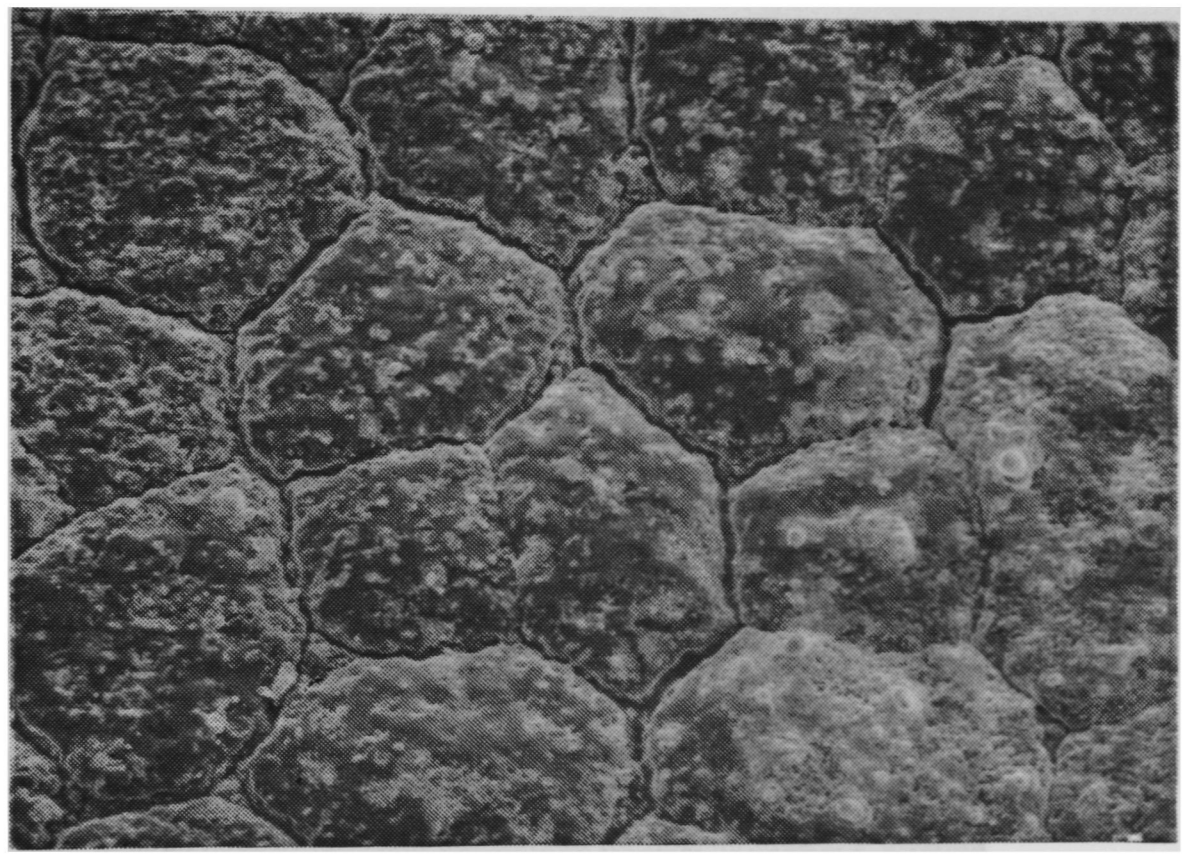

(x 100)

Figure 36. K-33 Electrode in SF_6, Exposed to Blue Nylon.

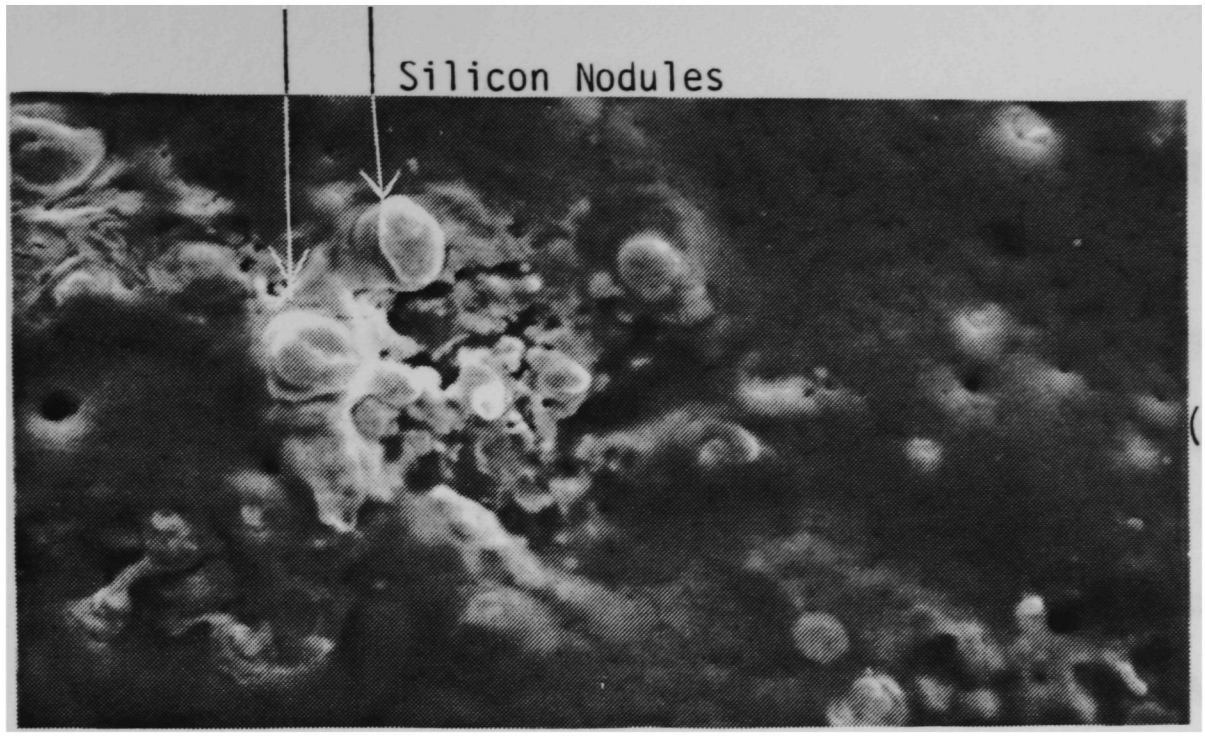

(a) SEM. (x 1000)

(b) Cu metal map. (x 1000)

(c) Si metal map. (x 1000)

Figure 37. Metal Maps of K-33 Electrode in SF_6, Exposed to Blue Nylon.

carbon oxides for graphite electrodes and tungsten oxides for K-33 electrodes. The third major difference is that after exposure to Blue Nylon, silicon is found on the electrode surfaces. Figure 37 shows the SEM photograph of the outer region of a single discharge site on a K-33 electrode in SF_6 and the corresponding metal dot maps for Si and Cu. The white nodules protruding through the smooth plastic-looking deposit are some form of silicon whiskers. The smooth plastic deposit surrounding the silicon nodules is a mixture of copper and copper fluorides ejected from the center of the discharge site and organic molecules from the Blue Nylon. The silicon is observed only in the presence of Blue Nylon insulators and may come from the mold release used in the manufacture of the Blue Nylon.[69] In a K-33 - Blue Nylon gap, the voltage distribution degrades significantly after a few thousand shots (both with N_2 and SF_6). This will be described further in the following section.

Breakdown Voltage Distributions

The breakdown voltage distribution for each gas-electrode-insulator combination was examined for shape (qualitative characteristics) and obvious changes during a shot series (0 to 50,000 shots). Since gas breakdown is a statistical process, it is impossible to have the ideal spark gap where 100% of the breakdowns occur at the same voltage. The optimum distribution, however, is narrow with a sharp peak (i.e., all breakdowns are concentrated about an average breakdown voltage V_B) and does not shift or widen

significantly during the lifetime of the gap. Spark gap performance deterioration occurs when the average breakdown voltage shifts, or the distribution widens, increasing the number of high and low voltage breakdowns. These variations from the ideal narrow distribution are described for several of the combinations tested.

Several reproducible, general observations can be made from the voltage distribution data. First, the voltage distribution for K-33 electrodes with either gas (N_2 or SF_6) tended to widen and give more low voltage breakdowns (i.e., a more gradual slope on the leading edge of the breakdown curve) than graphite electrodes. Second, the presence of Lexan had little effect on the breakdown voltage. It may have even slightly improved the graphite-N_2 breakdown distribution. Finally, the average breakdown voltage usually shifted 1-3 kV (out of 40 kV) during 50,000 shots. It was difficult to determine if this was caused by macroscopic external parameters (such as variation in gas pressure, electrode spacing, or temperature) or microscopic changes (electrode surface or gas composition).

Two electrode-gas-insulator combinations showed distinct changes in their voltage breakdown distributions over a test run of 50,000 shots. In a graphite-N_2 gap, the voltage distribution improved significantly between 500 and 10,000 shots. The distribution narrowed to 1/3 its initial full-width-half-max value; initially having a standard deviation of about 1 kV and improving to 0.2 kV after 10,000 shots. This distribution improvement was better than

any other combination. In fact, most other combinations (especially the ones with K-33 or Blue Nylon) tended to degrade after a few hundred shots. Figure 38a illustrates the voltage distribution of graphite-N_2 for shots # 0 to 450 and # 10,000 to 10,500. In addition to narrowing, the mean breakdown voltage dropped from 41 kV to 39 kV. The addition of Lexan to the graphite-N_2 system was observed to improve the distribution in one test run.

The worst case of voltage breakdown distribution degradation was observed in the K-33 - SF_6 - Blue Nylon combination. The mean breakdown voltage dropped from 40 kV to 35.5 kV, the standard deviation increased from 1.0 to 2.6 kV, and the number of low voltage breakdowns increased dramatically. Figure 38b illustrates the voltage breakdown distribution for this combination at the start of operation and after 10,000 shots. The distribution starts off poorly and gets worse, especially compared to the graphite-N_2 gap.

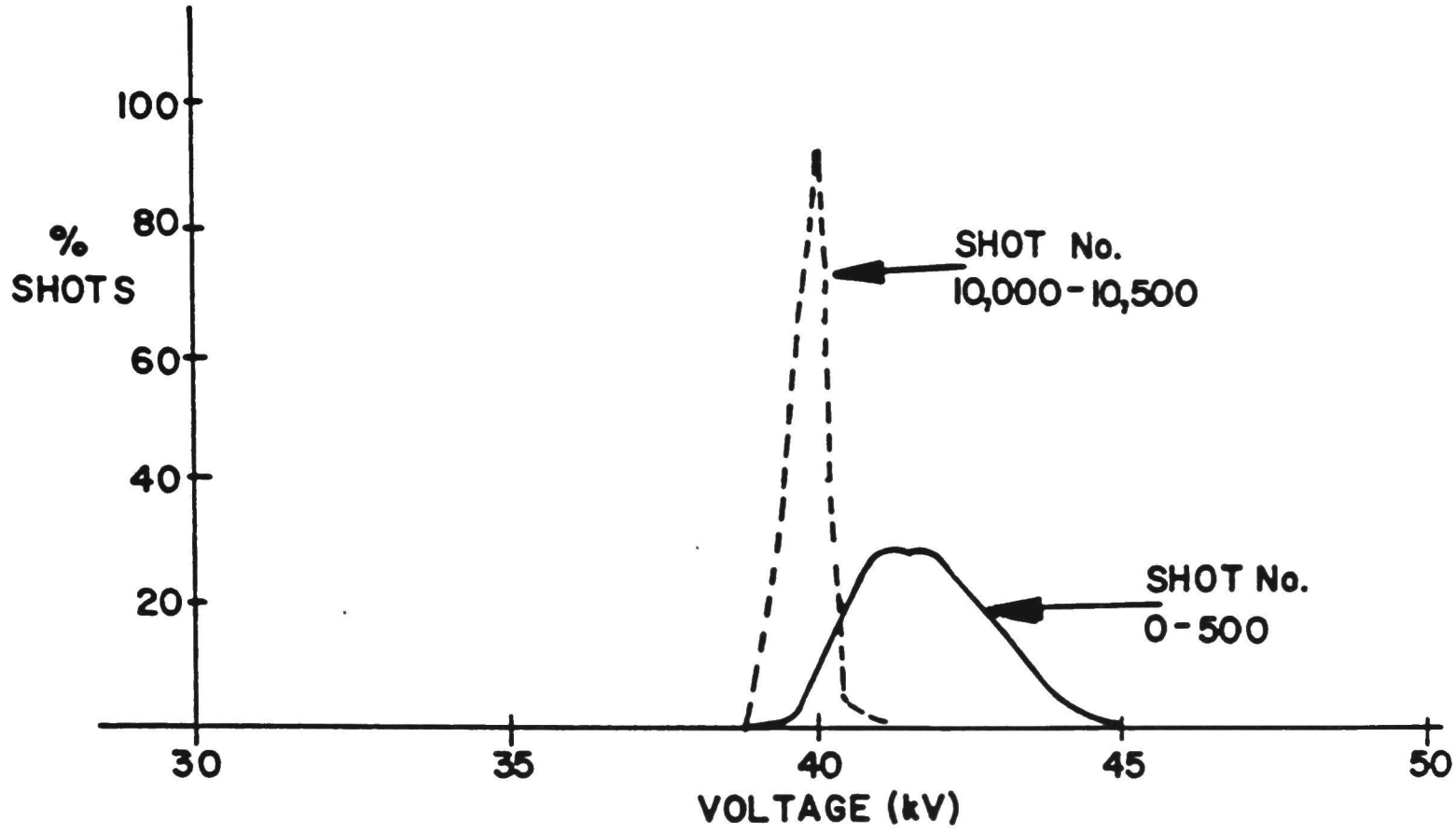

(a) Graphite- N_2.

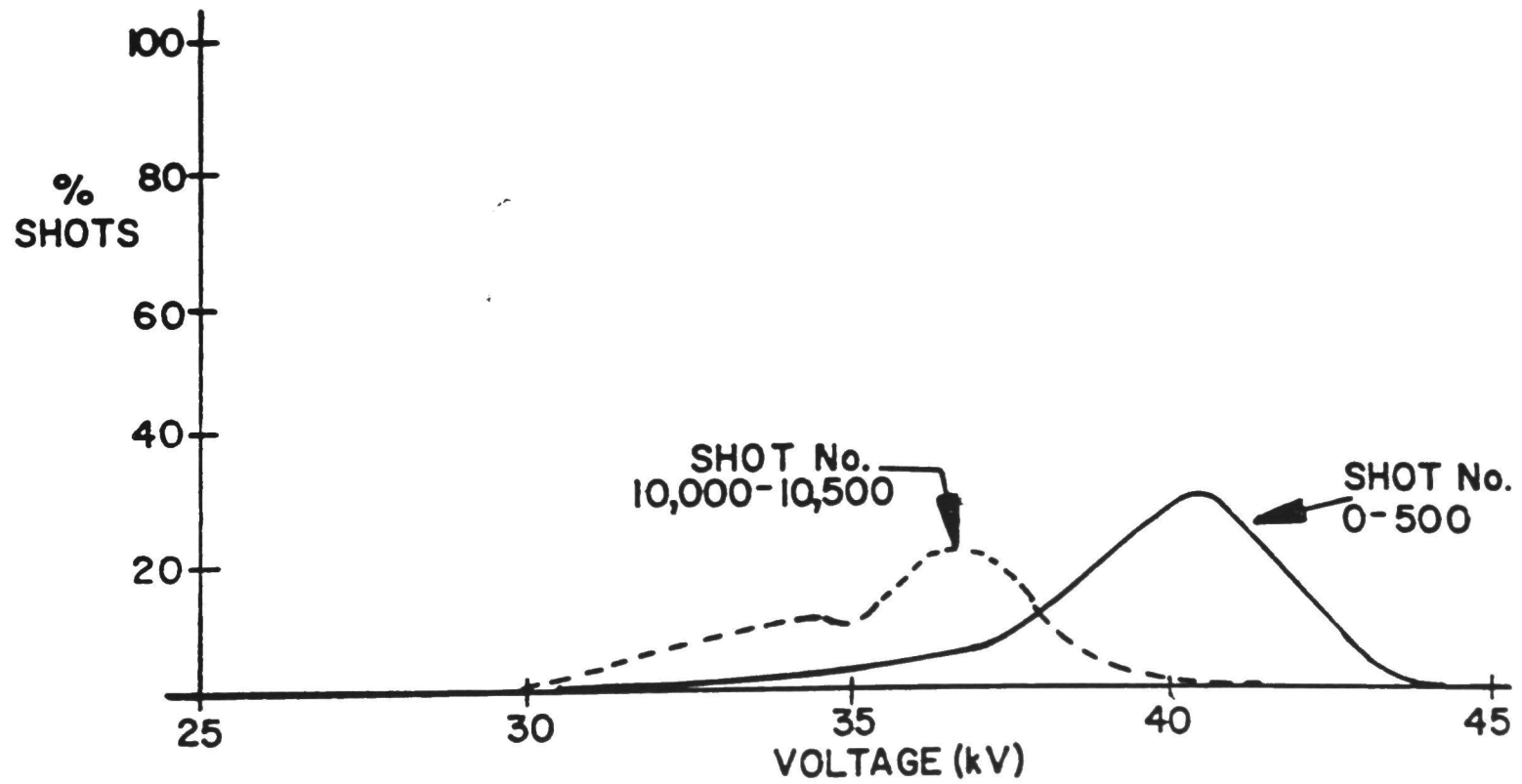

(b) K-33 -Blue Nylon -SF_6.

Figure 38. Breakdown Voltage Distributions.

CHAPTER VI

SUMMARY AND RECOMMENDATIONS

In the previous chapter, observations were made for each system considered; a system being a combination of certain electrode, gas, and insulator materials. Some general comments on the applicability of the results obtained in this specific experimental test-gap are discussed. To summarize the knowledge gained about the processes occurring in these systems, each individual material is discussed. Table II summarizes the principal characteristics for each electrode/gas combination and some general conclusions about insulator effects. In Table III, comparisons of materials of the same class (i.e., electrode, gas, or insulator) are given to illustrate the material dependence of the processes. Many questions about processes occurring in the different gap systems are left unanswered by this study, and many more arose. Some of these unanswered questions are presented, along with suggested methods to investigate the processes further. Suggestions are given for expanding the narrow parameter space which this study considered, and finally, suggestions are made for improving the diagnostics techniques used herein.

Conclusions

Many of the systems studied (each combination of electrode, gas, and insulator) were done with very few electrode samples for three reasons. First, with the 2 pps rep-rate of the high voltage system,

PROPERTY	GAS	GRAPHITE	K-33
erosion mechanism		vaporization and sublimation	Cu boiling, W ejection
surface texture		very smooth	rough
changes outside discharge region	N_2	none	Cu and WO_3 whiskers
gas/electrode chemistry		C-N bonds formed	non observed (involving N)
other chemistry		CO, CO_2, NO, NO_2	WO_3
breakdown voltage distribution		narrow and stable	some prefires
erosion mechanism		vaporization, sublimation, chemical	chemical, ejection
surface texture		smoothly pitted	crystalline (large)
changes outside discharge region	SF_6	AlF_3 deposit	thick deposit (unanalyzed to date)
gas/electrode chem.		CF_x	CuF, CuF_2, WF_6
other chemistry		S deposits, AlF_3	S deposits
breakdown volt. dist.		wider than in N_2	some prefires

PROPERTY (SF_6 or N_2)	LEXAN	BLUE NYLON
water content	3%	6%
contaminants	organic	organic, silicon
breakdown voltage distribution changes	little difference compared to no ins.	widening, increase in # of prefires

Table II. Summary of Chemical Results.

CHARACTER	GRAPHITE	K-33
visual erosion	smooth	rough
erosion scale	small	large
N_2 chemistry	some (CN)	none
SF_6 chemistry	some (CF_x)	much (CuF_x, WF_6)
individual discharge	little effect	distinct effect
breakdown voltage dist. changes with # shots	dist. narrows	dist. widens

	N_2	SF_6
electrode chemistry	low	high
decay products (gas)	almost none (NO, NO_2)	many (C & K-33)
insulator chemistry	none detected	some (CF_x)
impurities in gas	none	Cl
expense	low	high
breakdown voltage dist. changes with # shots	very little	more prefires

	LEXAN	BLUE NYLON
water content	lower	higher
impurities	nothing unusual	Si
organic contribution	some	greater
breakdown voltage dist. changes with # shots	little effect	much widening and more prefires

Table III. Materials Comparisons.

a 50,000 shot series took about 30 consecutive hours to produce. Second, the electrode materials, especially K-33, are expensive. Third, and most important, the highly sophisticated surface analysis techniques (ESCA, AES, EMPA, and XRF) are very expensive because they require expensive equipment, skilled personnel, and long times to complete. There is certainly going to be some sample to sample variation, due to sample handling and post-contamination, unstable spark gap system performance, changes in system operation personnel, and other factors. Without examining many samples, taken under identical system parameters, it is difficult to determine the error on quantitative measurements, to identify sources of external contamination of the samples, or to detect changing processes in the spark gap. For this reason, most of the final conclusions about spark gap processes were kept fairly qualitative in nature. Although not quantitatively described, conclusions on the general nature of the processes can be trusted for two reasons. First, samples from two or three combinations were analyzed twice in the process of reexamining certain combinations. These duplicated samples agreed with quantitative variations in the ESCA data of about 20%. Second, all combinations were rerun several times to accumulate data such as breakdown voltage distributions. Although careful surface analysis was not done on these duplicated samples, low power optical observations indicated the gross characteristics to be consistent; for example, graphite smoothing in N_2 and K-33 crystallization in SF_6, etc.

Although the breakdown voltage distribution data were preliminary, they did indicate that the spark gap materials have a definite effect on gas breakdown statistics. Most likely, this effect is ruled by processes which occur at the electrode surface. For instance, graphite erosion by vaporization and sublimation leads to a very smooth surface, void of sharp electron emitters. The graphite also recondenses as uniform monoatomic layers throughout the spark gap. A metal electrode, in this case K-33, not only melts, boils and recrystallizes, forming many sharp, jagged points, but also recondenses in a crystalline form to produce large, sharp metal crystals. Some insulating materials (Lexan) coat the electrodes with organic molecules, either not significantly affecting gap performance, or possibly improving it. Other materials, such as Blue Nylon, supply impurities detrimental to gap performance.

The range of application of spark gaps is extremely diverse, with widely varying parameter needs. For instance, spark gaps switch 10's of kA to 10's of MA, at 10 kV to 10 MV, transferring 10^{-3} to 100 C (the maxima are not achieved in the same system). They may require low jitter, low impedance, long lifetime, fast recovery, and/or high reliability. This study did not attempt to characterize the processes under all types of gap parameter ranges. As a result, although the techniques and some of the general results are applicable for all gaps, some of the processes may not apply under all gap conditions. For instance, the gap studied was a low energy system, transfering 0.03 C/shot. Other recent studies[70] indicate

that chemical and mechanical processes, breakdown voltage distributions, and erosion rates may be significantly different in a higher energy switch (~0.5 C/shot). Also, in the results presented here, the gas was static and not flushed and replaced during test runs. Although the gap chamber had a large volume (compared to the inter-electrode volume), the static system allowed volatile product accumulation and increased the effect of impurities as they were gradually released and concentrated. Certainly, many of the processes would be reduced or changed in a flowing or periodically flushed system.

Graphite proved to be a relatively simple and durable material in the spark gap environment. No large scale physical processes occur on the surface; i.e., no cracks, sputtering, or large particle ejection were observed. Erosion is primarily due to vaporization or sublimation or possibly chemical attack (CF_x). The resulting electrode surface is smooth and uniform across the entire discharge region (very flat in N_2 and smoothly pitted in SF_6). Generally, the self-breakdown voltage distribution tends to narrow initially as the electrode erodes. Some chemical surface interaction occurs with O, N, and F.

The copper-tungsten composite (K-33) tends to show large order (involving more material) physical and chemical processes. Melting, spattering, and surface crystallization are observed, resulting in metal component separation, material ejection, and deep chemical

interaction. Individual shot processes are prominent, and erosion occurs from boiling and ejection of copper vapor and possibly by chemical attack on tungsten. After many shots, the surface texture is rough and jagged, with metallic whiskers in N_2 and crystallized and cracked in SF_6. The breakdown voltage distribution widens after several thousand shots with many low voltage breakdowns. The surface undergoes strong chemical reaction with O and F.

Nitrogen is a stable, noncorrosive gas in the spark gap. No erosion mechanism can be attributed to chemical interaction with N_2 even though the plasma temperatures are very high. Some interaction with C and O (nitrous oxides were observed) does occur. The combination of N_2, graphite, and Lexan gives the best voltage distribution (narrowest and non-widening). This was due to the fact that the graphite eroded smoothly and few decomposition products accumulated in the N_2. The organic Lexan contaminants on the electrode surface may have helped to mask out any remaining high field emitters on the graphite surface.

Sulfur hexafluoride dissociates into many molecules producing a variety of decomposition products and reactive ions. Fluorine reacts with the metals (Al, Cu and C) and damages Al and quartz surfaces in the gap chamber, and sulfur tends to combine with H_2O and O_2 impurities and also collect at the bottom of the gap. Sulfur hexafluoride consistently shows a higher percentage of prefires (breakdowns lower than the average breakdown voltage) than nitrogen.

Insulators enter into the gap chemistry by donating H_2O, organic deposits, and Si contaminants. Blue Nylon definitely degrades gap performance, most likely by contaminating the electrode surfaces with Si.

Table III compares some of the processes observed for the different materials. Without accurate erosion measurements to correlate the chemical and physical processes, it is difficult to compare the performance of the different materials. Generally, graphite shows more uniform erosion than K-33, with small scale processes predominating on graphite and large scale processes predominating on K-33. Graphite interacts chemically more with N_2 than does K-33; conversely K-33 interacts more with SF_6 than does graphite. Graphite tends to develop narrower, more consistent breakdown voltage distributions.

Comparing SF_6 to N_2, it can be seen that SF_6 demonstrates more prefires, more insulator and electrode material chemistry, and more decay product accumulation. Blue Nylon contributes more water, silicon and organic contaminants, and leads to poor voltage breakdown distributions. Because of the chemistry observed and economic considerations, it seems that for a low voltage (not requiring SF_6), high rep-rate system a graphite-N_2-Lexan combination would give good voltage characteristics and long lifetime.

Further Studies

One of the primary purposes of this work was to demonstrate techniques to investigate the processes occurring in a spark gap. The parameter space was narrowed by choosing a few materials to investigate. Although many mechanisms were explained, to understand the processes occurring with these materials thoroughly, further investigations are needed to answer several remaining questions. To broaden the material studies of different types of spark gaps further, a few more materials should be investigated. Finally, some other parameters (besides materials) which were held fixed in this study, should be investigated to determine their influence on the spark gap mechanisms.

In the N_2-graphite system, the carbon-nitrogen interaction needs to be clarified. Is C-N formation observed on the graphite surface an erosion mechanism or are C-N bonds formed strictly in the arc plasma and at the electrode surface to bound carbon atoms? Most likely the C-N process is not a major erosion mechanism, but instead, erosion is primarily due to graphite evaporation and sublimation. What is the cause of the widely scattered craters in the graphite: impurities, vacancies, or other processes? In the graphite-SF_6 system, the exact nature of the chemical processes at the electrode needs to be studied. Although only fluorine was found attached to the graphite surface, sulfur also reacts readily with carbon at elevated temperatures.[66] Is there carbon in the sulfur deposits at the bottom of the gap chamber? Does demixing occur in the arc

channel, leading to fluorine concentration at the electrode spots? This would lead to enhanced chemical erosion of graphite and metals. In the K-33-N_2 system, what is the exact ratio of Cu to W at the surface and how much does it vary as a function of depth and distance from a discharge site? How is W removed from the electrode, since W has such a high melting point? Copper was observed spectroscopically in the discharge, but no tungsten lines were found. What is the exact composition of the metal whiskers and do they significantly degrade breakdown after a few shots? Since, in the K-33 - SF_6 system, no metal whiskers were observed, where does the tungsten go? How deep are the copper fluoride sites? How long does an electrode spot stay molten after a discharge, and how does this affect erosion? Exactly what is the composition of the material ejected at a discharge site? Finally, how strongly do impurities in the gases (Cl, O_2, H_2O, etc.) and electrodes (gases, hydrocarbons, etc.) affect the gap chemistry? Methods of answering many of these questions will be described in the next section.

The material parameter space needs to be expanded and other materials studied for three reasons. First, the materials studied were chosen because they were believed to be some of the best materials available. Are they? In other words, other common gap materials need to be studied to confirm that the materials chosen were indeed optimum. Since brass, stainless steel, copper, and air are commonly used in spark gaps, the processes occurring with these materials should be investigated. Second, there may be materials

which equal or exceed the performance of the materials studied. For instance, since SF_6 leads to detrimental gap chemistry, the "magic" 85% Ar -15% SF_6 mixture widely used in spark gaps to achieve multi-channeling should be investigated. The SF_6 available for chemical reaction would be reduced and yet this mixture would still have adequate high voltage switching performance. Copper impregnated graphite is a new material recently developed which may possibly exceed the performance characteristics of the ACF-10Q graphite. It is possible that Blue Nylon could be manufactured without the Si contaminant. Thirdly, a study of certain other gap materials may aid in understanding certain gap processes. For example, what processes occur in a pure Ar filled gap, since there should be no chemistry with this gas? How would graphite react in CO or CO_2 gas, since the oxygen is already combined with C? Possibly adding H_2O to a gas would help determine if and how it is detrimental to gap performance (very important if wet air is used as gas).

Other parameters, which need to be varied while studying chemical and physical processes, are electrode surface preparation, trigger method, charge per shot, peak current (affecting arc temperatures), gas pressure, gas flow, and gap voltage (or gap spacing). Also, careful correlation of recovery rates with the concentration of ionized gas molecules and numbers of vaporized metal particles will help explain recovery in terms of the chemical and physical processes occurring in the gap. Polarity effects should be studied, i.e., the surface of the cathode should be analyzed.

Although chemical processes may be more prevalent at the anode, recent results show that erosion is worse at the cathode.[71]

Although all of the above mentioned additional studies would be beneficial, certain key investigations would contribute more information to understanding spark gaps. For the materials presented here, key questions are:

(1) Does nitrogen contribute to graphite erosion (C-N)?

(2) How does SF_6 attack the graphite? Where does the graphite end up?

(3) How does the Cu/W separation in K-33 contribute to breakdown voltage distribution degradation?

(4) What removes the tungsten in the K-33 erosion?

New materials studied should include:

(1) brass - commonly used and easy to machine

(2) stainless steel - commonly used, fairly durable

(3) air - cheap

(4) SF_6/Ar mixtures - to reduce SF_6 erosion processes

(5) Cu impregnated graphite - possibly superior erosion characteristics, with good conductivity

(6) introduced controlled amounts of H_2O - how detrimental is it?

Gap parameters which most likely affect the spark gap processes observed, and should be investigated are:

(1) charge (energy) per shot - erosion processes may exhibit thresholds

(2) electrode surface preparation - how does the electrode surface influence the breakdown voltage distribution?

(3) gas flow - how does it affect the chemical processes and erosion?

(4) polarity - why are the chemical or mechanical processes different on anode and catnode?

Improvements in Analysis Techniques

Many of the current diagnostic techniques can be improved to obtain more information from the spark gap system. Also, some new techniques could help answer many of the previously listed questions. The technique improvements discussed below are divided into quantitative, electrical, surface analysis, chemical, and optical categories.

One analytical improvement would be the development of a quantitative approach to the chemistry. The erosion mass loss should be accurately measured. This might best be accomplisned in a larger discharge system (more charge transfer per shot) and also by redesigning the electrodes to increase $\Delta M/M$. The mass loss in the electrodes needs to be traced; i.e., where does the material go? Collection of solid debris in the gap in a drop tray at the bottom of the cylinder could help identify the total S lost in an SF_6 system. Careful metal and carbon particle density measurements on a cylindrically shaped insulator surrounding the discharge region could help track metal and carbon losses. Complete sealing of the gap chamber (since the mass spectrometer normally continuously samples the gas, requiring a slow, but finite gas flow) and analysis of total change and relative gas component content (after many shots) could

help identify total qualitative changes in the gas. These methods could be used to track W, C, Cu, and S quantitatively and thus help identify the significant chemical reactions.

Study of the breakdown voltage data will continue to be a very important tool to understanding the effect of different material combinations on gap performance. The present breakdown voltage measurement technique should be improved by more accurate control over system parameters, increasing the number of shots (record every shot), and eliminating the need for manual measurement. The gap voltage should be digitized and stored or recorded for later processing. If, instead of taking 500 shot samples every 2500 shots, all shot voltages were recorded and a sample averaging algorithm (averaging every 50 or so shots) were used continuously throughout the complete run of 50,000 shots, an accurate plot of gradual change in the breakdown voltage characteristics could be obtained. The error would be reduced and the number of man hours needed for data analysis would be shortened.

Although there are a few other surface analysis techniques which could be used (besides those described in this report), the best approach for additional surface information is to improve the sample preparation techniques and perform duplicate runs to improve the quantitative accuracy. Improved cross-section cutting and polishing techniques would help to answer damage depth questions. More single shot analysis using EMPA and AES techniques is needed, as well as sputtering or etching on many shot samples to study damage depths in

greater detail. Metal whiskers, copper/tungsten ratios, CuF crystal formation, and chemical deposit thicknesses could all be studied using these techniques. It is also very important to study the metal and carbon microparticles on the insulator surfaces to clarify the physical erosion processes.

The primary difficulty in gas analysis with the mass spectrometer is the large background-to-impurity gas ratio. A mass spectrometer used in conjunction with a gas chromatograph to separate out the background components would greatly increase the sensitivity for measuring small gas composition changes. More quantitative chemical analysis techniques need to be used to analyze the solid debris collected from the bottom of the spark gap chamber and from the gap surfaces.

Spectroscopic techniques could be greatly improved by using an optical multichannel analyzer (OMA) to look at sections of the emitted spectrum, gating the spectrometer to avoid the bright stages of the arc, and thus, being able to study the latter stages of gas recombination (giving more information on molecular species). Also, the formation of new molecular species, such as $(CN)_2$, could be detected by studying the UV spectrum of the discharge. Using improved spectroscopic techniques, plasma temperatures, electrode spot temperatures, metal vapor ejection, and demixing could all be investigated to learn more about the processes occurring in the discharge channel.

The more important diagnostic improvements are summarized:

chemical - quantitative chemical analysis of all solids with accurate erosion measurements

- gas chromatograph to separate the background gas

electrical - data acquisition system for the measurement, recording, and processing of breakdown voltage data

surface - improved sample preparation

- etching to study damage depth

- more single shot analysis

optical - spectroscopic techniques to look for C-N molecules, electrode spot temperatures, metal particle ejection

REFERENCES

1. Proceedings of the Workshop on Switching Requirements and R&D for Fusion Reactors, EPRI Special Report ER-376, July 1977 (M. Kristiansen, Ed.), sponsored by the Electric Power Research Institute, Palo Alto, California.
2. M. Kristiansen, ed., Switching Technology for CO_2 Laser Fusion, Final Report on LASL contract # N-68-2839E-1, pp. 49-64, Texas Tech University, Lubbock, Texas, June 1979.
3. T. R. Burkes, M. O. Hagler, M. Kristiansen, J. P. Craig, W. M. Portnoy, and E. E. Kunhardt, "A Critical Analysis and Assessment of High Power Switches," NSWC, Dahlgren Laboratory, Report NP 30/78, September 1978, (prepared by Texas Tech University, Lubbock, Texas).
4. G. Jackson, K. C. Yuan, L. L. Hatfield, and M. Kristiansen, "Surface Damage of Dielectrics in a Spark Gap," Proc. 3rd Int. Pulsed Power Conf., IEEE Pub. No. 81CH1662-6, pp. 289-292, Albuquerque, N.M., June 1981.
5. J. E. Gruber and R. Suess, "Investigations of the Erosion Phenomena in High Current, High Pressure Gas Discharges," Max Planck Inst. für Plasmaphysik, Garching bei Munchen, IPP 4/72, December 1969.
6. R. A. Burden and T. E. James, "Statistical Performance Data for a High Current 60 kV Spark Gap Switch," Proc. 7th Symp. Fusion Technology, Grenoble, France, pp. 24-27, October 1972.

7. J. Vargo and F. L. Taylor, "Electrode Erosion in Spark Discharges," J. Appl. Phys. 33 , pp. 2911-2913 (1962).

8. F. Llewellyn-Jones, "Electrode Erosion by Spark Discharges," Brit. J. of Appl. Physics 60 , pp. 60-65 (1950).

9. C. M. Cundall and J. D. Craggs, "Electrode Vapour Jets in Spark Discharges," Spectrochimica Acta 7 , pp. 149-164 (1955).

10. K. Schonbach and H. Fischer, "Explosive Anode Erosion in High Current Sparks," Applied Optics 9 , pp. 1695-1697 (1970).

11. F. M. Clark, "The Newer Insulating Gases," Engineering and Design, pp. 95-99 (1961).

12. H. I. Milde, "Dielectric Strength of a Spark Gap," Appendix D of Multimegavolt Modulator Feasibility Study, RADC-TR-68-241, pp. 43-158 (1968).

13. G. A. Farrall and J. D. Cobine, "Recovery Strength Measurements in Arcs from Atmospheric Pressure to Vacuum," IEEE Trans. Power App. and Systems PAS-86 , pp. 927-932 (1967).

14. E. P. Bel'kov, "Gas Cooling and Electric Strength Recovery after a Spark Discharge," Sov. Phys.-Tech. Phys. 16 , pp. 1321-1323 (1972).

15. M. P. Vanyukov, V. I. Isaenko, and G. N. Travleev, "Dielectric Strength Recovery of a Spark Gap in a Repeating-Discharge Regime," Sov. Phys.-Tech. Phys. 7 , pp. 544-548 (1962).

16. E. P. Bel'kov, "Dielectric Strength of Spark Gaps Following Strong Current Pulses," Sov. Phys.-Tech. Phys. 19 , 1210-1213 (1975).

17. J. J. Moriarty, H. I. Milde, and J. E. Hipple, "Megavolt Modulator Study," RADC-TR-70-107, 1970.

18. L. E. Murr, F. L. Williams, D. M. Smith, P. Predecki, and S. H. Wang, "A Preliminary Survey of High-Energy Switch Materials Degradation: Spectroscopic and Microscopic Characterization," Proc. 3rd Int. Pulsed Power Conf., IEEE Pub. No. 81CH1662-6, pp. 77-80, Albuquerque, N.M., June 1981.

19. E. W. Gray, "On the Electrode Damage and Current Densities of Carbon Arcs," IEEE Trans. Plasma Science PS-6, pp. 384-393 (1978).

20. M. T. Glancy and M. F. Rose, "Surface Aging in High Repetition Rate Spark Switches with Aluminum and Brass Electrodes," 2nd Int. Pulsed Power Conf., IEEE Pub. No. 79CH1505-7, pp. 301-307, Lubbock, Texas, June 1979.

21. B. Carder, "Gas Spark Gap Electrode Heating and Erosion," Internal Report, PI IR-13-74, Physics International Co., San Leandro, California, December 1974.

22. G. Marchesi and A. Maschio, "Influence of Electrode Materials on Arc Voltage Waveforms in Pressurized Field Distortion Spark Gaps," Proc. 5th Int. Conf. on Gas Discharges, pp. 145-148, Liverpool, U.K., September 1978.

23. D. Affinito, A. Fischer, and E. Bar-Avraham, "Design and Structure of an Extended Life High Current Spark Gap," IEEE Trans. on Plasma Science PS-7 , pp. 162-163 (1979).

24. EDM Technical Manual, 3rd Ed., Poco Graphite, Inc., Decatur, Texas, 1977.

25. S. Levy, "Spark-Gap Erosion Studies," USAELRDL Report No. 2454, U.S. Army Electronics Research and Development Labs, Fort Monmouth, New Jersey, April 1964.

26. F. Heitzinger, "The Properties of Tungsten-Copper Composite Materials on Arc Erosion Resistance," Seminar on Composite Materials in Electrotechnics, Oberursel, Germany, October 1977.

27. A. B. Parker, D. E. Poole, and J. F. Perkins, "The Measurement of Electrode Surface Temperature and Its Role in the Recovery of High Current Spark Gaps," Brit. J. of Appl. Physics 16, pp. 851-855 (1965).

28. W. C. Schumb, J. G. Trump, and G. L. Priest, "Effect of High Voltage Electrical Discharges on Sulfur Hexafluoride," Industrial and Engineering Chemistry 41, pp. 1348-1351 (1949).

29. J. Kulsetas, A. Rein, and P. A. Holt, "Arcing in SF_6 Insulated Equipment. Decomposition Products and Pressure Rise," Nordic Insulation Symposium, NORD-15-78, Vasa, Finland, June 1978.

30. P. Swarbrick, "Composition and Properties of a Sulphur Hexafluoride Arc Plasma," Brit. J. of Appl. Physics 18, pp. 419-426 (1967).

31. K. Hirooka, H. Kuwahara, M. Noshiro, and Y. Jitsugiri, "Decomposition Products of SF_6 Gas by High-Current Arc and Their Reaction Mechanism," Elect. Eng. in Japan 95, pp. 14-19 (1975).

32. J. P. Manion, J. A. Philosophos, and M. B. Robinson, "Arc Stability of Electronegative Gases," IEEE Trans. on Elect. Ins. EI-2, pp. 1-10 (1967).

33. D. Edelson, C. A. Bieling, and G. T. Kohman, "Electrical Decomposition of Sulphur Hexafluoride," Industrial and Engineering Chemistry 45, pp. 2494-2496 (1953).

34. R. Thorburn, "Permanent Dissociation of Sulfur Hexafluoride in Corona Discharges," Nature, pp. 423-424 (1955).

35. I. Sauers, L. C. Frees, H. W. Ellis, and L. G. Christophorou, "Mass Identified Ions from Spark Discharge of SF_6 in the Pressure Range 5-67 kPa," Proc. IEEE Conf. Plasma Science, Santa Fe, N.M., p. 127, May 1981.

36. M. T. Buttram and G. J. Rohwein, "Operation of a 300 kV, 100 Hz, 30 kW Average Power Pulser," Proc. 13th Pulsed Power Mod. Symp., IEEE Pub. No. 78CH1371-4, Buffalo, New York, pp. 20-27, June 1978.

37. D. L. Johnson, "Gas Switch Program," Sandia Report SAND-80-0974, p. 90, Sandia National Laboratory, Albuquerque, New Mexico, 1980.

38. B. A. Goryunov, "Dielectric Strength of Compressed Sulfur Hexafluoride and the Electrode Material and Surface Structure," Sov. Phys.-Tech. Phys. 20, pp. 66-67 (1975).

39. L. B. Gordon, M. O. Hagler, M. Kristiansen, and H. C. Kirbie, "Investigations of a 60 kV, 5 cm Spark Gap for Several Electrode, Insulator, and Gas Types," Proc. 3rd Int. Pulsed Power Conf., IEEE Pub. No. 81CH1662-6, pp. 376-379, Albuquerque, New Mexico, June 1981.

40. J. C. Martin, "Solid, Liquid, and Gaseous Switches," Lecture No. 30 from the Air Force Pulsed Power Lecture Series, AFOSR Grant 78-3675 (prepared by Texas Tech University, Lubbock, Texas, 1982, M. Kristiansen and A. Guenther, eds.).

41. N. K. Sukhodrev and S. L. Mandelstam, "On the Temperature of Electrode Vapors in a Spark Discharge," Optics and Spect. 6, pp. 473-476 (1959).

42. C. M. Cundall and J. D. Craggs, "Excitation Temperatures in Spark Discharges," Spectrochimica Acta 9, pp. 89-97 (1957).

43. S. Mandelstam, "Excitation of the Spectrum in a Spark Discharge," Spectrochimica Acta 3/4, pp. 255-271 (1959).

44. A. A. Mak, "The Channel Temperature of a Spark Discharge in Air," Optics and Spect. 8, p. 145 (1960).

45. E. Schulz-Gulde, "Temperature Determination for Arcs in Sulphur Hexafluoride Accounting for Demixing," J. Phys. D: Appl. Phys. 13, pp. 793-803 (1980).

46. T. Ito, Y. Ueda, H. Komura, and T. Nitta, "Spectroscopic Study of High Current Discharges," Proc. IEEE 99, pp. 573-578 (1971).

47. J. D. Cobine and G. J. Gallagher, "Current Density of the Arc Cathode Spot," Phys. Rev. 74, pp. 1524-1530 (1948).

48. R. L. Boxman, "Measurement of Anode Surface Temperature During a High-Current Vacuum Arc," J. Appl. Physics 46, pp. 4701-4704 (1975).

49. J. D. Cobine and E. E. Burger, "High-Pressure Arc Anode Phenomena," Physical Review 93, p. 653 (1954).

50. J. D. Cobine, Gaseous Conductors, Dover pp. 290-292 (New York, 1958).

51. CRC Handbook of Chemistry and Physics, "Table of Bimolecular Bond Strengths," 51st Ed., Cleveland, Ohio, 1970.

52. H. L. Roberts, "The Chemistry of Compounds Containing Sulfur-Fluorine Bonds," Q. Reviews Chem. Soc. 15, pp. 30-55 (1961).

53. R. W. Liebermann and J. J. Lowke, "Radiation Emission Coefficients for Sulfur Hexafluoride Arc Plasmas," J. Quant. Radiat. Transfer 16, pp. 253-264 (1976).

54. D. R. Airey, P. H. Richards, and J. D. Swift, "Time-resolved Temperature Profiles for 10 kA SF_6 Arcs," J. Phys. D: Appl. Phys. 8, pp. 1982-1993 (1975).

55. D. M. Barrett, R. A. Petr, and T. R. Burkes, "Spark Gap Electrode Erosion Data," Proc. 14th IEEE Pulse Power Mod. Symp., IEEE Pub. No. 80CH1573-5, pp. 25-27, Florida, 1980.

56. R. Petr and T. R. Burkes, "Acoustic Phenomena in Erosion of Spark Gap Electrodes," Applied Phys. Lett. 36, pp. 536-537 (1980).

57. G. Baruschka and E. Schulz-Gulde, "Transition Probabilities for FI Lines from Wall-stabilized Arc Measurements," Astron. and Astrophys. 44, pp. 335-347 (1975).

58. P. Cadman, J. D. Scott, and J. M. Thomas, "The Fluorination of the Surface of Elemental Carbon," Surface and Interface Analysis 1, pp. 115-121 (1979).

59. G. Jackson, "Application of Surface Analysis Techniques to Pulsed Power Problems," Technical Report AFOSR-PP-1, Texas Tech University, Lubbock, March 1981.

60. C. D. Wagner, W. M. Riggs, L. E. Davis, J. F. Moulder, and G. E. Muilenberg (Ed.), Handbook of X-Ray Photoelectron Spectroscopy, Perkin Elmer Corp. (Eden Prairie, Minn., 1979).

61. P. F. Kane and G. B. Larrabee, eds., Characterization of Solid Surfaces, Plenum Press (New York, 1975).

62. Poco Graphite, subsidiary of Union Oil Co., Decatur, Texas.

63. M. Hoch, D. Ramakrishnan, and T. Vernardakis, "Condensation and Vaporization Coefficients of Graphite," Advances in Mass Spectrometry, Vol. 6, Ed. by A. R. West, pp. 571-578, 1974.

64. R. P. Burns, A. J. Jason, and M. G. Inghram, "Evaporation Coefficient of Graphite," J. Chem. Phys. 40, pp. 1161-1162 (1964).

65. G. Jackson and L. L. Hatfield, private communication, Department of Physics, Texas Tech University, Lubbock (September 1981).

66. C. A. Hampel, ed., The Encyclopedia of the Chemical Elements, Reinhold Book Corp. (New York, 1968) pp. 106-115.

67. G. Buchet, et. al., "CN Molecular Bands in a Free Burning Metal Electrode Arc," J. Phys. Colloq. (France) 40, pp. 327-328 (1979).

68. Schwarzkopf Development Corp., Holliston, Mass, representative for Metallwerk Plansee, Reutte, Austria.

69. G. Jackson and L. L. Hatfield, private communication, Department of Physics, Texas Tech University, Lubbock, (November 1981).

70. A. L. Donaldson, R. Ness, M. O. Hagler, and M. Kristiansen, Proc. 15th Power Modulator Symposium, IEEE Pub. No. 82CH1785-5, pp. 84-88, Baltimore, Maryland, June 1982.

71. A. Donaldson and M. Kristiansen, private communication, Department of Electrical Engineering, Texas Tech University, Lubbock, Texas, (August 1982).